Characterization of Oilfield High Molar Mass Polymers Under Different pH and Mono-Di Valent Ion Environment Using Asymmetrical Flow Fluid Flow Fractionation.

by

Yogesh Kumar Dalsania

A thesis submitted in partial fulfillment of the requirements for the degree of

Master of Science
in
Petroleum Engineering

Department of Civil and Environmental Engineering
University of Alberta

Abstract

Various types of ultrahigh molar mass polyacrylamides (PAMs) or HPAMs and their co- and ter-polymers used not only in enhanced oil recovery, but also in drilling, fracturing, water treatment and tailing applications require an accurate description of polymer molar mass (Mw) and hydrodynamic size for their optimal design.

Molecular weight distribution (MWD) cannot be determined since either standard with low PDI, nor GPC/SEC techniques exist today for such ultrahigh molar mass polymers. Moreover, the solution environment in underground reservoirs, characterized by high temperatures, pH and the presence of monovalent and divalent ions, may often lead to changes in polymer macromolecular conformation. In this study the Asymmetrical Flow Field Flow Fractionation (AF4) system was utilized to fractionate ultrahigh molecular weight HPAM samples, varying in molar mass and commercially used for oilfield applications, in various carrier pH values ranging from 12 to 3 (pH 12, pH 7.4 and pH 3). In the second part of study effect of mono valent and di valent ion (salinity ranging from 1000 ppm to 10000 ppm) was investigated on post hydrolyzed, co polymer and associative polymer of PAM.

The results show that the observed molar mass of the polymer aggregate increased substantially as the pH of the carrier solution decreased from 12 to 3, especially for higher molar mass polymers. The samples radius of gyrations showed the opposite trend decreasing as the pH of the carrier solution changed from basic to acidic. The observations show that the molar mass value of polymer aggregate decreases as

salinity (monovalent ion) of the brine increases, similarly radius value also decreases as salinity increases. Di-valent ion has significant impact on radius of the polymer aggregate. A 31% decrement in radius values is observed as ions changes from Na^+ to Ca^{2+} at same salinity.

Preface

Chapter 3 and Chapter 5 of this thesis is partially based on a manuscript submitted for publication as Yogesh Dalsania, Ankit Doda and Japan Trivedi "Characterization of Ultra-High Molecular Weight Oilfield Polyacrylamides Under Different pH Environments Using Asymmetrical Flow FFF and Multi-Angle Light Scattering Detector" *SPE Peer Reviewed Journal*. A version of this work has been published at SPE Asia Pacific Enhanced Oil Recovery Conference, SPE 174624-MS. I was responsible for screening and analyzing the raw data and interpreting the results. I was also responsible for performing experiments, manuscript composition and addressing reviews. Ankit Doda assisted performing some experiments and Japan Trivedi was responsible for overall supervision and contributed to manuscript edits.

This thesis is dedicated to

My Guru,

H.D.H. Pramukh Swami Maharaj, whose serene and divine life will continue to inspire people across all humane boundaries.

My parents, without whose unconditional support this would not have been possible.

Acknowledgement

It is with immense gratitude that I acknowledge the support and help of my supervisor Dr. Japan Trivedi. I would like to thank him for his never ending support and persistence encouragement throughout my Masters. His novel technical ideas and methodology were instrumental in successfully achieving research goals.

I would like to thank my friends and fellow graduate student Tarang, Rajan and Ankit for providing fun filled atmosphere in the office. I would also like to thank Mit, Shivang, Gaurav and Urvesh for making my stay in Canada comfortable and memorable. I would also like to thank graduate lab assistant Mr.Todd Kinnee, for his help with instrumentation design and setup.

I would like to express my love and gratitude to my family, my sister Sona and Vidhi and brother-in-law Prashant and Keyur for their endless support.

I am also grateful to my parents for supporting me financially during the course of my studies.

Table of Content

List of Tables

List of Figures

Chapter 1

General Introduction

1.1Energy Outlook

The world energy needs will continue to grow at a steady pace for years to come. Population and income growth are underlying powerful forces behind the demand for energy. Real income has risen by a factor of 25 and world population has quadrupled since 1990. Rapid globalization and integration of low and middle-income economies will sustain the rising demand for energy. More people with more disposable income mean that demand for energy will continue to rise. Global energy consumption is estimated to increase by over 52% from the year 2010 to 2035.Currently, fossil fuels account for more than 85% of the world energy needs, and it will continue to be a major dependable source for energy needs. Out of fossil fuels, coal, gas and crude oil will continue to be a major source of energy (Figure 1). Given this fact, oil demand will increase from 81.2 to 100.2 mboe/d from 2010 to 2035 (OPEC World Outlook, 2013). This increased oil consumption will be realized by producing oil fields and newly to be discovered oil fields. Menard (Menard, 1981) in this article anticipated that the likelihood of discovering new fields with oil more than 100 billion barrels is extremely low. Also as current trends suggest, the rate of replacement of depleting fields by discovering new fields is decreasing faster (Alvarado, 2010).

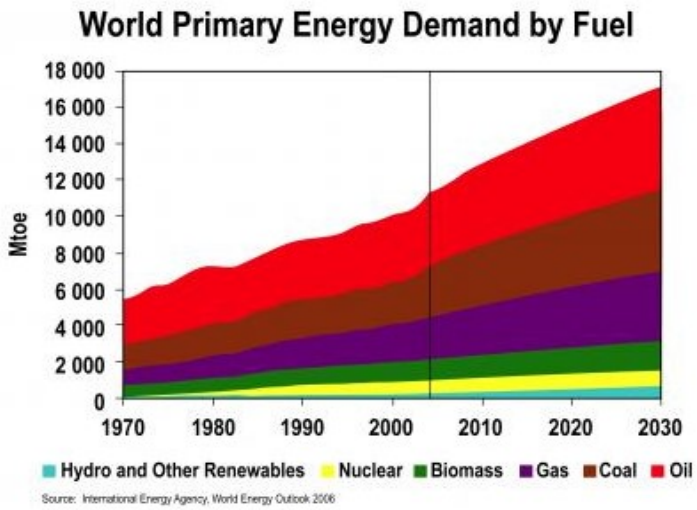

Figure 1: World Energy Demand (World Energy Outlook, 2006)

Also, an analysis of 1600 fields by IEA suggests that the production from a field declines at an average of 6% after it has passed peak production (IEA World Energy Outlook, 2013). Therefore considering the prospective shortage in oil resources and limitations in finding more oil by exploration the available option is to improve production techniques and extract more from existing reservoirs.

1.2 EOR Outlook

Life of a typical oil reservoir undergoes three stages. At each stage variety of techniques are engaged to optimize and maximize oil production. Three stages of oil recovery stages are primary, secondary and tertiary.

- Primary Stage: Initial stage in the production of the oil field. In this stage, oil recovery is by nature mechanisms. The various natural recovery methods

include rock and fluid expansion, solution gas drive, water influx, gravity drainage and gas cap drive.

- Secondary Stage: When the reservoir pressure declines and different methods for pressure maintenance and volumetric sweep efficiency are employed, the reservoir is called to be in secondary stage. Water injection and/or gas injection and artificial lifts is used in the secondary stage.
- Tertiary Stage: Third and last step of recovery and is also known as Enhanced oil recovery. Baviere (Baviere, 1991) defined EOR as "EOR consists of methods aimed at increasing ultimate oil recovery by injecting appropriate agents not normally present in the reservoir, such as chemicals, solvents, oxidizers and heat carriers to induce new mechanisms for displacing oil."

Generally, 5-30% of original oil in place (OOIP) is produced in primary stage (Castor, 1981) (Farouq Ali, 1970). Water injection in the secondary stage will increase recovery up to 40-60 %. During water flooding phase, the water-oil ratio in production stream steadily increases. When the water-oil ratio has reached high values, and it is not cost effective to operate the field, then it has reached its economical limit. At this point still 40-60 % of oil is in subsurface mainly due to heterogeneous rock properties and unfavorable wettability. It is this oil which is on target for production in EOR methods. The transition from a recovery method to other recovery method happens when the current recovery method becomes uneconomical.

In recent years EOR has gained enormous importance due to following reasons

- Lack of new discoveries.
- New discoveries tend to be in offshore or difficult to produce areas which add to capex and technological challenges.
- Producing unconventional resources is expensive in comparison to producing oil by EOR methods.

Depending on the basic mechanism which drives EOR, it can be classified mainly into three categories:

- Chemical EOR- It involves the injection of various chemicals in dilute solutions in the reservoir. It works by alternating capillary and viscous force in the subsurface.
- Thermal EOR- This method relies on heating the oil in the formation and thus reducing its viscosity. The increased heat also helps in reducing the surface tension.
- Gas Injection EOR – Miscible gas is pumped into the reservoir. It maintains pressure and improves oil displacement by reducing interfacial tension.

There are various techniques and methods which is used in EOR. Figure 2 shows various EOR methods and its category. Chemical methods have been used to increase macroscopic sweep efficiency. Polymer-gel treatment and polymer flooding have been used to increase the swept area in the reservoirs due to increases water viscosity (Chauveteau, 1991) (Clampitt, September 28 - October 1, 1975) and to shutoff high permeability zone (Sydansk, Spetember 27-30, 1998). Alkaline flooding and surfactant flooding works mainly by reducing interfacial tension

between oil and water. Thus it reduced the resistance to flow and made it easier for fluids to flow into the reservoir. Thermal recovery approach requires substantial capital investment in special equipment (Limited, 2013) and poses a safety risk in the larger production process. For this reason, thermal methods are not very common in a normal field. Gas injection methods are fairly common in the application. Carbon dioxide injection is preferred as it is cheap and it reduces oil viscosity.

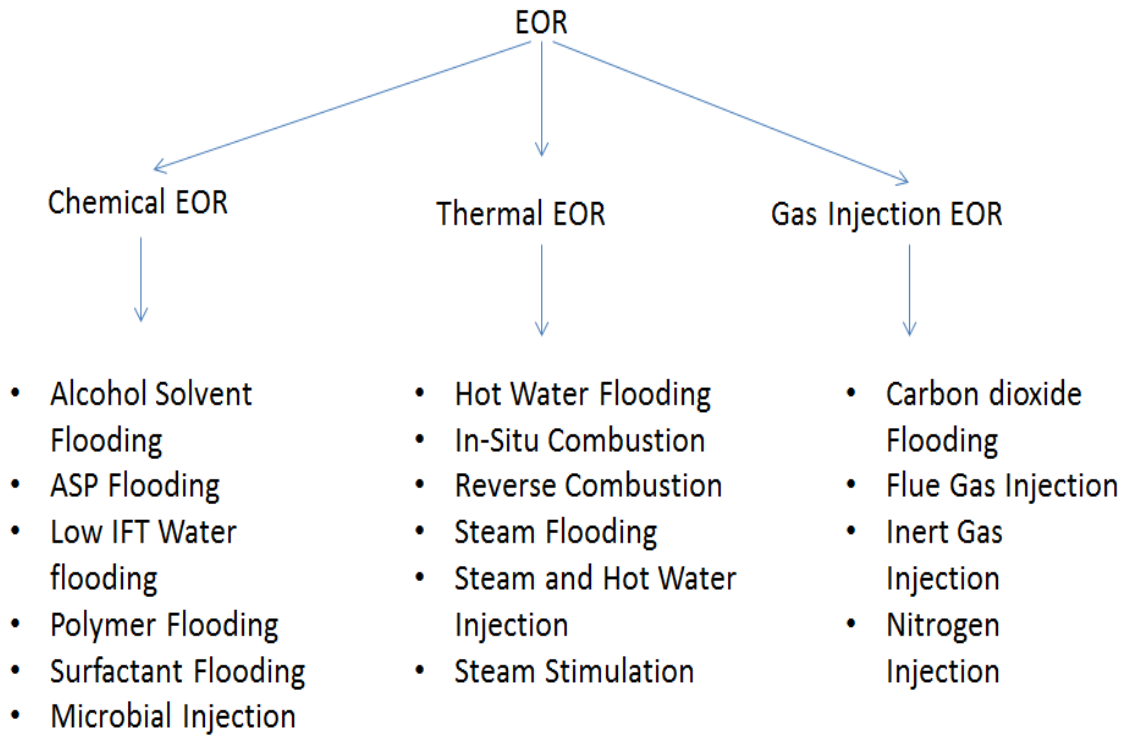

Figure 2- EOR Methods

1.3 Polymer Flooding Outlook

Polymer flooding is the most widely used chemical EOR technique and is in use since its introduction 50 years ago. The industry has implemented this technique

frequently and has achieved success to various extents. Water flooding has been used for pressure maintenance in reservoir however major concern associated with water flooding is poor sweep efficiency. High contrast in viscosity between oil and water results in unfavorable mobility ratio causing water to channel through oil. High mobility ratio leaves a major part of the recoverable oil in the subsurface leading to lower recoveries. Polymer flooding addresses this to a great extent. Added water soluble polymer in the water/brine in small concentrations increases the viscosity of the injected fluid and thus viscosity contrast decreases resulting in favorable mobility ratio which improves final oil recovery. From an engineering point of view which pursues economic viability and efficiency, polymer flooding technique is a very attractive method of increasing oil recovery with mobility control and pressure maintenance. Although polymer flooding is considered the economically modest method in comparison to other EOR techniques, it is still an expensive process, it has wide applicability across the different reservoir, the wrong design of polymer flood can lead to reservoir plugging and related problem; therefore it has warranted attention from researchers. Armstrong, 1967 (Armstrong, 1967) and Pye, 1964 (Pye, 1964) did early work on polymer flooding. Needham and Doe, 1987 (Needham, 1987) enlisted several polymer flooding cases and concluded that polymer flooding was an economical and technical success.

In USA Philips Petroleum implemented a 1440-acre freshwater polymer project in 1980. The project was based on North Burbank Unit in Osage County, Oklahoma. Philips Petroleum achieved incremental recovery of more than 2.5 MMSTB which bumped up the total project recovery nearly to 4.3MMSTB. It successfully

extended the life of the field by polymer flood. Philip Petroleum pumped in around 4 million lbs of aluminum citrate cross-linking solution and 4.2 million lbs of polyacrylamide (Moffitt, May 1993). Amoco conducted a polymer flooding at Sleepy Hollow, Nebraska in 1985. The field was a maturely water flooded containing 10 injectors and 45 producers on 40-acre spacing. Oil to be recovered has reported viscosity of 24 mPa.s and in comparison injected polymer solution had a viscosity of 10 mPa.s. Water oil ratio declined from 45 to 17. They injected 8kg of polymer for each incremental meter cube of oil recovered. Polymer they used was polyacrylamide (Christopher, 1988). In France, polymer flood was carried out at the Courtney in the Chateaurenard Field. Oil viscosity was 40mPa.s at 30^0 C. In this project 1 pore volume of the polymer solution at 900 ppm was injected via 4 injectors. Polymer solution injection was followed by water injection. Incremental oil recovery was reported as per the expectations (Putz, 1994). Largest polymer flood was implemented at Daqing, China. It started in 1996 and 2004 there were over 31 commercial scale projects involving 2427 injection wells and 2916 production wells. This project encompasses 67759 acres of aerial extent. Incremental oil recovery In Daqing and Shengli fields' (Chang, 2006) incremental oil recoveries of 6 to 12 % of OOIP have been reported (Singhal, 2011). In Canada CNRL and Cenovus has implemented field scale polymer flooding in there Pelican Lake asset. CNRL has an area of 187000 acres with 1000 producing wells and 200 injecting wells. Cenovus has 397000 acres with 445 producing wells and 280 injecting wells. Both the projects are currently producing and it started in 2004(Cenovus) and 2006 (CNRL). The industry has continuously improvised

technically in response to newly faced challenges in the polymer flooding. The most common polymer used for this application is polyacrylamide group (Jung, 2013). Partially hydrolyzed polyacrylamide (HPAM) has the shape of straight chain polymers of acrylamide monomers which some of it has been hydrolyzed. Other EOR projects active or planned during 2011 in Canada is given in Table 1 (Singhal, 2011).

Table 1: EOR Projects in Alberta, 2011.

Company	Formation	Field Name	Injection Type
Harvest Operations Corp.	Upper Mannville U	Suffield	Polymer Flood
Cenovus Energy	Sparky JJ	Viking-Kinsella	Polymer Flood
Harvest Operations Corp.	Wainwright B	Viking-Kinsella	Polymer Flood
Husky Oil Operations	Mannville B	Taber South	Polymer Flood
CNRL	Athabasca Oil Sands Area	Oil Sands Area	Polymer Flood
Murphy Oil Company	Peace River Oil Sands Area	Oil Sands Area	Polymer Flood
Enermark Inc	Lloydminister A, Sparky E	Wildmere	Polymer Flood
Blackpearl Resources Ltd.	Bluesky A	Mooney	ASP Flood
Cenovus Energy	Upper Mannville UU	Suffield	ASP Flood
Husky Oil Operations	Glauconitic K	Taber	ASP Flood

Major points which govern polymer flooding applications are

- The solution viscosity of the injected solution.
- Polymer absorption.
- Polymer degradation.
- Reservoir plugging.

The viscosity of the solution increases with increasing polymer concentration. Using higher molecular weight polymer also causes higher viscosity. In theory higher the viscosity more favorable mobility ratio and hence more oil recovery. However, high viscosity solution constraints injectivity of the solution in the reservoir. The polymer solution can undergo various changes in between the time from which polymer solution was made by the time it encounters oil in the reservoir. The apparent viscosity of polymers is usually much higher within the porous medium than in bulk i.e. when in pumping equipment. The increase is due to various permeability reduction phenomena. Polymer solution undergoes progressive mechanical degradation as shear rate increases. This phenomenon has been studied widely from 1970's (Warner, 1976 (Warner, 1976)) to current time (Zaitoun et al., 2012 (Zaitoun A. P.-M.-H.-G., 2012)). Polymers fail to retain/attain high viscosities in the presence of high salinity or high temperature. Some polymer is absorbed on the rock surface resulting in decreased solution viscosity. Smaller pores in the reservoir become inaccessible due to the large relative size of the polymer. Straining out of large polymer aggregate is known as plugging; it leads to higher pumping pressures.

1.1 Problem Statement

The success of polymer flooding applications depends on the proper selection of the polymer. Selection of such a polymer is dependent on reservoir characteristics and polymer characteristics. A critical factor that governs the success of flooding is polymer interaction with the brine in the reservoir. It is well known that high salinity causes polymer viscosity to decrease which results in unfavorable mobility ratio and subsequently lower recovery. Salinity present in the form of mono-valent and di-valent ion causes chemical degradation of the polymer. Interaction of metal ions shields the mutual repulsion from the carboxylic groups along the HPAM backbone, which leads to polymer coil to collapse. Another factor that affects HPAM is mechanical degradation. When polymer solution is pumped into the reservoir it passes through chokes, pipes, valves, nozzles, pumps, perforations near wellbore; HPAM chains are subject to both shear and elongation. Shear stress result in chain breakage that is mechanical degradation of the polymer. It may change the conformation of molecule and molar mass distribution of the polymer, this hinders the efficiency of the technique (Dupas, 2012) (Noik., February, 1995). Thus characterizing polymer before and after exposure to these external factors can substantially help to understand polymer behavior. Charaterization is really important because beforehand knowledge of polymer conformational change and structural changes in the reservoir will help immensely in polymer selection and polymer flood design such as to optimize recovery. Since almost every reservoir has different subsurface and brine conditions, it is important to study and investigate polymer in that specific environment. Thus polymer characterization

regarding molar mass, radius and molar mass distribution and radius distribution is crucial in understanding the polymer. Currently, industry uses the very crude method to characterize polymer; it is an indirect method based on the viscosity of the polymer solution. Molar mass is derived from calibrated standards from the viscosity measurement. The problem with this approach is that pre-determined calibration standard are required. Calibration standards may not be available for atypical polymers and it fails to encompass effect of varying salinity for the same polymer. Gel permeable chromatography(GPC) is also not effective for characterizing high molar mass polymers. It requires pre-filtering to avoid choking of the GPC column. The process of pre-filtering causes sample loss in high molar mass oil polymers and thus the filtered solution is not a true representation. Thus a direct method of measurement is required to characterize the polymer under different influences. Asymmetrical Flow Fluid Flow Fractionation(AF4) is one such direct measurement method which can be used for the said purpose. It has been extensively used in protein analysis (Botana, September 7, 1995) (Southan, 1999). AF4 coupled with Multi-Angle Light Scattering(MALS) is capable of providing complete molar mass distribution and radius distribution for the polymer. AF4-MALS is capable of accurately characterizing polymer under different brine environments. In this study the effect of pH, mono valent ion and divalent ion was investigated on polymer solution about conformational changes and structural changes i.e. molar mass and radius changes.

Chapter 2

Literature Review

2.1 Mechanics of Polymer Flood

Water soluble polymers are dissolved in the brine and then it is injected into the reservoir. The polymer dissolved in the brine makes brine viscous leading to extended sweep efficiency and better oil displacement. Figure 3 shows a typical schematic of a polymer flood. It is a single 5 spot pattern. As visible in Figure 3, the polymer solution is injected from the 4 injected wells placed in the corners. Flow is clear with the help of yellow marking. The formation is produced through one production well which is visible in the center.

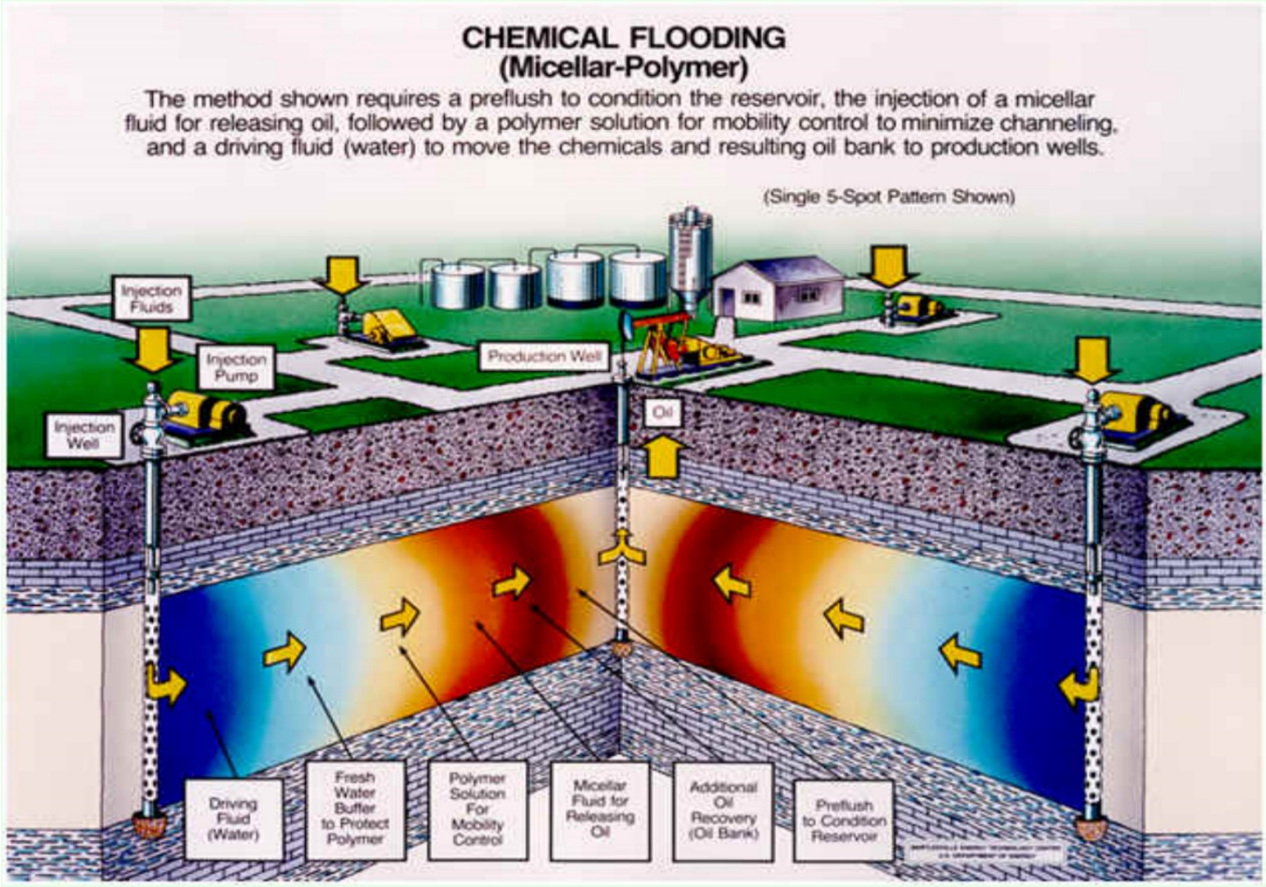

Figure 3: Schematics of Polymer Flood (Chemical Flooding Polymer, 2001)

2.1.1 Mobility Ratio

The concept of mobility ratio is widely discussed in the literature to describe the efficiency of the displacement processes such as water flood (Dake, 1978) (Willhite, 1986) (Aronofsky, 1956). Mobility ratio is the ratio of mobility of displacing fluid to the mobility of displaced fluid. It provides a measure of the relative movement of fluids during a displacement process. Relative movement of the fluid in the subsurface has a direct effect on the displacement of the trapped oil

and hence will subsequently affect the oil recovery of the process. For the purpose of EOR, mobility ratio for water floods can be defined as:

$$\boldsymbol{M = \frac{\lambda_w}{\lambda_o} = \frac{\left(k_w/\mu_w\right)}{\left(k_o/\mu_o\right)}} \qquad \textbf{Equation 1}$$

where,

μ_o and μ_w are the viscosities of oil and water respectively

k_w and k_o are the effective permeabilities of water and oil phases respectively.

λ_o and λ_w are the mobility of displaced fluid which is oil and the mobility of displacing fluid which is polymer solution.

When the mobility ratio for the displacement process is less than one, it is considered to be favorable for oil displacement. The mobility ratio higher than one suggests that the displacing fluid (water) has more tendency to flow than the displaced fluid (oil). Higher mobility ratio leads to inefficient displacement and can eventually cause fingering. Higher the mobility ratio, higher is the chance of

fingering.

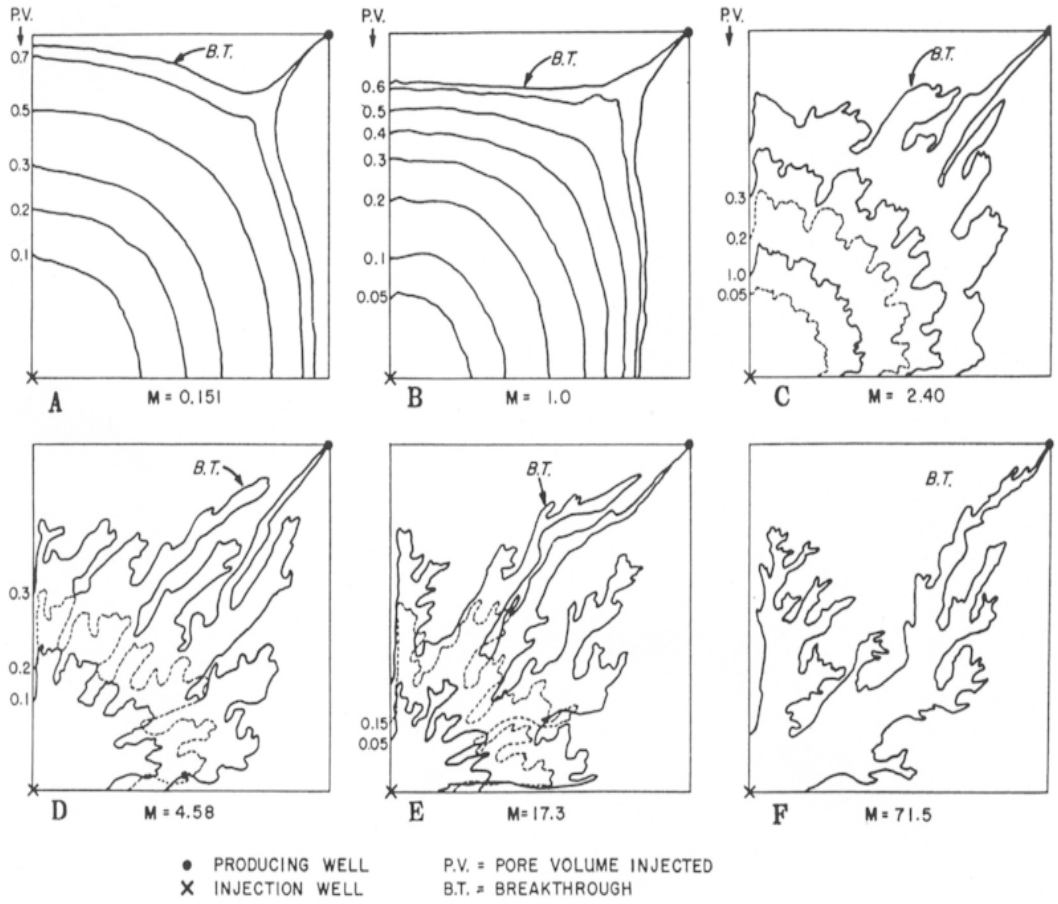

Figure 4: Different mobility ratio and its effect (Richardson, 1965).

Effect of mobility is apparent in Figure 4. Six different mobility ratios are showed i.e. 0.151, 1, 2.4, 4.58, 17.3, and 71.5. Mobility ratio values are varied to observe the effect it has on displacement process effectively. As seen in the case when the ratio is 0.151 and 1, displacement is progressing symmetrically, and it is covering the area uniformly. It can also be observed that breakthrough was reached earlier when the ratio is 1. So, the area swept more in displacement is when the ratio is less that is 0.151. When mobility ratio of 71.5 and 17.3 are compared, it is quite noticeable that both of them exhibit prominent fingering. When the ratio is higher,

the area swept is less, and breakthrough is reached very early. It is clearly visible that as mobility ratio increases the effect of fingering also increases. It also evident that sweep area also decreases as mobility ratio increases. Pore volume after which breakthrough is also reached decreased as mobility ratio increases.

So, lower mobility ratio is desired, and to do that either water viscosity has to be increased, or oil viscosity has to be decreased. There is not much in the subsurface that can be done to decrease oil viscosity, but water viscosity is easy to influence. So, increase in viscosity by dissolving the polymer in the brine and hence brings down the mobility ratio. Reduction in mobility ratio also improves and increases sweep efficiency.

2.1.2 Fractional Flow

Fractional flow is a fundamental concept of two-phase flow displacement process. As the name suggests, it represents the fraction of the flow of the displaced fluid(oil) or displacing fluid(water) in the total flow. Flow equation for the displaced fluid (oil) is given as:

$$f_o = \frac{q_o}{q_w+q_o} = \frac{1}{1+\frac{k_{rw}\mu_o}{k_{ro}\mu_w}} = \frac{1}{1+M} \quad \textbf{Equation 2}$$

Similarly, the equation for the displacing fluid (water) is given as:

$$f_w = \frac{q_w}{q_w+q_o} = \frac{1}{1+\frac{k_{ro}\mu_w}{k_{rw}\mu_o}} = \frac{1}{1+\frac{1}{M}} \quad \textbf{Equation 3}$$

In context to polymer flooding, polymer added to the injection water will increase the viscosity and hence reduces the relative permeability to water. As a result, the denominator term decreases in f_o and hence the value of f_o increases. Thus adding polymer aids in improving oil recovery performance.

2.1.3 Sweep Efficiency

Sweep efficiency acts as an indicator to judge the effectiveness of an enhanced oil recovery process that depends on the volume of the reservoir contacted by the injected fluid. Sweep efficiency is a broader parameter which depends on injection pattern selected, off- pattern wells, fractures in the reservoir, the position of gas-oil and oil/water contacts and reservoir thickness, areal and vertical heterogeneity, mobility ratio, the density difference between the displacing and displaced fluids.

The total efficiency factor, E can be given as:

$$\boldsymbol{E = E_D . E_{AS} . E_{VS}} \quad \textbf{Equation 4}$$

E_D is displacement efficiency

E_{AS} is aerial sweep efficiency

E_{VS} is vertical sweep efficiency

2.1.4 Displacement Efficiency

Displacement efficiency in also referred as microscopic sweep efficiency or local sweep efficiency. It can be defined as the ratio of the volume of oil displaced to the volume of oil contacted by the displacing fluid (polymer solution).

$$\mathrm{E}_D = \frac{Volume\ of\ oil\ at\ start\ of\ flood - Remaining\ oil\ volume}{Volume\ of\ oil\ at\ start\ of\ flood}$$

If the displacement process just involves oil and water and no gas is present, then displacement efficiency can be expressed using water saturation.

$$\boldsymbol{E_D = \frac{S_w - S_{wi}}{1 - S_{wi}}}$$ **Equation 5**

Where,

S_w is water saturation behind the font at the time of breakthrough

S_{wi} is connate water saturation

2.1.5 Buckley Leverett Equation

One of the most widely used methods of estimating the advance of a fluid displacement front in an immiscible displacement process is given by Buckley Leverett. It lays the basic analytical foundation for fluid displacement in sands. Buckley and Leverett (Buckley, 1942) showed that using material balance it can be proved that:

$$\boldsymbol{\left(\frac{\partial S_D}{\partial \theta}\right)_u = -\frac{q_t}{\phi A}\left(\frac{\partial f_D}{\partial u}\right)_\theta}$$ **Equation 6**

Where,

S_D is saturation of displacing fluid

θ is time

u is the distance along the path of flow

q_t is total rate of flow through section

ϕ is porosity

A is cross sectional area

f_D is fraction of flowing stream comprising displacing fluid

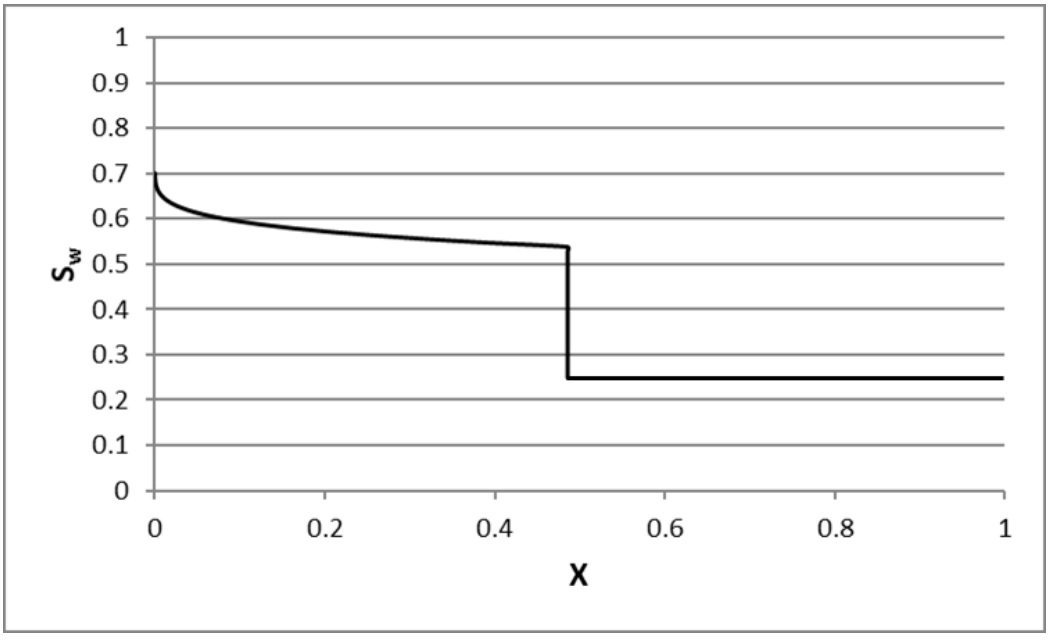

Figure 5: Plot of water saturation and distance.

Figure 5 shows water saturation in the reservoir. It shows that when water flooding technique is implemented, the saturation profile of injected water in the reservoir. It shows that saturation of the water front is little above 0.5 and has flooded half of the reservoir. Irreducible water saturation is just above 0.2. The “vertical line” represents the shock front. When the water breakthroughs, the water shock front has reached the producer well and well will produce water. Similar conclusion can be drawn for polymer flooding.

2.2 Polymers Used

The two most usually utilized polymers in enhanced oil recovery applications are the polyacrylamide in its partially hydrolyzed form and the biopolymer xantham. The recorded purpose behind these two polymers being utilized as a part of oil operations depends on the fact that both the polymers i.e. xantham biopolymer and polyacrylamide has broad application in other industries. Polyacrylamide is utilized as a major flocculant in an industrial process. It is also used in paper manufacturing industry. Xantham is extensively used as a thickener in food processing industry. As specified before HPAM is more broadly utilized polymer as a part of oil industry than the xantham biopolymer.

HPAM molecule exhibits a flexible chain structure which is also known as a random coil in basic polymer chemistry. Structurally HPAM is a synthetic straight chain polymer of acrylamide monomers, some of which have been hydrolyzed. Figure 6 shows the structure of HPAM. The level of hydrolysis is perhaps

imperative in certain physical properties, for example, polymer adsorption, shear steadiness, and thermal stability. All commercial polymers available have a stated degree of hydrolysis. There are three main chemical methods which may be used in principle to synthesis HPAM. The three process are –

- Direct free radical polymerization to produce PAM followed by hydrolysis of some of the amide group.
- Co-polymerize selected proportion of acrylamide and acrylic acid.
- Polymerize acrylic acid to give polyacrylic acid followed by aminolysis of PAA.

First and second reaction paths have been used in industrial production of HPAM. The fundamental and main solution property which is of importance in the context of polymer flooding is the viscosity of the polymer. It is defined as resistance to deformation b shear or tensile stress. Generally speaking, the viscosity of a fluid indicates to how "thick" the fluid is; that is water is less thick and flows easily than maple syrup. So, syrup has more viscosity than water. One important factor to observe is that unlike water which is a Newtonian fluid, polymer solution at high concentrations is generally non-Newtonian fluids. That is polymer solution do not display the same viscosity at all flow rates (shear rate) in a capillary or a porous medium.

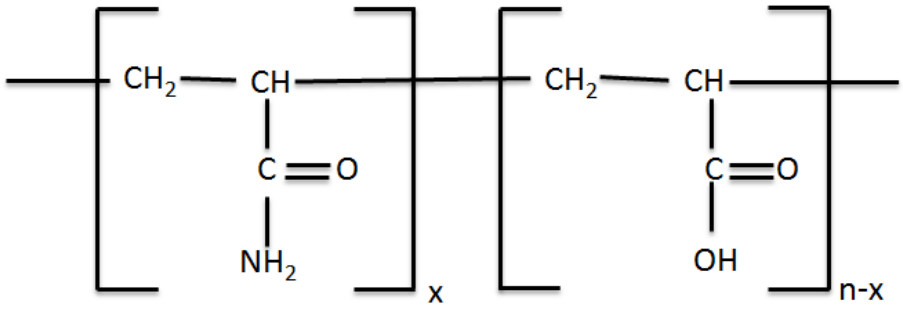

Figure 6: Structure of HPAM.

2.3 Polymer Degradation

Polymer degradation refers to any process that will break down the molecular structure of the polymer macromolecules. The change in polymer structure results in changed physical properties of the polymer solution like reducing viscosity, precipitation, etc. Change in the physical properties of the polymer solution leads to change in polymer flood performance. Change in viscosity of the solution will alter the mobility ratio of the fluid system. This change will be detrimental for polymer flooding. Increases mobility ratio will lead to inefficient sweep of the pore volume reducing the recovery of the oil. Practically in field applications, water flooding precedes polymer flood which implies that it is important to retain viscosity contrast in the polymer solution to sweep area bypassed by water flood, as pathway affected by water are relatively more favorable to flow than the others. Since almost all reservoir has different subsurface conditions and different brine with varying salinity, the polymer will undergo structural change resulting in

changed physical properties of the solution. Different HPAM have different performance under different physical and chemical environment. It is critical to "know" this changes and design the flood accordingly. To effectively design polymer flood, it is imperative to not only know the qualitative change but to quantify these change.

There are three main degradation pathways for the polymers used in oil field applications. They are -

- Chemical Degradation

  The breakdown of the polymer molecules, either through long term attack of the molecular backbone by a process such as hydrolysis or short-term attack by contaminants, such as oxygen.

- Mechanical Degradation

  The degradation through mechanical forces. Like a breakdown of a molecule in a high flow rate region close to the well as a result of the high mechanical stresses. This degradation is short term and is prominent near wellbore only.

- Biological degradation

  In this pathways of degradation, bacteria are responsible for the degradation. Bacteria may be encountered in the reservoir or during the storage. It will lead to the microbial breakdown of the macromolecules. Biological degradation effect both synthetic polymers and biopolymers and is a concern at a lower temperature or in the absence of effective biocides.

2.3.1 Chemical Degradation

As mentioned earlier, in chemical degradation two distinct processes can be identified. One is the short-term attack on the polymer molecule by contaminants, additives or other components present in the fluids or encountered in the process of injecting polymer solutions for example oxygen, iron, etc. The second process is long term attack on polymer backbone which results in intrinsic instability of the molecule. Hydrolysis is a critical factor in this type of attack. The practical methodology for efficient polymer flooding is to inject such a polymer solution (molecular system) that is resistant or insulated to short term degradation, and long term degradation takes place in such a way that polymer solution retains its viscosity long enough to be effective on the time scale of the oil recovery mechanism. Short term attack on polymer solutions can significantly decrease the polymer flooding performance.

Polymer degradation due to chemical effects has been of interest to researchers since 1970's. Akstinat (Akstinat, 28-30 May, 1980) in 1980 did a prominent study on the effect of high salinity brines at temperatures up to 80^{o} C. More than 300 different polymers were investigated. Polymers included cellulose derivatives, gelatine, mucilages, biopolymers, natural gums, polyvinyl alcohol, polyethylene oxide, synthetic resins, PAM and HPAM, and copolymers of the various group listed. Akstinat investigated at a range of properties which included solubility, the effect of pH, thermal stability, shear stability, and absorption behavior. To test the thermal stability of the polymer solutions, a polymer solution of different concentrations was prepared in a synthetic saline brine and was allowed to stand

for 48 hrs in the absence of air. Atkinson noted that over 90% of the polymer solution decomposes above 40^{o} C. Subsequently after the second step of exposure at 80^{o} C for 150 hrs only 7% of the original polymers showed promising behavior. These polymers were further stored for 3 months at 80^{o} C to investigate long-term stability of the polymers. Akstinat did not present very detailed results for stability for the polymers. However, polymers of HEC (hydroxyethyl cellulose) type and xantham were found to be acceptable. Another early work which is famous is a study done by Davison and Mentzer (Davinson, June 1982). They investigated 140 polymers for viscosity retention and porous media flow performance under high temperature and high salinity. They classified polymers as polyacrylamide(HPAM),polyvinylpyrrolidones(PVP),hydroxyethylcellulose(HEC), cellulose sulfate, guar gums, xantham and scleroglucan(glucan). Polymer solutions were made up using 0.45 μm filtered sea water. This method was described earlier by Hill (Hill, 1974). The solution used in the stability experiments were deoxygenated. This study concludes that polyvinylpyrrolidone and scleroglucan exhibit the most thermally stable behavior under test conditions. However, PVP had to be used in high concentrations (20000 ppm) to achieve adequate viscosity and therefore not very efficient. The precipitation time for polyacrylamide was found to decrease rapidly with increasing temperatures.

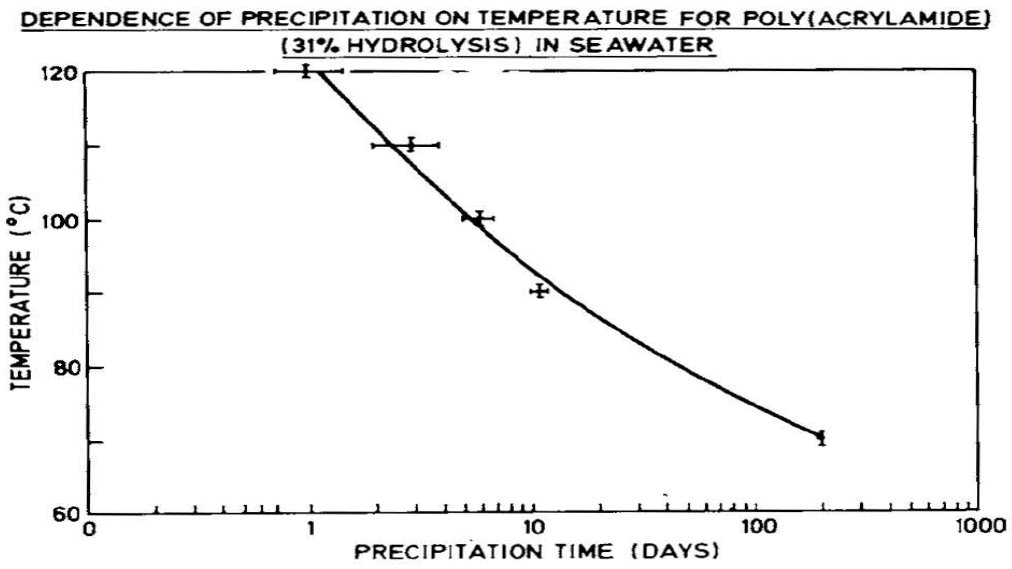

Figure 7: Dependence of precipitation time on temperature for HPAM.

Davison and Mentzer (Davinson, June 1982)

Figure 7 shows precipitation time varying with temperature for HPAM with 31% hydrolysis in the seawater. Moradi also investigated the dependence of precipitation and was found similar as found by Davidson and Mentzer.

Ryles (Ryles R. , 1983) reported that polyacrylamide was very stable for many months with or without the addition of chemical scavenging agents in the absence of oxygen. It is also to be noted that synthetic brine in the study had 22 ppm of divalent ions and total salinity was 3387 ppm. Figure 8 shows plot between residence time and viscosity for 2 polyacrylamides and xantham polymer in alkaline condition. It can be clearly observed that polyacrylamide retain its viscosity for significantly longer time than xantham polymer. Xantham polymer experiences a sudden loss of viscosity as seen in Figure 8.

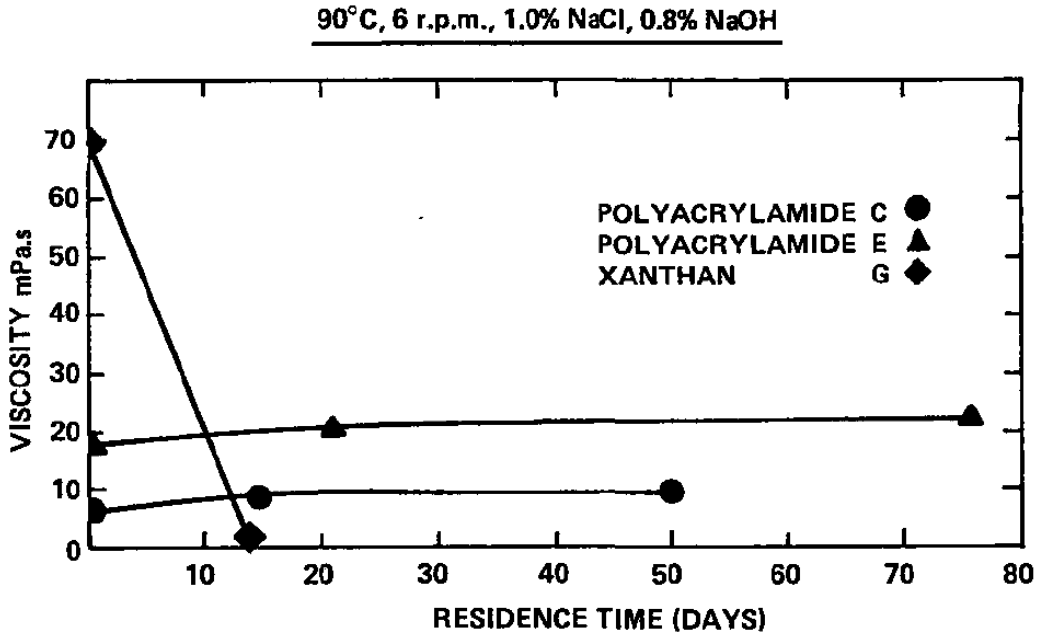

Figure 8: Thermal Stability in Alkaline conditions.

Ryles (Ryles R. , 1983) concluded few important observations regarding polyacrylamides. Observations are given below.

- At temperatures above 70° C, HPAM use will be restricted to brines with calcium ion concentration less than 200 ppm.
- At 50° C and below the rate of hydrolysis is low and HPAM remains stable for longer periods irrespective of brine composition.
- High molecular weight polyacrylamide is more sensitive to divalent ions.
- Polyacrylamide was stable for long periods in alkaline brines at a temperature up to 90° C.

Ryles in the extension of the study in 1986 (Ryles R. C., April, 1986), investigated a wider group of polymers of unknown structure. Another work on the

investigation on polyacrylamide on hard brines containing divalent ions was done by Moradi and Deo (Moradi -Araghi, May, 1987). When the temperature of a solution of polyacrylamide containing divalent cation is increased, the solution turns cloudy and then precipitation follows. This cloud point represents a stability limit for that particular polyacrylamide in that particular brine. Moradi and Deo studied hardness level (using equal concentration of $Mg^{2+}$and Ca^{2+}) over the entire range from 1 to 10,000 ppm, particularly in the range of 10-100 ppm where a reduction in polymer cloud point is first observed. Figure 9 shows the effect of brine hardness and degree of hydrolysis on the cloud point of polyacrylamide. It represents the concentration of 1000 ppm in 5% NaCl solution. It can be observed that PAM with higher degree of hydrolysis

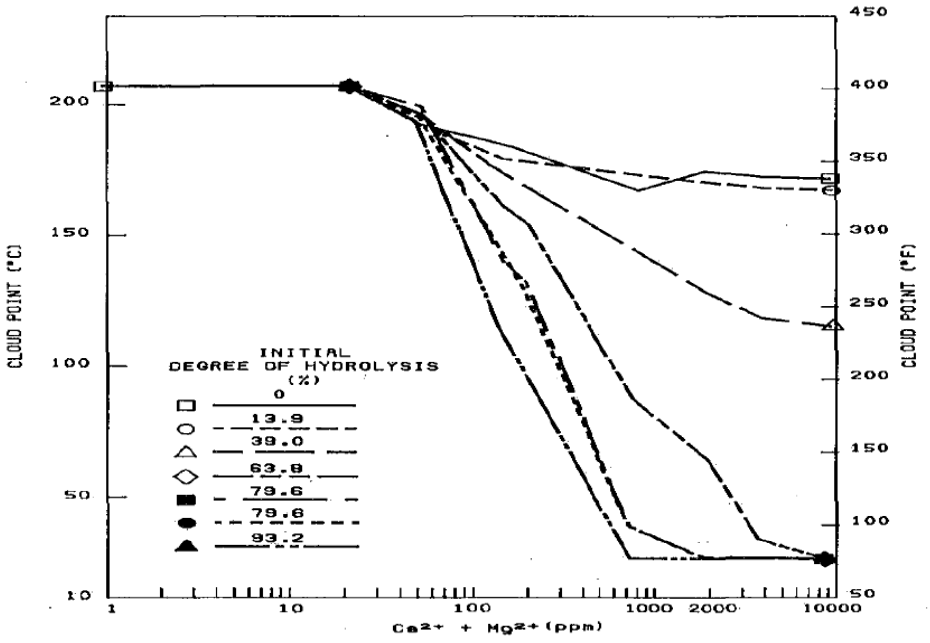

Figure 9: Effect of brine hardness and degree of hydrolysis on cloud point.

Moradi and Doe (Moradi -Araghi, May, 1987)

Have lower cloud point in the high presence of divalent cations. It can be seen that cloud point for 93.2% hydrolyzed PAM is around 75° C and cloud point for 0% hydrolyzed PAM is around 340° C when the divalent ion is 10000 ppm. Another significant observation is that degree of hydrolysis does not affect cloud point when divalent ion concentration is less than 10 ppm. Important inferences from Moradi and Doe work is –

- When hardness level is between 20ppm and 800 ppm, a small increase in divalent ion concentration results in a significant drop in cloud point(stability).
- Polyacrylamide is influenced by molecular weight as well as polymer concentration but the effect of hydrolysis supersedes.
- At equal molar levels, Ca^{2+} is more potent in reducing cloud point than Mg^{2+}, Sr^{2+}or Br^{2+}.
- Polyacrylamide solutions are stable at all hardness levels up to 75° C. Beyond this; they precipitate at increasingly shorter times as temperature is increased.

Seright et al (Seright R. C., June 2010) conducted a study on the stability of HPAM at elevated temperature in the presence of 0.3 % NaCl. It can be observed in Figure 10 that at 120° C, polymer solution loses half of its viscosity in 500 days. For 140° C, polymer solution significantly loses its viscosity over the course of 500 days. As temperature increases rate of loss of viscosity also increases. Polymer solution loses its viscosity in 60 days only when the temperature is 180° C with decane.

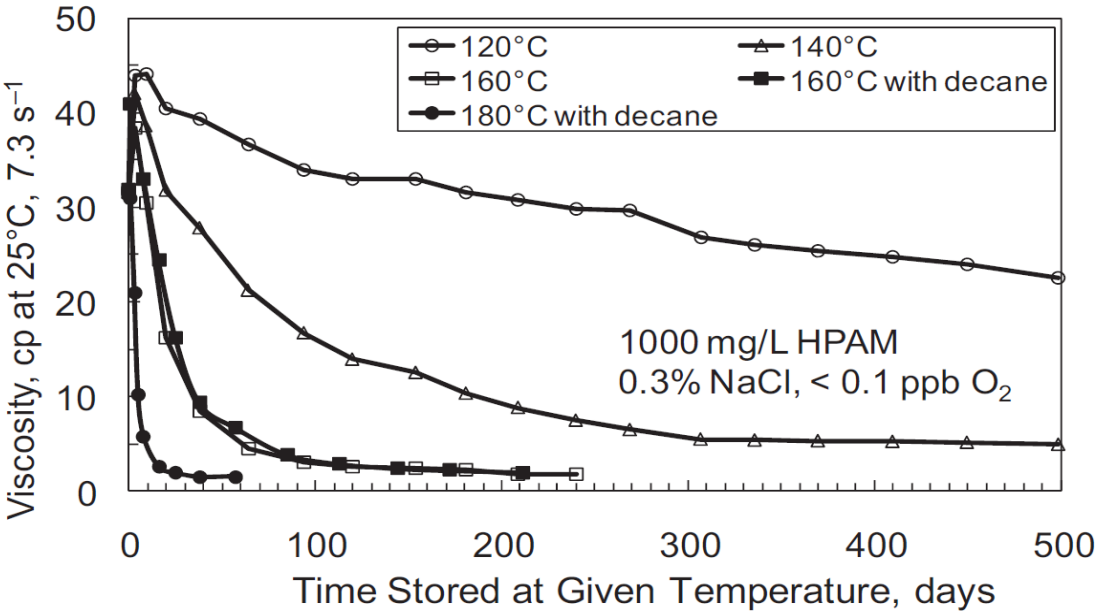

Figure 10: Stability of HPAM at 0.3% NaCl. Seright et al (Seright R. C., June 2010).

Xin et al. (Xin, 15 September, 2007) conducted an interesting study on the effect of CaCl2 on partially hydrolyzed polyacrylamide. HPAM investigated had a viscosity averaged molecular weight of 1.7 * 10^7 Dalton and degree of hydrolysis are 23-25 % and was supplied by Chang'a Corp. Rheological measurements taken in the study was carried out on HAKKE RS75 Rheometer. Two different temperature of 25° C and 75° C; four different concentrations of CaCl2 were taken i.e. 100 ppm, 200 ppm, 300 ppm and 400 ppm were considered for the study. It can be observed that viscosity decreases as the concentration of Cacl2 increases. Effect of temperature is also as discussed earlier. Viscosity decreases with increase in temperature. It can also be seen that at different concentrations too, higher

temperature shows low viscosity. The trend of viscosity on shear rate remains similar in each case.

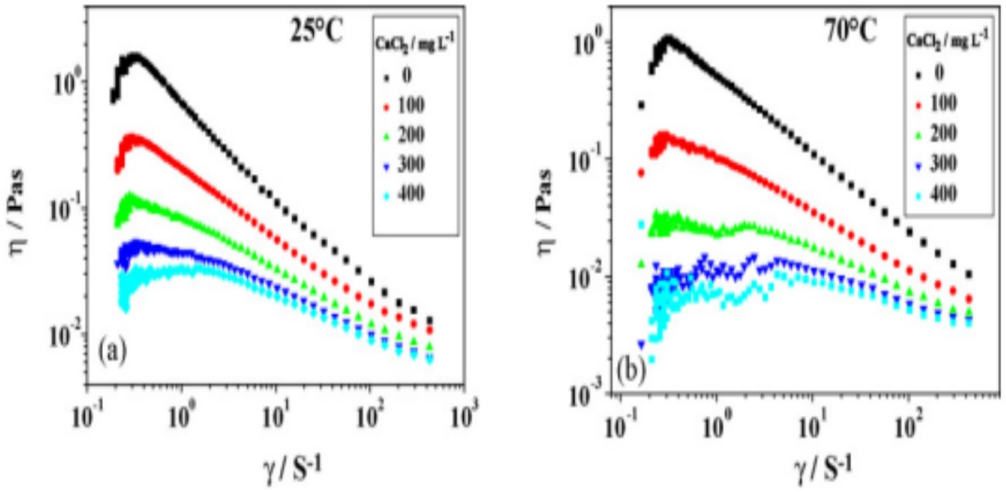

Figure 11: Viscosity of HPAM under CaCl2.Xin et al (Xin, 15 September, 2007)

2.3.2 Biological Degradation

Biodegradation can either take place on the surface before injection or within the reservoir. The biological attack can effect more synthetic and biopolymers, but the problem is prominent in the case of biopolymers. Damage can be reduced by adding a biocide, the most common biocide used is formaldehyde. The concentration of biocide is kept between 500 to 5000 ppm (Sorbie, Polymer - Improved Oil Recovery, 1991). A biocide may also interfere with other additives added in the flooding process; it should be taken care that added biocide is compatible with the other additives. There are several field reports of polymer flooding in which biological degradation of the polymer has been reported as a problem, one of the

prominent project which reported biological degradation as a problem was Exxon's Loudoun pilot (Bragg, October, 1983).

2.3.3 Mechanical Degradation

Mechanical stability of the polymers commonly used in oil recovery operations is an important factor as polymer undergoes shear stress and other physical stresses in the polymer injection projects. It leads to the cessation of large molecular weight chains of polymer into lower molecular weight chains; this leads to reduced effective molecular weight distribution. It leads to changes properties of the polymer solution i.e. lower viscosity and hence higher mobility ration which is detrimental to the success of polymer flood. Among common polymers, Xantham appears to be extremely shear stable, and a synthetic polymer such as HPMA are very sensitive to shear degradation. Degradation of HPAM from this mechanism can occur at various locations from the mixing step till the point it encounters oil in the subsurface. On the surface, facilities required for injection for example chokes, pumps, etc. can lead to mechanical degradation (Zaitoun A. P.-M.-H.-G., 2012). Another area where degradation is prominent is near well bored area where the apparent viscosity of polymer solution decreases reduces due to high flow velocities (Seright R. S., October 2009) (Gumpenberger, November, 2012). Work done by Seright et al. concluded that HPAM is sheared at high flow rated and as a result molecular weight distribution changes. Larger molecules offer more resistance to flow and therefore experience larger shear stress and are as a result more likely to

breakdown (Agarwal, 1980) (Basedow, 1979). So, larger molecular weight polymer is more prone to mechanical degradation. The rate of mechanical degradation or polymer chair rupture in high shear flow depends on molecular weight, the shear rate, and fluid viscosity (Ram, 1970) (Abdel-Alim, December, 1973).

2.3.4 Polymer Retention

When the polymer is hydrated in reservoir brine and injected into the reservoir, the objective is to increase the viscosity of injected fluid using the polymer. However, there are significant interactions between the polymer hydrated and the porous medium (reservoir). Such interactions cause the polymer to get restrained in the porous medium due to various reasons. Retention allows the injected fluid to get accumulated in the reservoir; this will lead to decreased efficiency of the polymer flood. This polymer retention in the porous medium will also result in a reduction of the rock permeability. Polymer Retention potentially can have a huge impact on the technical and economic success of a water flood. Therefore, it is estimated by conducting polymer flood experiments in the lab on the desired reservoir subsurface rock.

Classically, retention level, Γ, is expressed in g/g that is, in the mass of polymer per unit mass of solid. Since the polymer retention phenomenon takes place in micro scale, it is more appropriate to measure it in $\mu g/g$. Generally, retention in practical application in porous media is reported in mass of polymer per unit

volume of the rock, Γ_m. The most prevalent oil field unit for retention is lb/acre-foot (lb/AF). Conversion from, Γ = x $\mu g/g$ to field unit of Γ_m in lb/AF, where ρ_{RG} is grain rock density of rock without pore space and φ is porosity is given by-

$$\boldsymbol{\Gamma_m = x2.7194(1-\varphi)\rho_{RG}\ lb/AF} \quad \textbf{Equation 7}$$

There is three main retention mechanism which is considered to be active when polymer solution flows through porous media. They are –

- Polymer Adsorption
- Mechanical Entrapment
- Hydrodynamic retention

Polymer adsorption takes place due to the interaction between the polymer molecules and the solid surface which is interfaced by the solvent. This interaction causes polymer molecules to get attached to the surface of the rock in contact. Physical adsorption is predominant than chemical adsorption. Van der Wall bonding and hydrogen bonding plays an important role in physical adsorption. It is evident that larger the surface area, larger will be the polymer adsorption. Also, it is the only mechanism which can take place in the absence of a porous medium. Polymer adsorption will take place in varying amount wherever the solution comes in contact with a surface, which potentially means that adsorption transpires right from the mixing tank. Although tangible adsorption occurs in the reservoir as surface area encountered is enormous. Mechanical entrapment is “straining out” of

large polymer molecules from smaller pore throat. It acts like a filtration process where large polymer molecule's entry in small pore radius is strained and thus the polymer molecule is strained out of the smaller pore opening. There are several implications in light of this mechanism. If entrapment is widespread in the reservoir and the number of such entrapment sites/incidents exceeds a certain critical number, then it will lead to drastic permeability reduction to unacceptable levels. Even for the subcritical number for the entrapment events, there will be a significant reduction in the permeability accompanied with a large level of retention. Retention can be a problem as this effect is largest close to the immediate porous media to the polymer injection. This chronology of the polymer injection also suggests that retention due to mechanical entrapment along the reservoir would be largest close to the inlet of the polymer solution and decreases as solution progress through the reservoir. Another implication is reduced concentration of the effective polymer solution. Reduced concentration of effective polymer solution can also decrease due to polymer adsorption mechanism. As the polymer get retained in the pores, polymer bulk "decreases" from the polymer solution resulting in lower concentration than the intended polymer concentration. Reduced concentration will directly affect the viscosity of the solution which in turn will change the mobility ratio unfavorably. Increased mobility ratio can result in an inefficient sweep. Oil lost due to this and too inaccessible pore volume due to pore plugging (mechanical entrapment) can potentially reduce recovery of the polymer flood to noticeable levels. It can be said that if entrapment mechanism operates to about the average size of the pore distribution, then it can lead to significant problems in polymer

flooding. It can lead to palpable pore blocking which will cause unsatisfactory and uneconomic polymer flood. Hydrodynamic retention is the least understood retention mechanism. This mechanism is not a very significant contributor to overall polymer retention in porous media and is not an important factor for field scale polymer floods. As shown in Figure 12, it can be explained as the polymer molecules that are trapped probably temporarily in stagnant flow region by hydrodynamic drag forces. In such localized region, there may be a possibility for increased polymer concentration than the injected fluid. When the flow ceases and drag force is reduced, these polymer molecules may again blend in the main flow channel and when the flow restores, they are produced.

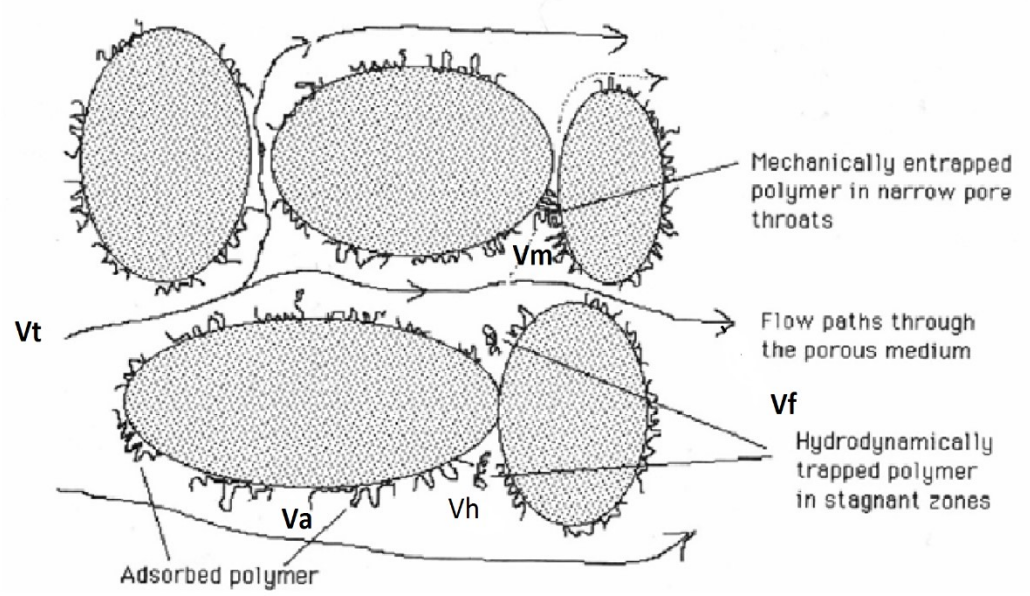

Figure 12: Schematic of polymer retention mechanism. Reproduced from Sorbie,1991 (Sorbie, Polymer - Improved Oil Recovery, 1991)

As seen in Figure 12 as polymer solution enters the localized pore system, different retention mechanism commences. The total volume of Vt enters the localized pore system. Va is the "volume" of the polymer solution adsorbed on the surface area of the rock. Vm is the "volume" of the polymer solution that is constrained in due to smaller pore opening about the polymer molecule size. Vh is "volume" of polymer solution confined due to hydrodynamic drag force. Vf is the final volume which will exit the local system. Vf gives vf = Vt – Va – Vt -Vm.

Smith in 1970 (Smith, Feb, 1970) studied permeability reduction caused by HPAM with three different molecular weight through Berea cores. It was observed that residual resistance factor increases as the molecular weight of the polymer increases. As seen in Figure 13 Polymer H (higher molecular weight) shows greater permeability

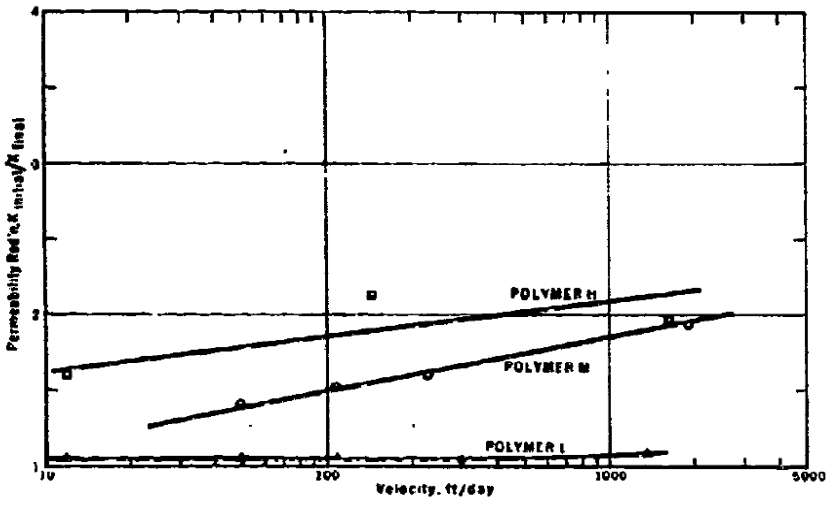

Figure 13: Effect of Molecular Weight on permeability reduction. Smith (Smith, Feb, 1970)

Reduction than polymer M (medium molecular weight) and polymer L (Lower molecular weight). Polymer L shows the lowest reduction and shows negligible reduction with increases velocity. Another important conclusion was that it showed that polymer effectiveness in reducing mobility is highest in lowest salinity. Higher polymer concentration leads to higher residual resistance factor. Vela et al.,1976 (Vela, Evaluation of Polymer flooding in the Layered reservoir with cross flow, retention and degradation, April, 1976) studied the retention behavior of HPAM with a molar mass of 5.5 * 10^6. It was observed that higher polymer concentration corresponds with higher resistance factor. It was also noted that level of retention and resistance factor also depends on permeability. Lecourtier et al (Leourtier, 1990) investigated the effect on adsorption of polyacrylamides on siliceous minerals. The study reported that increase in pH leads to decrease in adsorption of HPAM. This pH dependence can be explained with electrostatic repulsion between polymer and surface as well as between polymers. Similar behavior was observed by Lee et al (Lee L. R., December, 1991). Lee et al. conducted a study on different faces of kaolinites. It was also observed that adsorption density increases as salinity increases. Zhang and Seright (Zhang G. S., 2014) reported that HPAM adsorption on rock surfaces could be considered as instantaneous and irreversible. Another observation was that polymer adsorption is concentration independent at dilute regions (low concentration) and concentrated region (high concentration). In semi-dilute region, retention is polymer concentration dependent. Tekin et al (Tekin, 2005) reported that adsorption process becomes more favorable as temperature increases. It has also been suggested that low-cost additives (adsorption inhibitors)

can be used with brine to reduce the effect of adsorption. Tay et al (Tay, 2015) demonstrated that properly selected low-cost additives can be used as adsorption inhibitors to reduce adsorption. Simple solubility, static adsorption test, and microemulsion phase behavior were used to screen the best additive. Screened additive showed the promising result on lab scale.

For hydrolyzed polyacrylamide, mechanical entrapment is the dominant retention mechanism as it is flexible coil polymer. Polymer adsorption still occurs, but in porous media mechanical entrapment is dominant. Szabo (Szabo, August, 1975) in 1975 studied retention oh HPAM on sand packs and Berea cores. The level of retention observed in dynamic flow test was up to 5 times than the retention observed in static measurements. Ignoring the hydrodynamic entrapment, the only possible explanation is mechanical entrapment. The study also determined the distribution of retained HPAM post long brine flush. Figure 14shows retained HPAM profile along the sand pack after injection of 0.2pv polymer solution followed by brine post flush with 5pv.

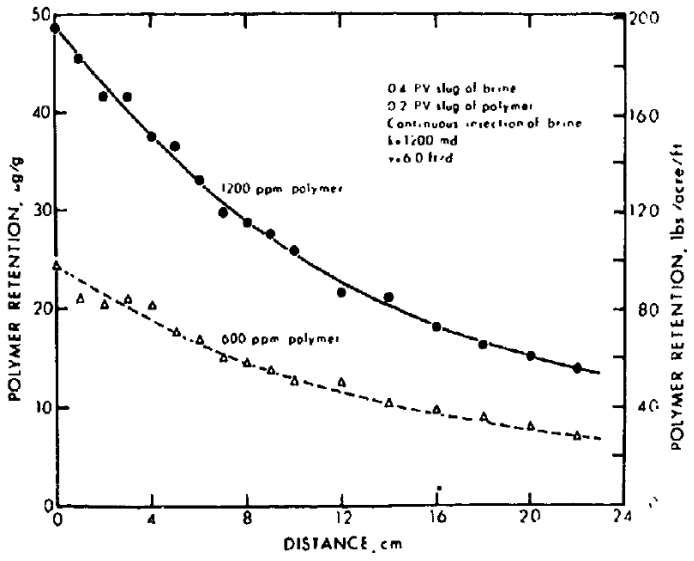

Figure 14: Retained HPAM profile along sand pack. Szabo (Szabo, August, 1975)

For the two cases shown (600ppm and 1200ppm), mechanically retained polymer levels range from 600 ppm was 6 – 24 (inlet – outlet) $\mu g/g$ and for 600 ppmit was 15- 50 (inlet-outlet) $/g$. Static adsorption for this particular HPAM/sand was 2.5 $\mu g/g$ and was independent of polymer concentration. Clearly by observation mechanical entrapment is dominant here. Also the fact that retention values increases as concentration increases further substantiate the conclusion. Retention level of HPAM also decreases along the sand pack and is lowest at outlet, this is as per intuitive expectation. Dominguez and Willhite (Dominguez, April, 1977) conducted similar study with HPAM and core of compacted Teflon. This study also found mechanical entrapment as predominant.

More recently Zhang and Seright (Zhang G. S., 13-15 April, 2015) studied retention of commercially available HPAM SNF Floopam 3230S. Floopam 3230S is in the

molecular weight range of 6-8 million daltons, and degree of hydrolysis is 30 % approximately. Dundee Sandstone with the permeability of 1.9 Darcy and 24.1 % porosity. Retention was investigated under flux or superficial velocity from 3.26 ft/day to 104 ft/day. Different levels of retentions were observed with different flow rate. As flow rate increases, retention of the polymer also increases. Table 2 shows retention values with changing velocity. It can be observed that retention can increase up to almost 50% when velocity changes from 3.26 ft/day to 104 ft/day Similar observation regarding flow rate and retention level has previously been reported by Huh et al (Huh, 1990).

Table 2: Retention Values for SNF 3230 S. Zhang and Seright [57].

V, ft/day	Γ $\mu g/g$ rock
3.26	20.3
6.52	23.0
13.0	25.7
26.1	28.3
52.2	28.4
104	29.5

The permeability of the porous media also plays a role in polymer retention. In a range of high permeability porous medias (more than 500 md), polymer retention is insensitive to permeability change. Zaitoun and Kohler (Zaitoun A. K., 1988) reported polyacrylamide retention values of 140 $\mu g/g$ in 520 md Vosges sandstone and 155 $\mu g/g$ in 2.1 darcy Vosges sandstone. However, for lower permeability

porous medias, polymer retention generally increases dramatically with decreasing permeability. Vela et al (Vela, Evaluation of Polymer Flooding in a Layered Reservoir With Crossflow, Retention and Degradation, April, 1976) found that for Pusher 700 (HPAM) retention value increases from 12 $\mu g/g$ in 137 md sandstone to 130 $\mu g/g$ in 17 md sandstone. More recently Chen et al (Chen, 2016) observed that HPAM with molecular weight of 8 million Daltons, initial retention decreased from 96.1 $\mu g/g$ to 13.9 $\mu g/g$ as core permeability increased from 135 mD to 1650 mD

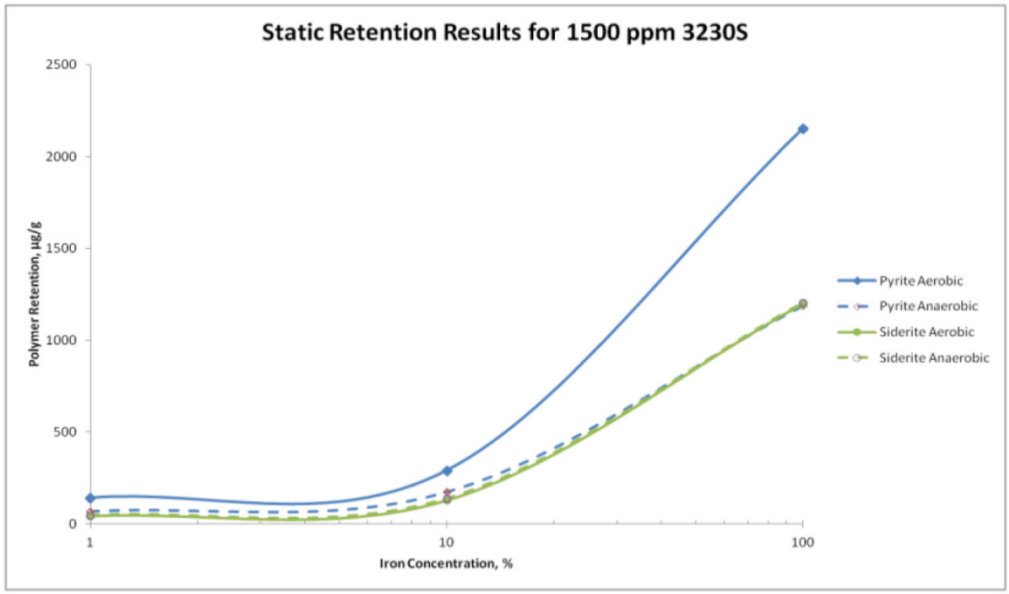

Figure 15: Effect of iron mineral concentration and oxygen on polymer static retention.

In 2016, Wan and Seright (Wan, 2016) studied polymer retention under anaerobic and aerobic conditions. Commercially used polymer 3230S and 3630S were used for investigation. The study reported that for both aerobic and anaerobic conditions,

HPAM retention increased significantly with increase in pyrite and siderite content. From observing static retention measurements on pure silica, it showed little difference in retention values between aerobic and anaerobic conditions. Manichand and Seright (Manichand, 2014) reported theoretical delay factor (Figure 16) associated with polymer flooding and polymer retention.

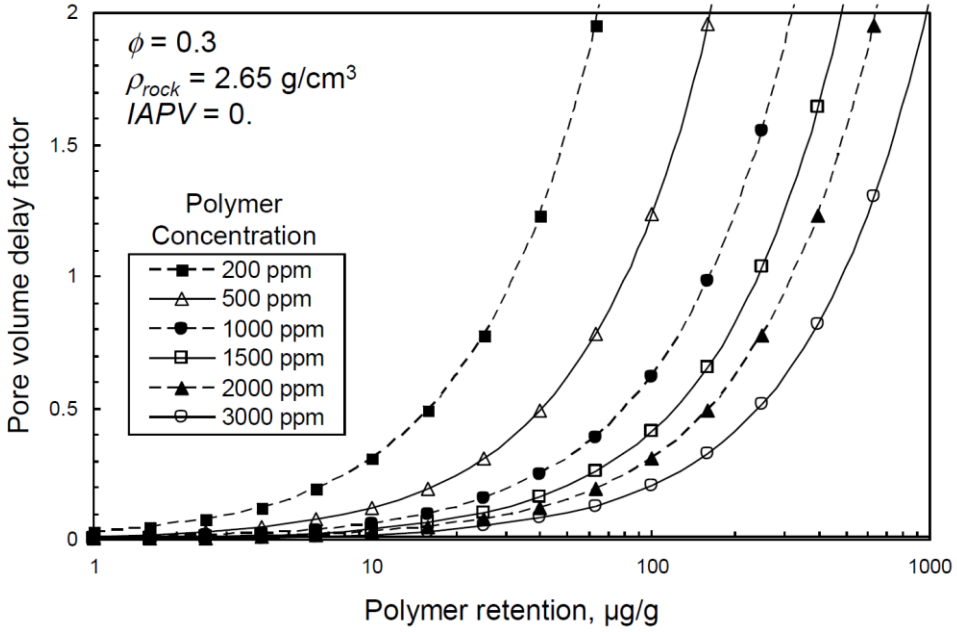

Figure 16: Polymer delay factor associated with polymer retention. Manichand and Seright (Manichand, 2014).

In Figure 16, IAPV stands for inaccessible pore volume, the density of rock is 2.65 g/cm3 and porosity of 0.3, Pore volume delay factor represents an incremental fraction of one pore volume required to access target distance in the formation about the case for no polymer retention. It is observed that at same retention value of polymer, incremental pore volume required increases with decreasing concentration. For polymer concentration of 1240 ppm and retention value of 100 $\mu g/g$, pore volume delay factor is 0.5 meaning that 50% more polymer must be

injected to reach target distance in relation to the case when there is no polymer adsorption. Study also pointed that polymer retention calculation in the field indicates much higher retention value than polymer retention from laboratory test.

2.1 Method of Characterization

2.4.1 Viscosity Method

A relatively simple and highly empirical polymer characterization method that has been widely used to estimate the average molar masses of polymer samples is based upon a determination of the intrinsic viscosity of a polymer in solution. Intrinsic viscosity can be estimated through extrapolation of viscosity vs. concentration data (Buchholz, 2001). Although modern rotational viscometry instruments can be used for these measurements, a simple Ostwald or Ubbelohde viscometer is more typically applied. Polymer molar mass can be empirically related to the intrinsic viscosity through the Mark-Houwink-Sakurada relationship (Kasaai, 2005).

$$[n] = KM_v^a \qquad \textbf{Equation 8}$$

where [n] is the intrinsic viscosity, K and a are empirical constants that are specific for a given polymer, solvent, and temperature, and Mv is the viscosity average molar mass.

This method is restricted to the analysis of polymers for which Mark-Houwink-Sakurada constants are already known. Also, MHS constants only work for the solvent or closely related solvent for which the constants are determined (Brandrup, 1999). It is recognized that brine composition changes as reservoir changes, which makes it difficult to analyze behaviour of a polymer as MHS constants may not be

necessarily known for that brine. This method also has a limitation in case of novel polymers or copolymers being designed specifically for a purpose (Young, 1991). This method of characterization is extremely crude. It only gives one value for the molar mass and gives no information on the mass distribution of the polymer. It also doesn't give the value of the radius of gyration. Hence, intrinsic viscosity has limited usefulness for novel ultrahigh molecular weight polymers and copolymers that are being developed specifically.

2.4.2 Gel Permeation Chromatography (GPC)

GPC is a common method of polymer characterization in use. Especially it is used when higher molecular weight is involved (Al-Sabagha, 2013) (Wever, 2013) (Pourjavadi, 2013) . GPC is also extensively used in characterization of poly-acrylamide (Su, 2008) (Liberatore, 2004) (Ouyanga, 2011).

In this method, the polymer sample is first dissolved in a solvent. Once the polymer is dissolved, the molecules coil upon themselves to form a coil conformation, which resembles a ball of string. Higher molecular weight polymers coil up to form larger coil conformed structure. These coiled up polymer molecules are then introduced into the mobile phase and flow into the GPC column. The dissolved polymer molecules move past the beads as the mobile phase carries them down the column. As the polymer coils move past each bead, several things can happen. If the polymer coils are much larger than the biggest pores in the beads, they cannot enter the pores and so are carried straight past by the mobile phase. If the polymer coils are a little smaller than the biggest pores they can enter the larger, but not the smaller pores as they pass by,

occupying some, but not all of the available stationary phase. If the polymer coils are smaller than the smallest pores in the beads, then they can enter any of the pores and so can potentially occupy all of the stationary phases.

As the molecules enter the column, this partitioning repeatedly occurs, with diffusion acting to bring the molecules into and back out of any pores they pass as they travel down the column. As a result, small polymer coils that can enter many pores in the beads take a long time to pass through the column and therefore exit the column slowly. Conversely, large polymer coils that cannot enter the pores take less time to leave the column, and polymer coils of intermediate size exit the column somewhere between these examples. Thus, the way in which the samples elute from the column depends very much on the size of the pores in the beads.

As the components exit the column, they are detected in various ways, and the elution behavior of the sample is displayed in a graph or chromatogram. The chromatogram shows how much material exited the column at any one time, with the higher molecular weight, larger polymer coils eluting first, followed by successively lower molecular weight (and therefore smaller) chains emerging later. The primary separation is according to elution volume.

An inherent assumption in this method of molar mass estimation is that the analyte polymer travels through the column at the same velocity (Buchholz, 2001) as would a given polymer size standard of the same molar mass. This assumption is clearly an approximation since coil size and specific mode of migration is dependent not only on molar mass but also on polymer persistence length and the extent of solvation.

Shear degradation is another problem faced in analyzing high molecular weight polymer (Cave, 2009) (Barth, 1984) (Žigon, 1997) . Nicolai Aust (Aust, 2003) showed that molecular degradation happens due to mechanical forces acting on the

chromatographic system when the molecular weight of the sample is higher than 5000kg/mol. This effect has also been studied as a function of flow rate (Slagowski, 1974) (Kirkland, 1976) and the column packing material (Ling., 1982).

Due to above-mentioned limitations, it is difficult to employ GPC for characterizing high molecular weight oil field polymers.

2.4.3 Field-flow fractionation (FFF)

Over the years, FFF has advanced rapidly and has become a very useful analytical separation technique for characterization of macromolecules. It is a standard method for quantification regarding size and molar mass characterization of ultra-large biopolymers, protein aggregation, and synthetic polymers. The technique is a strong alternative GPC/SEC when it comes to separation of large proteins and ultra-high molar mass (>10^6 g/mol) polymers, which are not accessible by GPC/SEC since their molecular size prevents them from penetrating the pores in the packing material. As FFF relies on a combination of field-driven and diffusive transport mechanisms.

General Principles of FFF

The fundamental principle if FFF can be explained with the help of Figure 17.The separation takes place inside a narrow channel which is composed of two highly polished plane parallel surfaces. The solvent is flown continuously into the inlet port of the channel. Polymer sample to be characterized is injected. It is to be noted that it is desirable to use the same solvent to hydrate /dissolve the polymer which

is being injected into the channel. An effective later field is applied to the channel in the direction of the x-axis. The later field can be a physical (Pressure FFF, Electrical FFF, Magnetic FFF), chemical (Concentration FFF) or any other field. Due to this later field applied, the solute particles in the injected polymer sample gets concentrated on the channel and thus forms a concentration gradient depending on the solute concentration accumulated. The accumulation of the solute will depend on the behavior of the solute to the applied later field. Thus it can be potentially be used to characterize a specific solute selectively. The concentration gradient thus formed induces a diffusion flux in the reverse direction than that of the cross flow applied. As a result of this solute particle accumulated under the influence of cross, particles tends to disperse back into the channel.

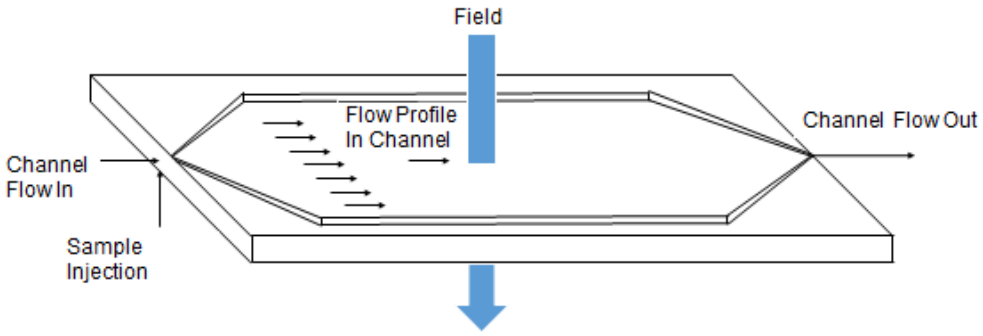

Figure 17: Principle of Field Flow Fractionation

Due to the solvent flowing in the channel, this dispersed solute particle gets carried away in the direction of the flow of the solvent which is along the longitudinal axis. Finally, the dispersed solute in the solvent along with the solvent exits the channel as seen in Figure 17. The outflow of the channel is connected to a detector or a

series of detectors. Detectors like Refractive Index(RI) Detector, Ultraviolet detector, MALS detector. The choice of the detector is made according to the requirement, design, and applicability of the experiment.

The streamline velocity of flow of the solvent inside the channel exhibits a parabolic profile under laminar conditions. The solute particles which are transported due to the solvent will vary in time because of the varying velocities which depend on the distance from the channel walls. For example, in the channel there are two solute species, out of which one species is relatively smaller, and the other species is relatively larger. Now due to the lateral field effects, these solute species will get concentrated on the accumulation wall. They will get distributed across the channel to different extent due to the field effect. The smaller particles will have more tendencies to move along the channel due to induced concentration flux in comparison to the larger particles. Thus the smaller particles are less compressed to the accumulation wall than the larger particles. Due to relatively high compression of the larger particles, they have retained more in the channel then, the smaller particles. So by this mechanism, separation is achieved. Hence the elution sequence proceeds from the molecules with smaller dimensions to the larger particles. FFF mode, when the intensity of the lateral field applied is homogenous and constant along the entire channel is referred as classical FFF. Practically, however, intensity of the lateral field is varied from high intensity to low intensity with the help of field intensity programming.

Different techniques of FFF

There are several different techniques of FFF. They are grouped according to the nature of the field applied, and the intensity of the field applied. Table 3 shows physiochemical properties and application for various flow fluid fractionation systems. Few of the FFF techniques are -

Thermal FFF

Thermal field flow fractionation is arguably the oldest FFF technique (Thompson, 1969). It is usually composed of two metallic blocks. Electricity heats the upper block and water cools lower black. A temperature gradient or rather thermal energy flux causes thermal diffusion of the solute species leading to the accumulation.

Sedimentation FFF

It uses either natural gravitational or centrifugal forces in the centrifuge machine to serve as an effective lateral field which forces accumulation of the solute particles.

Electrical FFF

The electrical current induces the homogenous field across the channel. Walls for Electrical FFF are semipermeable that permits passage of ions.

Flow FFF

Flow field flow fractionation is widely used FFF technique. In this technique, the external lateral field is provided by the flow of the solvent in the perpendicular direction to the flow of the basic medium in the channel. This thesis employs a type of Flow FFF known as Asymmetrical Flow Field Flow Fractionation to characterize and investigate oil field polymers.

Table 3: Physiochemical properties and application for various FFF systems (Leenders, 2014).

FFF subtype	Physiochemical properties	Applications
Electrical	Size, electrophoretic mobility	Cells and organelles, bacteria and viral separations, characterization of emulsions, liposomes, protein adsorption
Thermal	Size, thermal diffusion coefficient	Separation of dissolved and suspended polymers, polymer and silica nanoparticle analysis
Dielectrophoresis	Dielectric permittivity, size	Cell separation and dielectric property measurements and cancer cell separation
Asymmetrical flow	Diffusion, size	Proteins, DNA, polymers, cell, micro, and nanoparticles

2.5 Asymmetrical Flow Field-Flow Fractionation (AF4)

It differs in design with other FFF methods in two major aspects. First is that it only has one permeable wall which is the accumulation wall. Traditional FFF methods have both walls permeable. The second aspect is that it has asymmetrical channel dimensions in the form of a trapezoid. Traditionally FFF methods use rectangular channels. Schematics of AF4 can be seen in Figure 18. Separation in AF4 is carried out in a thin ribbon like channel in which the channel is constructed by clamping a thin spacer between porous and non-porous plates as shown in Figure 18. Carrier liquid entering at the tip of the channel quantitatively makes up for the both longitudinal flow (channel flow) and the horizontal flow (cross flow). The crossflow is created because the porous wall allows the carrier liquid to exit through the bottom channel wall. The porous wall referred here is a membrane supported by a frit as seen in Figure 18. Thus the carrier flow or the tip flow entering the channel divides between flow down the channel and flow across the channel. The crossflow forms fluid lines which are perpendicular to the channel flow. It causes a viscous force which drags the sample material to the membrane surface (accumulation surface). The viscous drag results in species being distributed across the channel to a different extent. Distribution will depend on diffusion and size properties of the sample species and the magnitude of the cross flow. Components which are compressed tightly against the accumulation wall are carried slowly by the flow because they encounter streamlines of low velocity nearer to the wall.

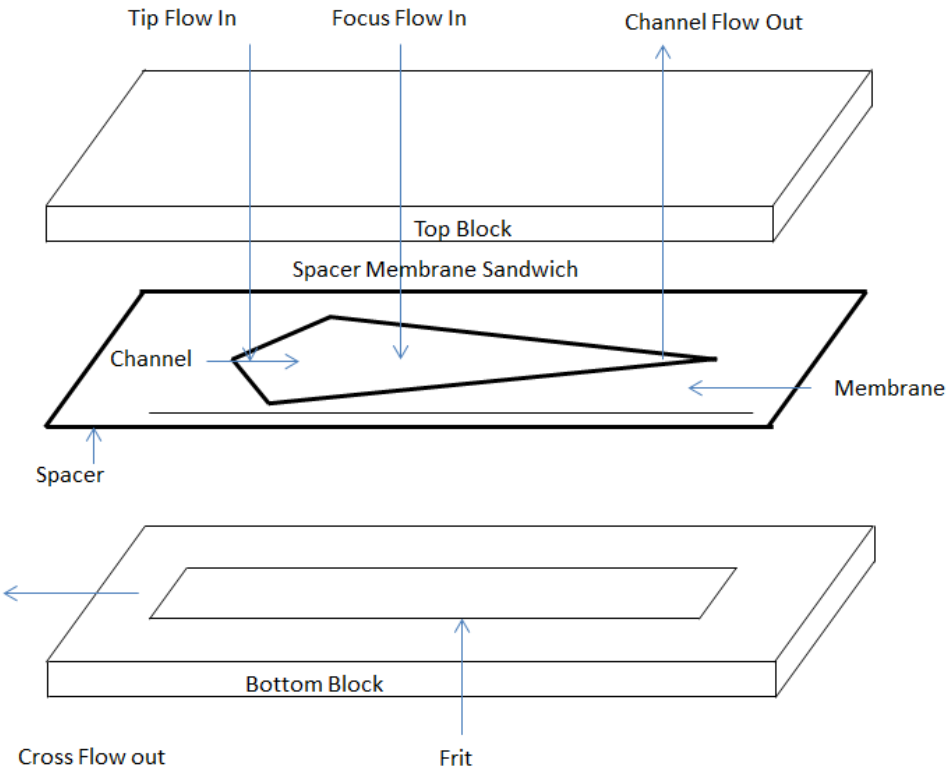

Figure 18: Schematics of Asymmetrical Flow Fluid Flow Fractionation.

Sample components with higher diffusivities will travel more rapidly and elute earlier which results in differential elution of sample components.

AF4 has several advantages over GPC/SEC for ultrahigh molecular weight polymer characterization.

- Andersson et al (Andersson, Ultra high molar mass component detected in ethylhdroxyethyl cellulose by AF4 couples with MALS, 2001) and Roger et al (Roger, 2001) reported that time taken in the process of GPC is more than AF4

- GPC/SEC requires pre-filtering of the sample to avoid clogging of the columns and in AF4 it is possible to inject samples without any pre-treatment.
- Size range analyzed can be adjusted by the flow rates using one simple channel as opposed to GPC /SEC where some columns with different packing material must be chosen.
- A study (Wittgren, 1998) revealed the principle feasibility of AF4 in the analysis of unprepared samples, allocating AF4 greater application range and more information power.
- Adsorption phenomenon in AF4 is minor, considering FFF channel has significantly less surface area (Giddings, 1979).

Fraunhofer and Winter (Fraunhofer, The use of asymmetrical flow field flow fractionation in pharmaceutics and biopharmaceuics, 2004) and other researchers (Jungmann, 2001) (White, 1997) have used this method to study and investigate conformational changes and aggregation tendencies of macromolecules.

Due to its unique separation mode, AF4 is also applied for analysis of dissolved sample components aside undissolved particles. This feature was applied in the analysis of soluble polyvinyl pyrrolidone which is prevalently used as pharmaceutical excipients (Fraunhofer, The use of asymmertrical flow field flow fractionation in pharmaceutics and biopharmaceutics, 2004). About a broad range of analysis, it can be used to analyze colloidal and particulate systems running the gamut from nm to um range. Heterogeneous mixtures of cationic lipid-DNA colloidal were characterized via MALS regarding the shape and size distribution

(Lee H. W., 2001). AF4 has found its relevance in a wide range of applications. From biopharmaceutical analytics, a complex mixture of colloids or even cells, high molecular weight protein aggregate to shear sensitive samples, AF4 can be used to for successful characterization.

Additional information (i.e. the size and shape of the separated compounds, the molar mass and the radius of gyration) is simultaneously obtained with online light scattering techniques, such as multi-angle light scattering (MALS), together with concentration sensitive devices such as a refractive index detector (RI).

Multi-Angle Light Scattering

MALS is a powerful technique for polymer characterization when the molar mass and molecular radius is of interest. Static light scattering takes advantage of two basic physical principles that are if light interacts with matter:

- The intensity of scattered light is proportional to the product of the concentration times molar mass of the sample.
- Small particles scatter light in every direction with the same intensity; large particles scatter light mainly in the forward direction.

A fundamental equation which is the basis of calculation of Mw and Rg for MALS system is well known and was given by Rayleigh (Rayleigh, 1910).

$$R_\Theta / Kc = M\,P(\Theta)$$ **Equation 9**

R_Θ is Rayleigh ratio, which is directly proportional to the ratio between the scattered intensity at angle Θ and incident intensity. K is contrast factor, c is the

concentration of the scattering species, M is the molar mass of the sample, P(Θ) is foam factor of the sample, it describes angular dependence.

The first principle described for light scattering is clearly evident as scattered intensity is proportional to the concentration times molar mass of the sample. The second principle is reflected in the foam factor P(Θ). The foam factor describes the angular dependence of the scattering; it is defined as the intensity scattered under the angle Θ divided by the intensity scattered under the angle 0. For scattering angle zero, the foam factor is equal to 1.

The ideal way to calculate Mw by light scattering would be to use the scattered intensity at 0^o scattering angle where the relationship between molar mass, concentration, and intensity of scattered light is simple. However, it is not practically possible to measure intensity at 0^o experimentally. Alternatively, to address the issue, measurements for scattering intensities can be made at angles larger than 0^o and then extrapolate it to find scattering intensity at 0^o .

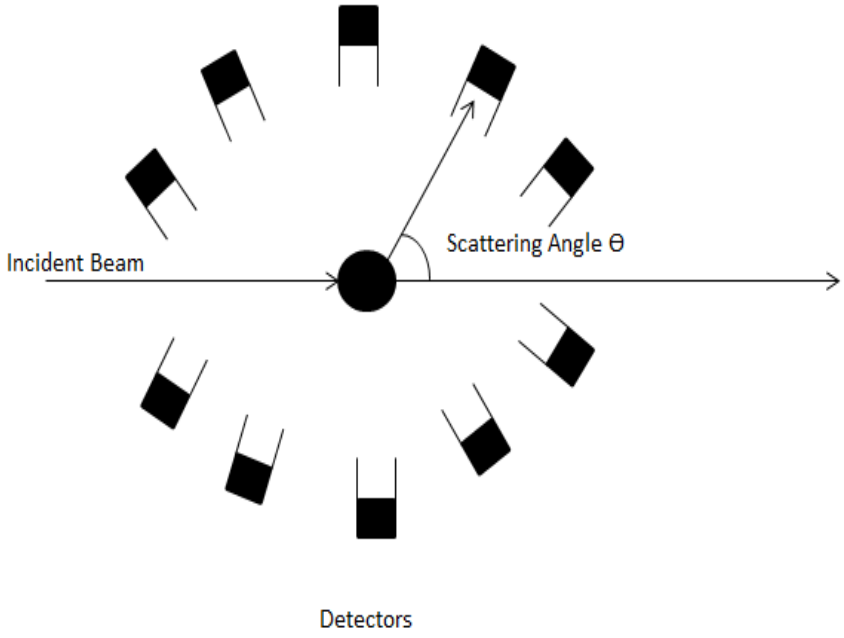

Figure 19: Light Scattering under MALS.

Equation 9 is solved for every slice of the data. For solving this equation, a plot is drawn for R_Θ/Kc against $\sin^2 \Theta/2$. R_Θ is known by the experiment for all detector angles. The concentration is known by the signal of the RI detector. The radius of gyration can now be calculated by taking the slope value at the interpolation at $\Theta=0$. Molar mass can be calculated as the intercept with the y-axis in this plot. So the evaluation based on light scattering measurements is by plotting Rayleigh ratio divided by the sample concentration and contrast factor against the square of half of the scattering angle, interpolate to zero and calculate from the intercept with the y-axis the molar mass and from the slope at $\Theta=0$ the radius of gyration.

Chapter 3

Methodology and Validation

3.1 AF4-MALS-RI Instrumentation and Separation Parameters

The experimental setup for AF4-MALS-RI can be seen in Figure 20. The major parts of the setup are an AF4 module, focus and tip pump, MALS detector, and RI detector.

AF4 module was AF2000 MF supplied by Postnova Analytics, Landsberg, Germany. Its general purpose is to control or measure every operating variable required to run the system and to analyze the elution data. Pumps, valves, and flow rates are controlled and NovaFFF Data Acquisition and Control Software acquire elution data.

Focus and Tip pump were PN 1130 by Postnova Analytic. PN 1130 is a dual piston solvent delivery pump. MALS system used was PN3621 by Postnova Analytics. It works with 532 nm laser bean and has 21 different scattering angles at which it detects the scattering intensity, i.e. 7º, 12 º, 20 º, 28 º, 36 º, 44 º, 52 º, 60 º, 68 º, 76 º, 84 º, 90 º, 100 º, 108 º, 116 º, 124 º, 132 º, 140 º, 148 º, 156 º and 164 º. Its measurement range for molar mass is 10^3 Dalton to 10^9 Dalton. Refractive index detector was PN 3150 supplied by Postnova Analytics.

Figure 20: AF4-MALS-RI Setup.

The channel geometry created due to spacer membrane sandwich is a trapezoid. The dimension of the channel were the tip-to-tip length of 27.9 cm and breadths at the inlet and the outlet of 2 cm and 0.6 cm, respectively. Total area for the channel is 34 cm^2. The spacer used for definition of the channel has a nominal thickness of 300 μm. A regenerated cellulose membrane was used for the separation channel with an average molar mass cut-off of 10 kDa (Z-MEM-AQU-631, RC amphiphilic, Postnova Analytics).

The method used for experiments performed can be seen in Figure 21. The samples were introduced into the channel by manual injection. Experiments were started with sample injection and focusing with a main pump flow rate of 0.20 mL/min and a focus pump flow rate of 0.80 mL/min. The low inlet flow rate was used to prevent

shear degradation. The cross-flow rate was constant at 0.50 mL/min during the injection and focusing phase. The focusing time was typically 3 min and focusing position was at 8.9 cm. The transition time from injection/focusing phase to elution mode was 1 min. Elution started at an initial cross-flow rate of 0.50 ml/min for 2 minutes, which then decrease to 0.1 ml/min in 35 minutes according to the power function available, built in the software (Nova FFF) with an exponent of 0.3. A final cross-flow of 0.1 ml/min was applied for 15 minutes. After each experiment, rinsing was done using tip pump flow rate of 1 ml/min and purge valve was kept open for 5 minutes.

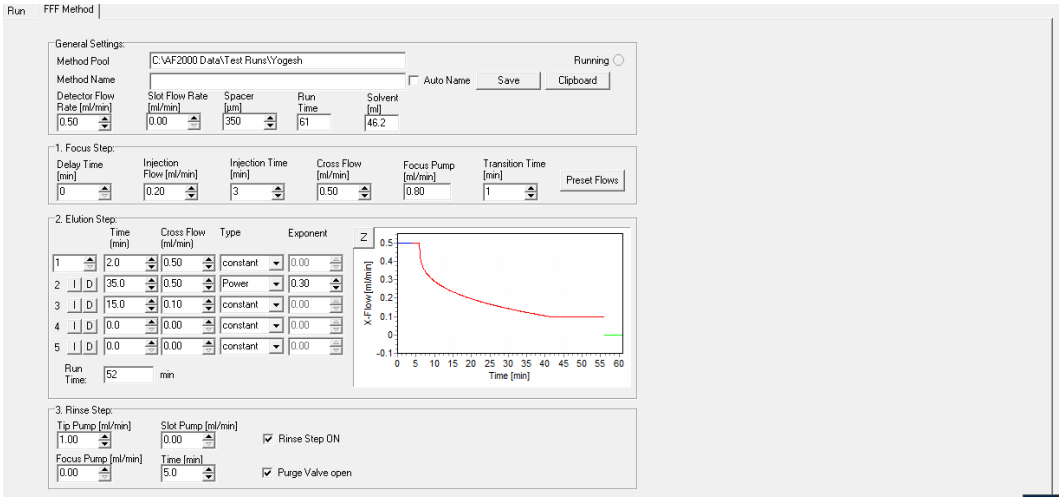

Figure 21: Method used for the experiments.

For each separation experiment, ~50 µL sample was injected into the membrane. All the separation experiments were performed at room condition. Following the separation in the channel, the eluent from the channel enters in-line detectors, MALS detector, and RI detector. The coupling of the MALS and RI detectors to the separation channel outlet will enable the determination of molar mass and radius of the eluted fraction directly without the use of any standards. The entire system

is connected to a single software (Nova FFF software, Postnova Analytics, Landsberg, Germany) platform to control data acquisition and to evaluate the system and all of the connected detectors.

3.2 Data Processing

MALS measurements work by calculating the amount of scattered light at each angle detected. Every part of the aggregate will scatter light in different intensities directions. The angular dependence of the scattered light can be measured to determine the size, which is known as the radius of gyration. MALS was used to determine the radius of particles using the random coil model. This process overcomes the problems associated with low angle light scattering detectors (typically there is around ten times the noise at an angle of 11° or below compared to 90°) and allows a reliable and accurate measure of the light scattered. The amount of light scattered is then related to the molar mass. MALS also determines the size of the molecule, because angular dependence of the scattered light is measured.

MALS data were collected at a frequency of 2 Hz. The averaged fractograms from MALS and RI were then processed. The value of dn/dc is assumed to be 0.17. Concentrations and recoveries were determined by integrating across the RI fractogram using a known dRI calibration constant and the dn/dc value to transform the RI-signal×elution time into polymer concentration and total eluted mass. To obtain structural conformation, the logarithm of Rg of each polymer sample is plotted against the logarithm of the corresponding molar mass. The slope of the plot provides the information of fractional increase of Rg upon the increase of molar

mass. The plot shades light on conformational information regarding molecular structure in solution.

AF4-MALS-RI measures molar mass and radius for each aggregate that enters the detectors. Thus it is capable of determining the entire distribution. It starts from the first eluted aggregate from the membrane, and it continues to measure all the particles till no eluted particles come. Thus it is possible to get entire molar mass distribution to be plotted against elution time, and similarly entire radius distribution plotted against elution time. From this distribution which is calculated by the software, it also gives out three different averages for molar mass and radius. The number average Mn and Rn, the weight average Mw and Rw and z-average Mz and Rz. These values will be extensively used in results and discussion section of this thesis.

The number average:

$$\boldsymbol{M_n = \frac{\sum \frac{c_i}{M_i} M_i}{\sum \frac{c_i}{M_i}}} \qquad \textbf{Equation 10}$$

$$\boldsymbol{R_n = \frac{\sum \frac{c_i}{M_i} R_i}{\sum \frac{c_i}{M_i}}} \qquad \textbf{Equation 11}$$

The weight average:

$$\boldsymbol{M_w = \frac{\sum c_i M_i}{\sum c_i}} \qquad \textbf{Equation 12}$$

$$R_w = \frac{\sum c_i R_i}{\sum c_i}$$ **Equation 13**

The z-average:

$$M_z = \frac{\sum c_i M_i M_i}{\sum c_i M_i}$$ **Equation 14**

$$R_z = \frac{\sum c_i M_i R_i}{\sum c_i M_i}$$ **Equation 15**

Here M is molar mass, R is radius, c is concentration and M_i, R_i, c_i represents results for the i^{th} slice/ aggregate. The different averages differ in how particles with higher masses effect the calculation. Due to the square dependence, the z-average is most sensitive for particles with higher masses. The in-built program gives out two different distributions and the differential distribution. Both the distributions are extensively used to analyse and interpret results.

The cumulative distributions C(r) or C(m) is an addition of all concentrations that belong to a smaller value than r or a smaller mass than m. For the radius, cumulative distribution is defined as

$$C(r) = \frac{\int_0^r c(r')dr'}{\int_0^\infty c(r')dr'}$$ **Equation 16**

Here c(r) is the concentration of particles with the radius r. Due to larger range of molar masses, the cumulative distribution for the masses is expressed in logarithmic

$$C(m) = \frac{\int_0^m c(\log m')\, d\, \log m'}{\int_0^\infty c(\log m')\, d\, \log m'} \quad \textbf{Equation 17}$$

The differential distribution c(r) and c(m) can be calculated by building the first derivation of the cumulative distribution on r or m.

MALS and RI detectors were calibrated using BSA (Bovine Serum Albumin) with the molar mass of 63,900 g/mol. To confirm the applicability of AF4-MALS-RI to high molar mass polymers, a high molar mass PAM standard was analyzed. PAM standard was procured from Polysciences Inc. The molar mass of 9 million g/mol is reported for the PAM standard, and the analyzed molar mass is found to be 8.59 million g/mol. Table 4 shows results for the PAM standard. Replicate experiments were also performed on PAM standard. Figure 22 shows RI and MALS 90° for the replicate experiments of PAM standard.

Table 4: Molar Mass and Radius of Polymer Standard

	Mn(g/mol)	**Mw(g/mol)**	**Mz(g/mol)**	**Rn(nm)**	**Rw(nm)**	**Rz(nm)**
Results	8.306E+06	8.59E+06	8.87E+06	176.9	180.4	183.8

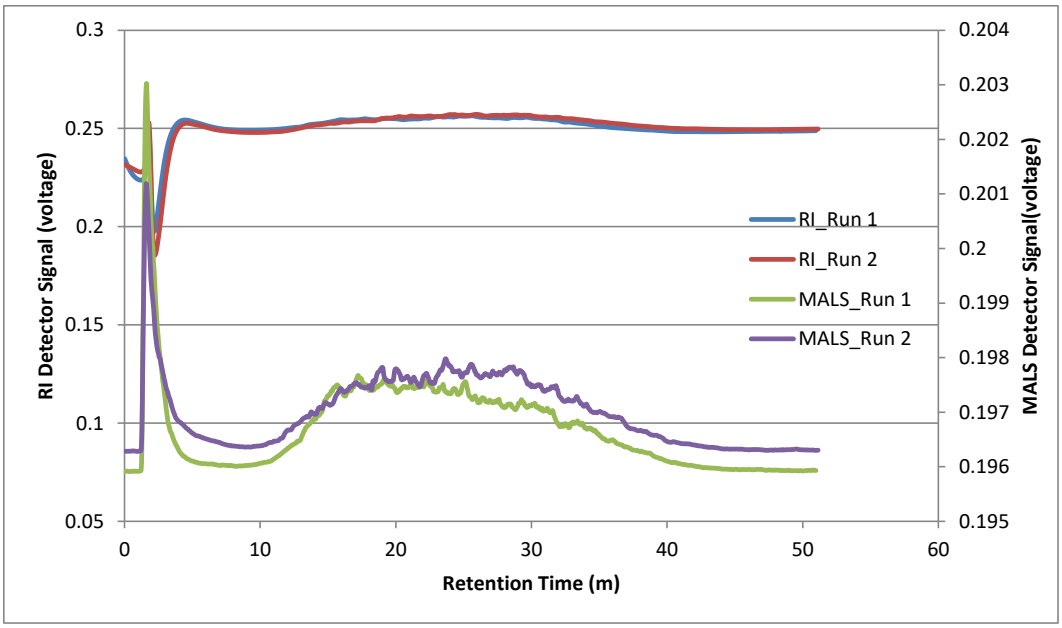

Figure 22: Replicate experiments of RI response and MALS response (90^0), for 9 million g/mol PAM standard.

3.1 Replication Analysis

The replicate analysis was done to establish the reproducibility of the method. Replicate experiments were done on HPAM 3130 S in pH 3 and HPAM 3630 S in pH 3. Two replicate experiments were performed on each polymer with same parameters. Figure 23 shows RI and MALS response at 92^0 for two replicate experiments of HPAM 3130 in pH 3. Radius value profile (Figure 24) with elution time and molar mass profile (Figure 25) along with elution time are also shown for the replicate analysis.

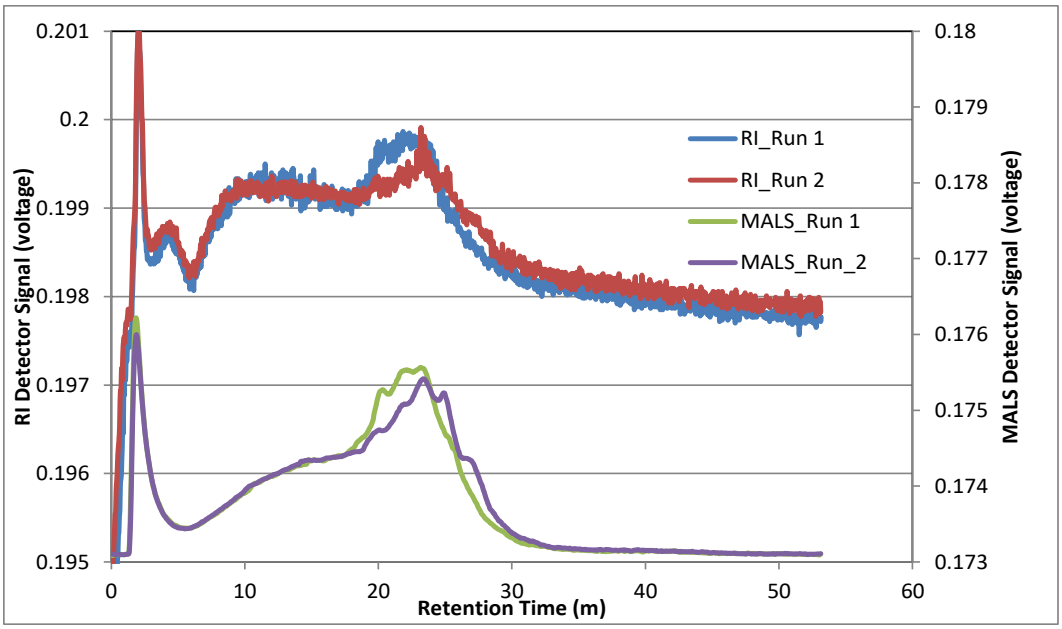

Figure 23: Replicate experiments for HPAM 3130 in pH 3. RI and MALS response at 90^0

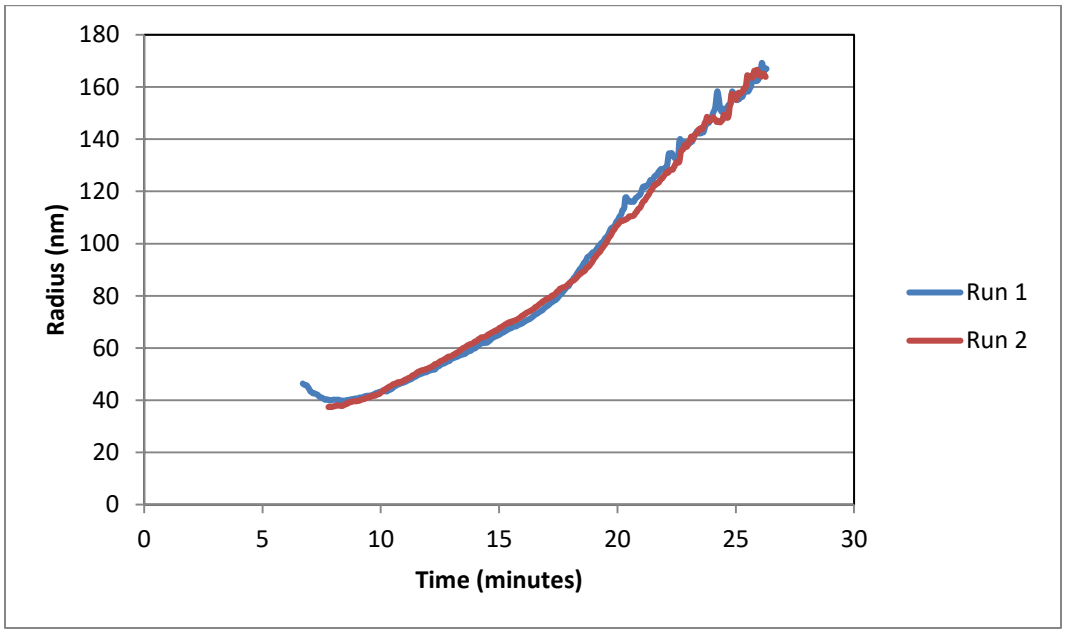

Figure 24: Replicate experiments for HPAM 3130 in pH 3. Radius values with time (elution).

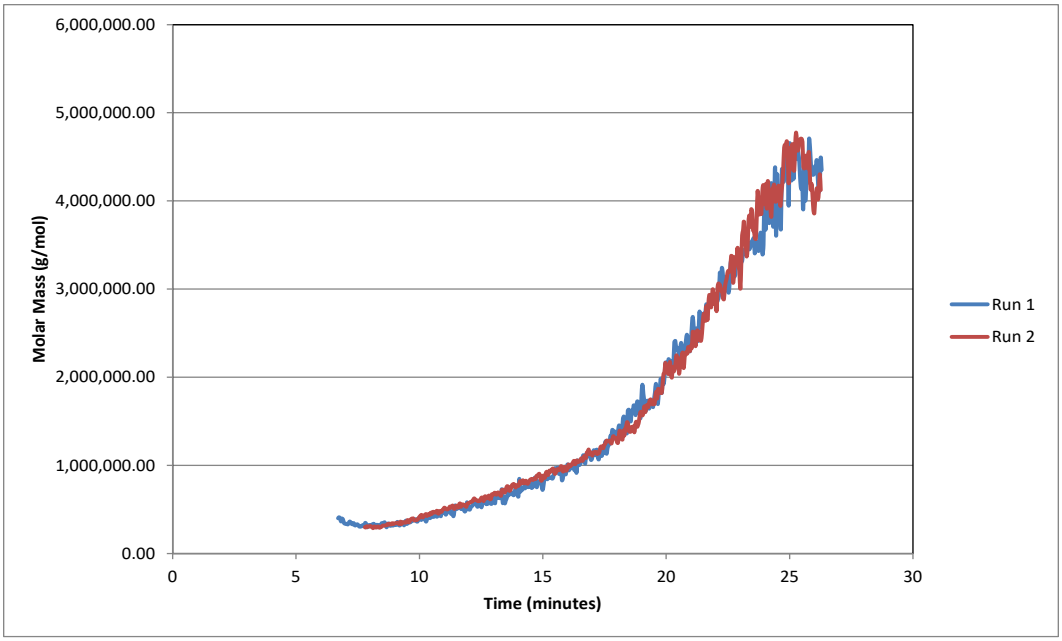

Figure 25: Replicate experiments for HPAM 3130 in pH 3. Molar mass values with time (elution).

RI and MALS response at 90^0 for HPAM 3630 in pH 3 is seen in Figure 26. The molar mass profile and radius profile with elution time for HPAM 3630 at pH 3 is seen in Figure 27 and Figure 28 respectively. It can be observed that replicate analysis for both the polymers has similar angle response and similar profiles for radius and molar mass distribution. Thus it can be concluded that results are reproducible. More RI responses for replicate results can be seen in the appendix.

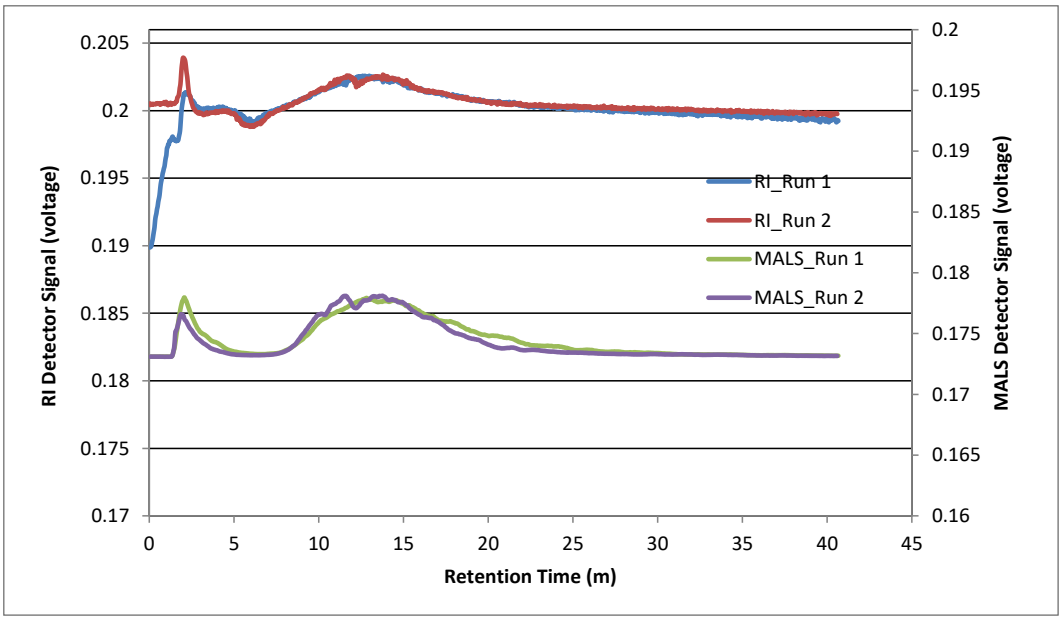

Figure 26: Replicate experiments for HPAM 3630 in pH 3. RI and MALS response at 90^0.

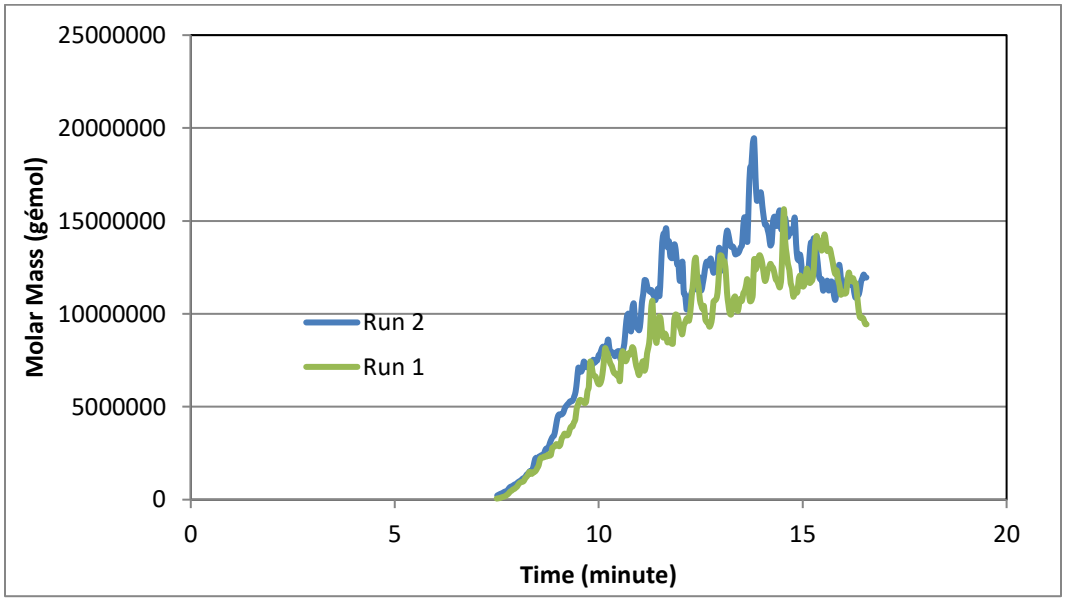

Figure 27: Replicate experiments for HPAM 3630 in pH 3. Molar mass values with time (elution).

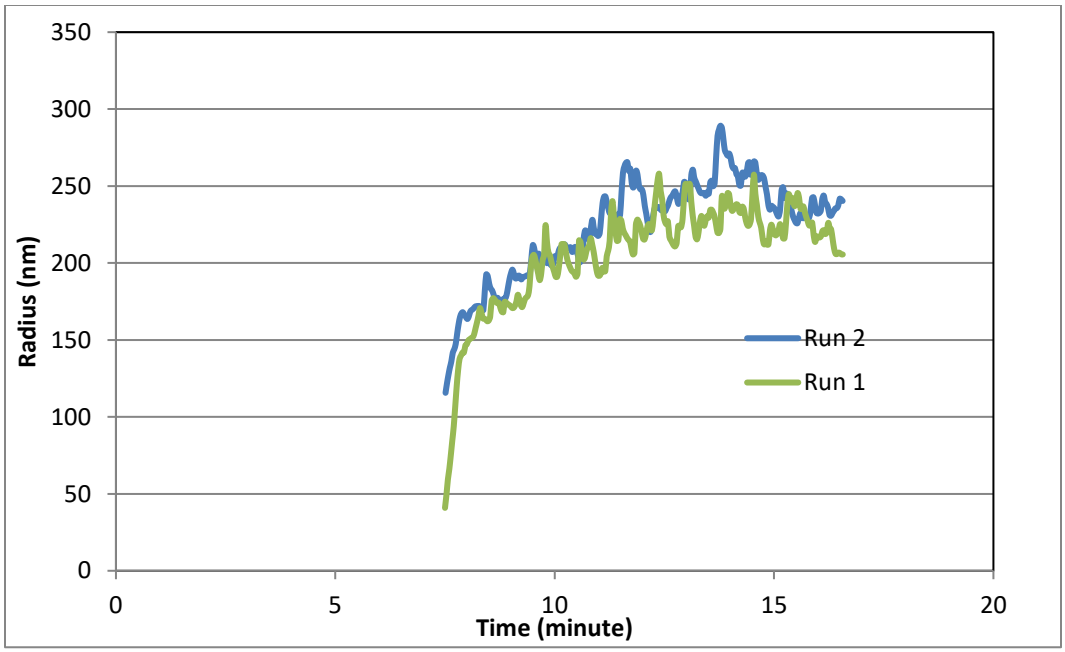

Figure 28: Replicate experiments for HPAM 3630 in pH 3. Radius values with time (elution).

Chapter 4

Effect of HPAM Concentration

It is very important and intuitive to investigate the effect of polymer concentration on the characterization done by AF4-MALS-RI system. In practical applications according to the requirements, the concentration of the polymer can vary. Therefore, it is essential to know if change in polymer concentration will affect the characterization of the polymer solutions regarding molar mass and radius distribution.

To investigate the effect of concentration on analysis, three different concentration of polymer was considered i.e. 1000 ppm, 2000 ppm, 1500 ppm. A polymer solution with above said different concentration were characterized by using AF4-MALS-RI method. The polymer used is HPAM 3630 S and were supplied by SNF SAS in dry powder form. 3630 S is a copolymer of acrylamide and acrylic acid. The polymer is anionic and water soluble with a degree of hydrolysis of 25-30 mol %. Two different brine solutions with different NaCl concentration (5000 ppm, 500 ppm) were considered. Table 5 shows polymer and brine pair, which were used for the investigation.

Table 5: Brine composition to study the effect of polymer concentration.

Case	**Brine**	**Polymer**
Case 1	5000 ppm NaCl	HPAM 3630 S
Case 2	500 ppm NaCl	HPAM 3630 S

4.1 Case 1

Figure 29 shows MALS scattering response at 90° for HPAM 3630 S at different concentration in 5000 NaCl. Similarly, refractive index response can be seen in Figure 30. It can be observed that signal response for 2000 ppm polymer is stronger than other concentrations and covers more area under its curve. The same trend can be observed for both MALS and RI response. It is to be noticed that in both MALS and RI, response starts and ends at a similar time for all the concentration. The difference in response of the detector is more visible in case of RI response.

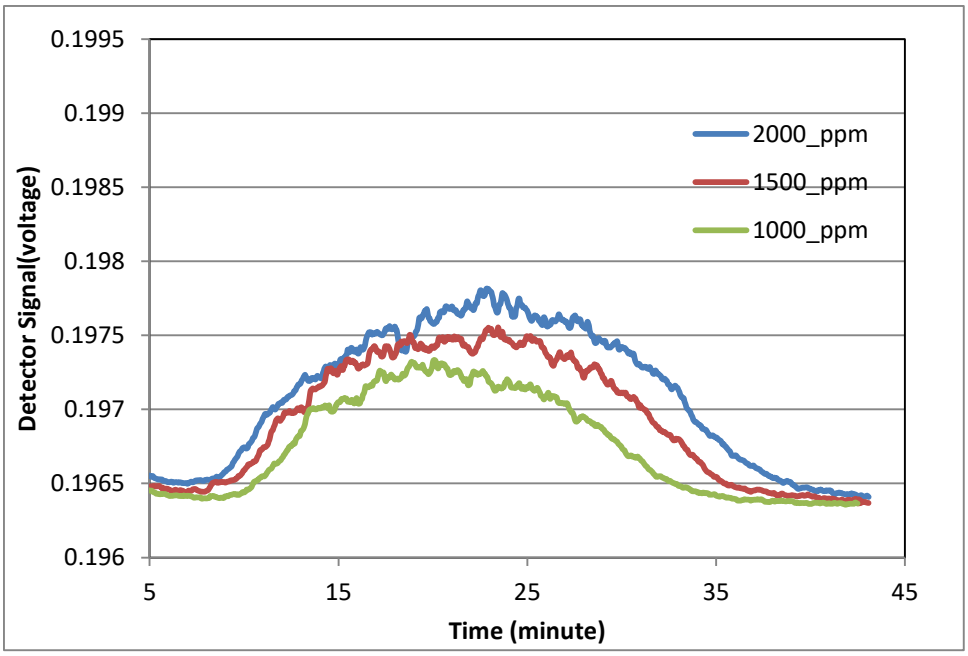

Figure 29: MALS 90° Response for Case 1.

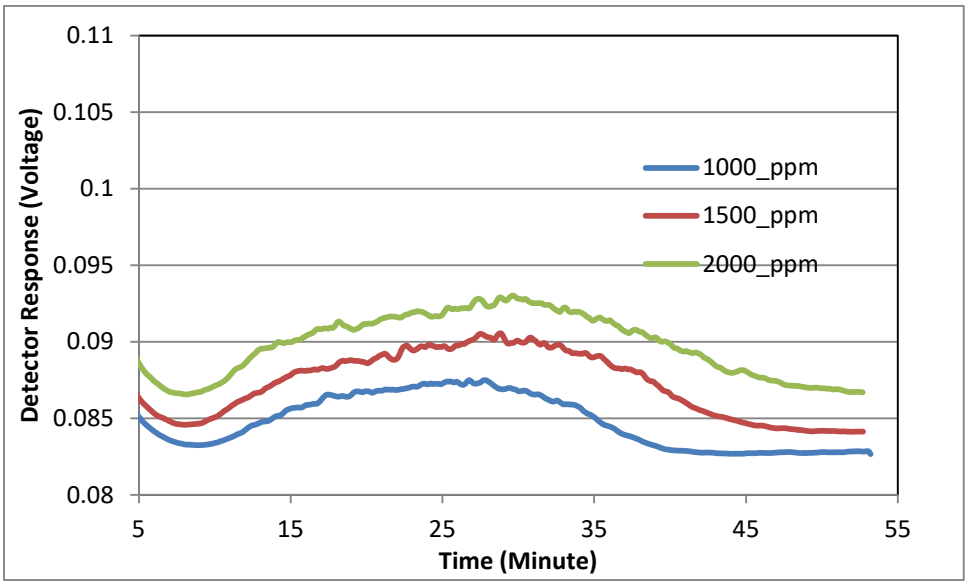

Figure 30: RI Response for Case 1.

Table 6 shows molar mass and radius values for different polymer concentration in 5000 ppm NaCl brine. It can be observed that Mw values are similar. In the case of 1000 ppm polymer concentration, Mw is 1.046×10^7 g/mol which is close to 1.041×10^7 g/mol when the concentration is 2000ppm. At 1500 ppm, Mw is also similar to that of observed in 2000 ppm and 1000ppm polymer concentration. Rw values are very close to each other. In 1000 ppm NaCl, Rw of 219.1 nm is observed which is very close to 218.7 nm which is Rw in 1500 ppm. Rw of 210.6 nm is seen in 2000 ppm polymer concentration which is near to that of previous observations.

Table 6: Molar Mass and Radius for Case 1.

	Mw(g/mol)	**Rw(nm)**
2000 ppm	1.041E+07	210.6
1500 ppm	1.123E+07	218.7
1000 ppm	1.046E+07	219.1

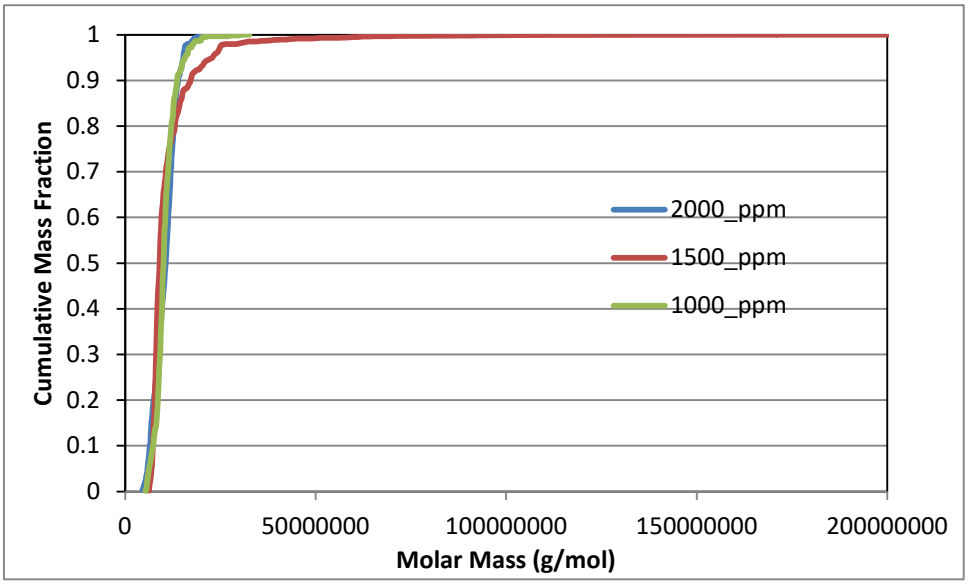

Figure 31: Cumulative Mass fraction plot for Case 1.

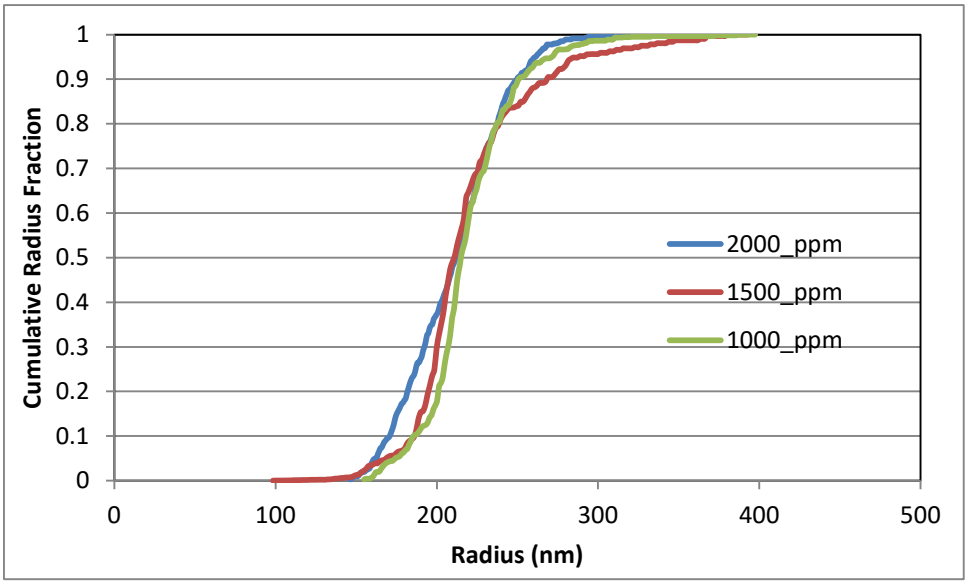

Figure 32: Cumulative Radius fraction plot for Case 1.

Cumulative mass fraction plot for HPAM 3630 S in 5000 ppm NaCl brine can be seen in Figure 31. It can be clearly noticed that curve for all concentration overlaps

each other. Figure 32 shows cumulative radius fraction plot. It is clearly observable that curves are close to each other. Cumulative radius and molar mass plots indicates that radius and molar mass distribution is similar for different polymer concentration. Even the conformance plot for different polymer concentration shows high similarity. It can be seen in conformance plot for Case 1 in Figure 33. Conformance curve for 2000 ppm concentration and 1000 ppm concentration are extremely near to each other and the conformance curve for 1500 ppm is minutely steeper.

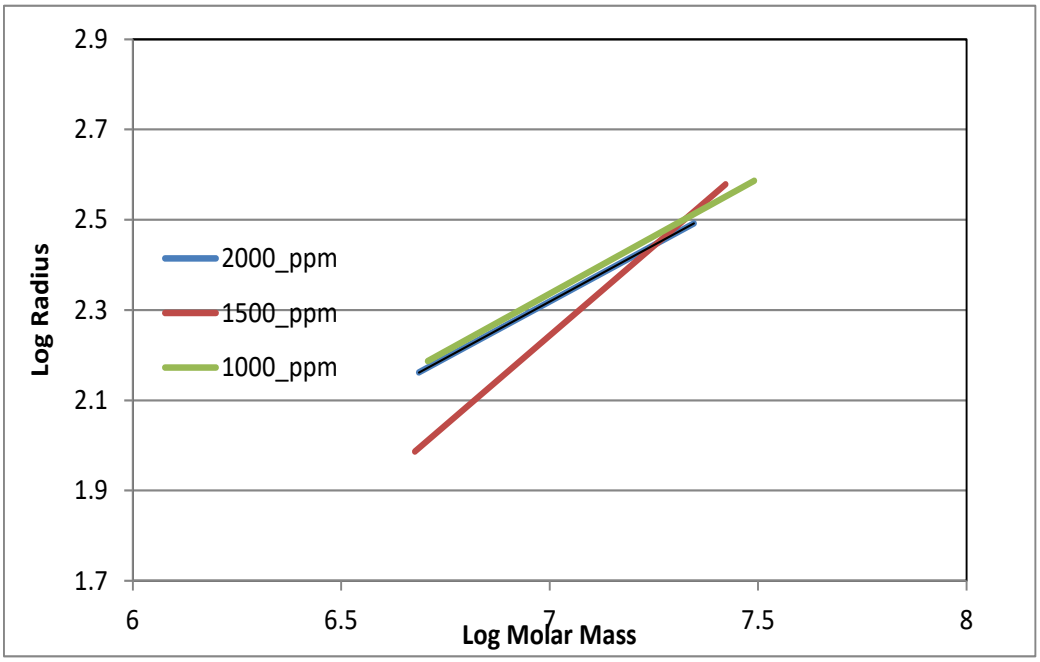

Figure 33: Conformation plot for Case 1.

4.2 Case 2

Figure 34 shows MALS response at 90° for HPAM 3630 S in 500 ppm NaCl brine. It can be seen that response for 2000 ppm is stronger than 1500 ppm and 1000 ppm response. 1000 ppm response can be seen to be weakest and cover least area under its curve.

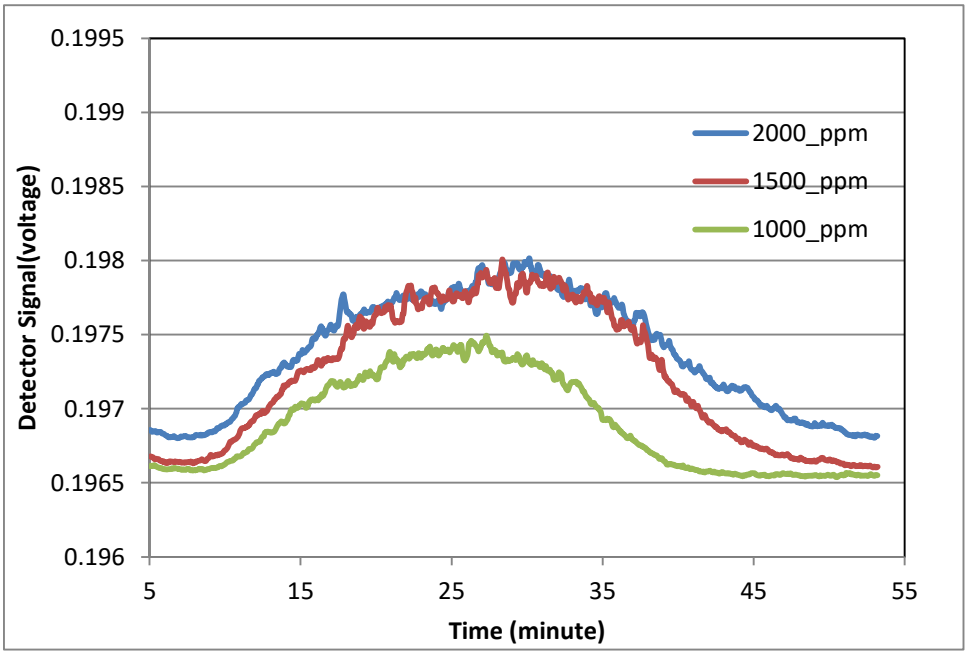

Figure 34: MALS 90° Response for Case 2.

Refractive index response can be seen in Figure 35. It can be clearly observed that detector response gets bigger and stronger as polymer concentration increases. With biggest response for 2000 ppm concentration and then for 1500 ppm concentration and finally 1000 ppm concentration has least area under its curve. It is also to be observed that response envelope in the curve for the response for all concentration starts and ends at the similar time. Same can be observed in MALS response in Figure 34.

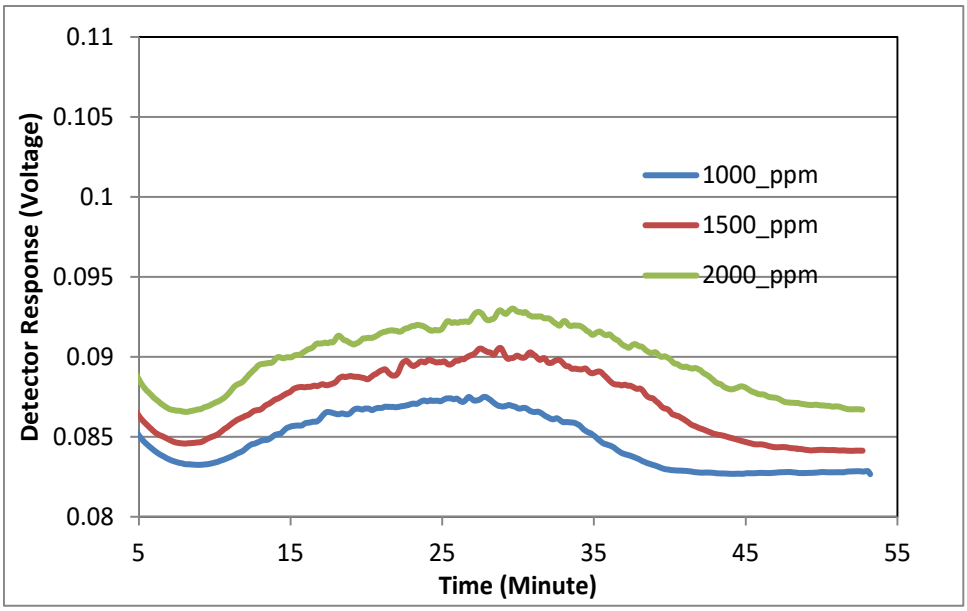

Figure 35: RI Response for Case 2.

Table 7 shows molar mass and radius values for different concentration in 500 ppm NaCl brine. From observation, it is evident that molar mass values are very close to each other. Molar mass of 1.793×10^7 g/mol is observed in 2000 ppm concentration, molar mass of 1.629×10^7 g/mol in 1000 ppm concentration and 1.777×10^7 g/mol in 1500 ppm polymer concentration. Radius value for 2000 ppm concentration is 264.3 nm which is close to 254.7 nm (1500 ppm). In the scenario of 1000 ppm, the radius of 294.6 nm is observed, it can be considered as an outlier.

Table 7: Molar Mass and Radius for Case 2.

	Mw(g/mol)	**Rw(nm)**
2000 ppm	1.793E+07	264.3
1500 ppm	1.777E+07	254.7
1000 ppm	1.629E+07	294.6

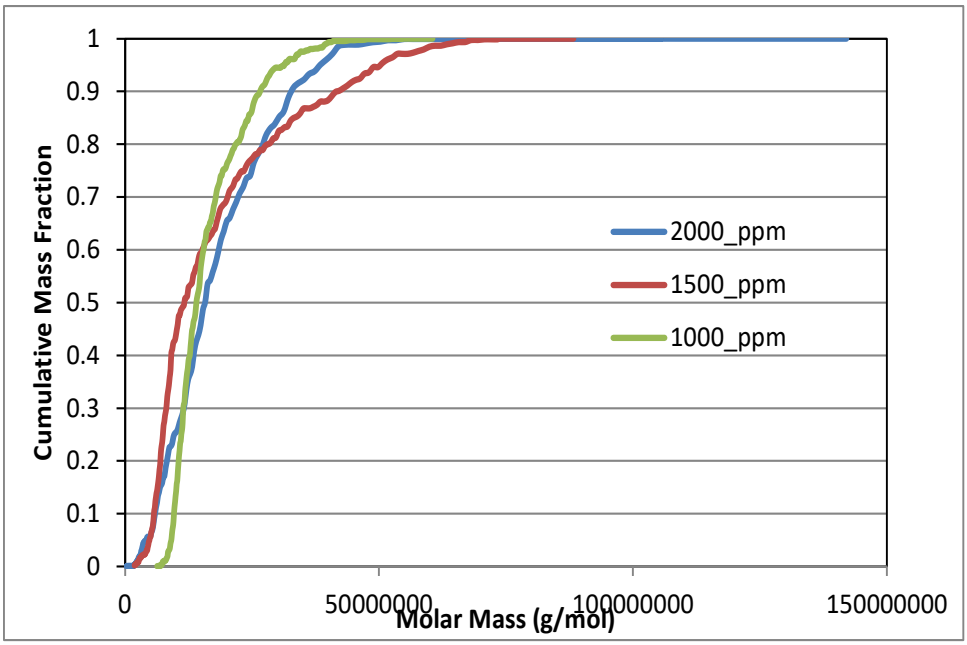

Figure 36: Cumulative Mass fraction plot for Case 2.

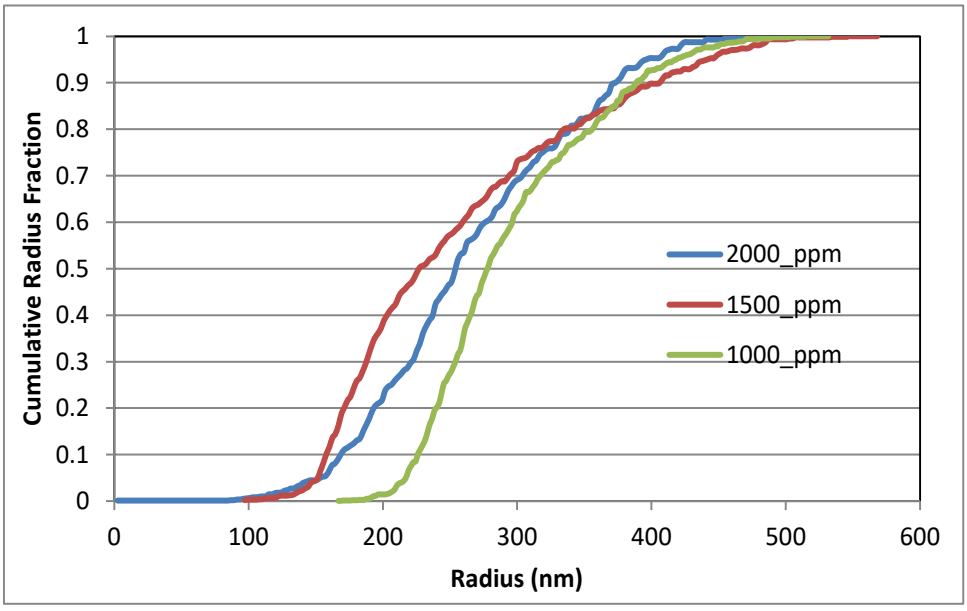

Figure 37: Cumulative Radius fraction plot for Case 2.

The cumulative mass fraction for HPAM 3630 in 500 ppm is seen in Figure 36. It can be seen that curve for 1000 ppm, 1500 ppm, and 2000 ppm are close to each other suggesting that molar mass distribution is similar to each other for different polymer concentration. Similarly, it can be seen that in cumulative radius curve can be seen in Figure 37, curves are close for different polymer concentration suggesting that radius distribution is similar with change in polymer concentration.

The conformational plot for HPAM 3630 S in 500 ppm NaCl brine is Figure 38. It is evident from the observation that conformational curve for 2000 ppm, 1500 ppm and 1000 ppm polymer concentration overlap each other. The similarity in curve suggests that polymer exhibits similar conformation under different polymer concentration conditions. The RI responses for other experiments with different polymer concentration in different brines can be seen in the appendix.

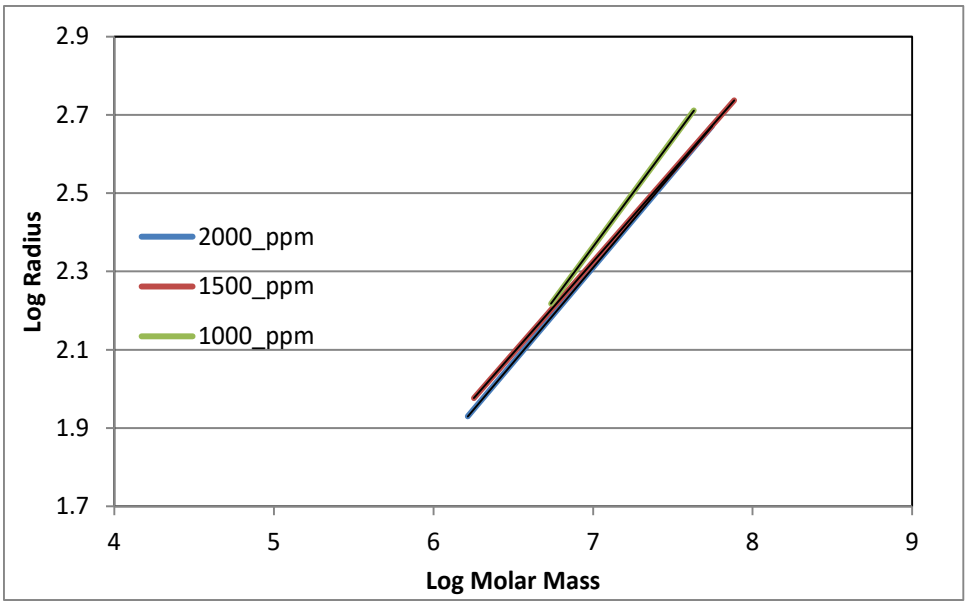

Figure 38: Conformation plot for Case 2.

4.1 Summary

Within the range of concentration studied i.e. 2000 ppm to 1000 ppm, polymer concentration has no significant impact on final results i.e. molar mass and radius values. However, brine composition does affect the results. Signal strength from MALS and RI detector is stronger and covers more area under its curve as polymer concentration increases.

Chapter 5

Effect of pH on HPAM

5.1 Polymer Used

Four different types of polymers namely AB005V, 3130 S, 3330 S and 3630 S were used. SNF SAS supplied all the polymers in dry powder form. 3130 S and 3330 S is a copolymer of acrylamide and acrylic acid. AB 005V is a non ionic bead polymer. These polymers are anionic and water soluble with a degree of hydrolysis of 25-30 mol %.

5.2 Solution preparation

The solution of various pH were made by adding specific quantity chemicals into the deionized water. The solution of pH 3 was prepared by adding 3mM NaN_3. The pH of NaN3 solution was adjusted by adding few microliters of a 5% HCl solution. For the preparation of pH 7.4 solution, 150mM NaCl was used, and for pH 12 solution 25 mM NaOH was used. The 150 mM NaCl solution was buffered by 10 mM Phosphate di and mono basic salt. The pH of 25 mM NaOH solution was measured several times and stayed constant during the measurement. Polymers were added to the solutions and were mixed with using a magnetic stirrer at 350 rpm for 3 hours. All the sample solutions were clear after three hours of mixing. In total, 12 different polymer solutions were prepared (each polymer at 3 different pH condition). The pH values of the solution used in the experiments were all measured.

5.3 Result and Observation

5.3.1 AB 005V

The average values of radius and molar mass for AB 005V in the different pH environment are presented in Table 8. In acidic environment polymer radius (Rw) is 18.6 nm, it increases to 30.9 nm at pH 7.4, and further increases to 42.8 nm when pH increased to 12. Values of Rn and Rz also show a similar trend. Rn increases from 16.7 nm to 25.2 nm when pH is 7.4 and to 38.9 nm when pH increases to 12. Similarly, Rz increases from 22.1 nm in pH 3 to 36.9 nm in pH 7.4 and increases further to 47.5 nm in pH 3. So, the radius increases as pH of the brine increases.

Table 8: Molar Mass and Radius of AB 005V under different pH

	Mn(g/mol)	**Mw(g/mol)**	**Mz(g/mol)**	**Rn(nm)**	**Rw(nm)**	**Rz(nm)**
pH 3	1.379E+05	2.045E+05	2.998E+05	16.7	18.6	22.1
pH 7.4	1.313E+05	2.017E+05	2.667E+05	25.2	30.9	36.9
pH 12	1.928E+05	2.422E+05	2.946E+05	38.9	42.8	47.5

Figure 39 shows molar mass and radius vs. retention time for AB 005V in all brines. At pH 12, the average molar mass of AB 005V is ~2.42×10^5 g/mol, and that reduces to ~2.02×10^5 g/mol at pH 7.4 and marginally increases to 2.045×10^5 g/mol at pH 3. The Same trend can also be observed for Mn and Mz. The increase in Mw value as pH changes from 7.4 to 3 is not significant, and it can be said that effect of pH on Mw diminishes as pH decreases beyond 7.4.

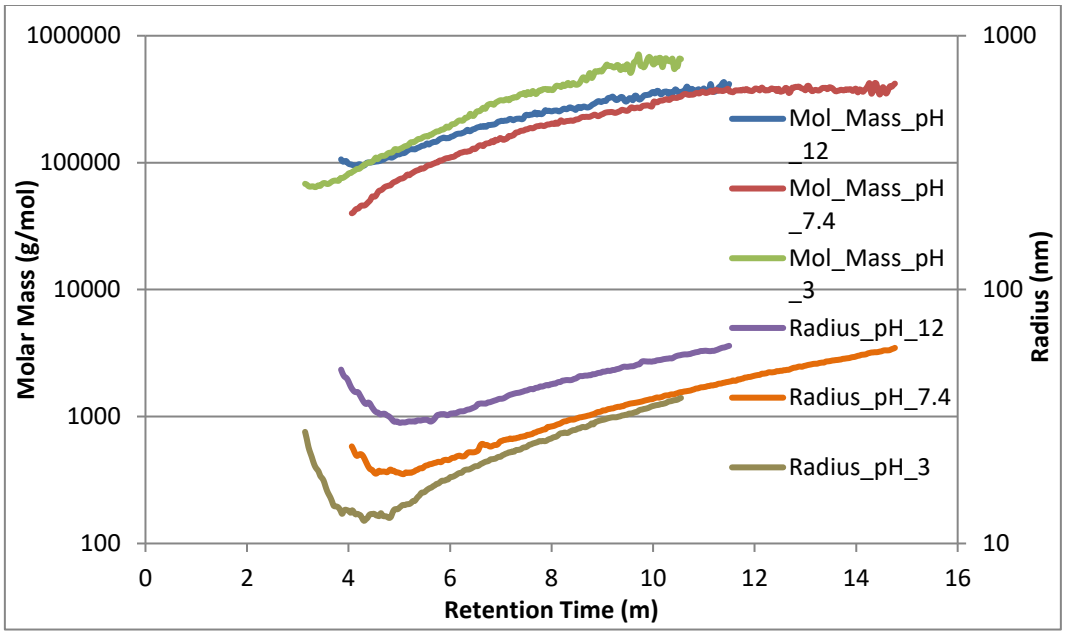

Figure 39: Molar mass and radius v/s retention time of AB 005V.

The conformational plot shows that AB 005V exhibits a high value of slope and are therefore more linear in conformance. (Figure 40). AB 005V is most linear in pH 12 with a slope value of 0.6582 and then polymer coils as pH decreases with a value of .6325 for pH 7.4 which further decreases to 0.5708 at pH3. It can be said that polymer coils as pH of the solvent decreases. It can also be noticed that decrease in slope value from pH 7.4 to pH 3 is more than the decrease in slope value from pH 12 to pH 7.4 which points that AB 005V has high conformational sensitivity in the acidic environment than basic environment.

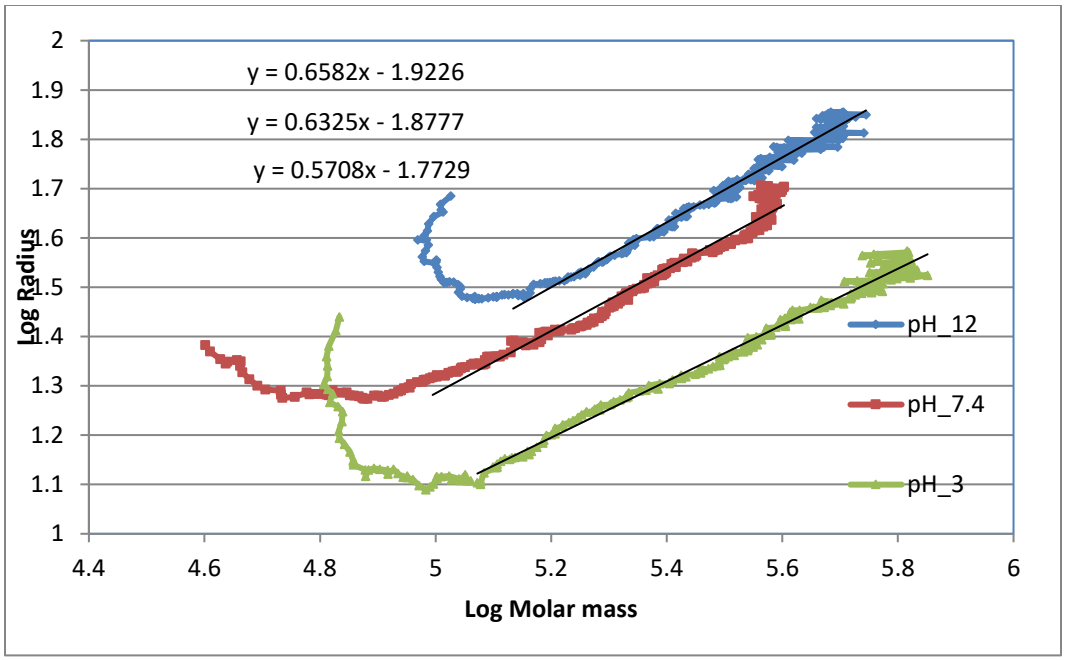

Figure 40: Conformation Plot of AB 005V.

The molar mass trends of AB 005V in all pH case are close to each other (Figure 41). It can be observed that mass distribution is wider in the case of pH 3, also initially the slope of the line is steeper and then gradually decreases. Molar mass distribution in pH 12 and 7.4 is fairly similar. It can also be observed that curve for pH 3 and pH 7.4 starts close to each other and eventually when the curve ends, they are relatively far, which indicates that nature of distribution of mass is different for pH 3 and pH 7.4.

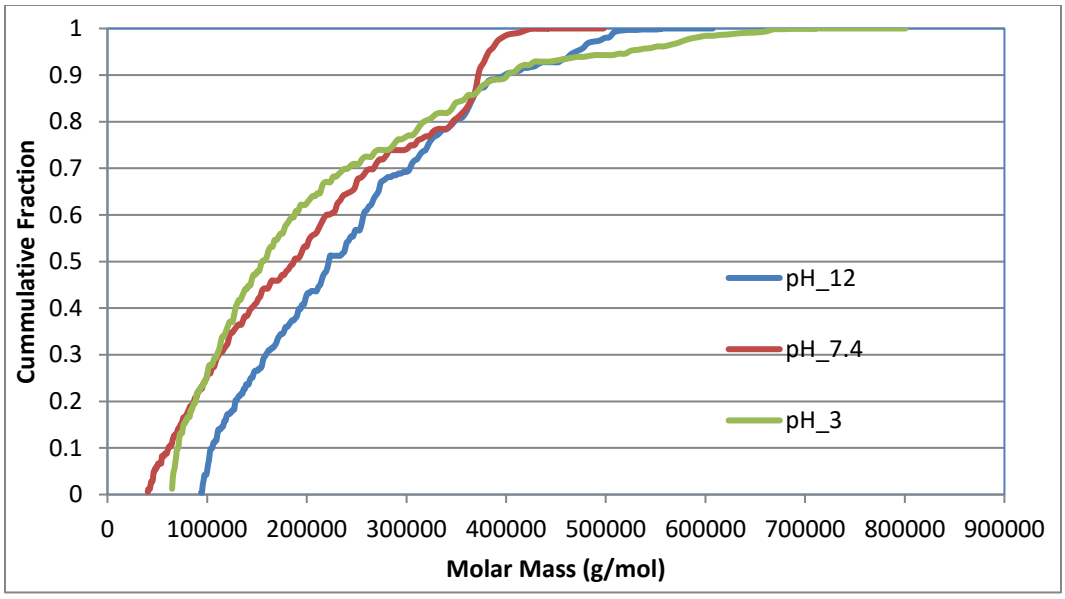

Figure 41: Cumulative Molar Mass Fraction of AB 005V.

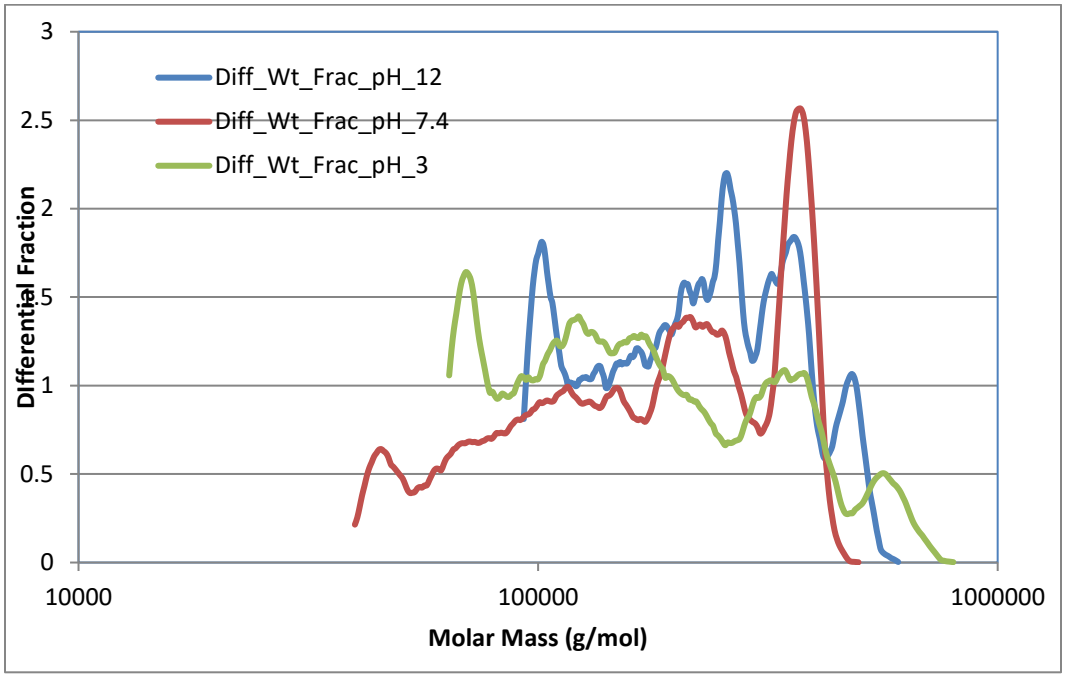

Figure 42: Differential Mass Fraction of AB 005V.

Differential molar mass fractions for AB 005V polymer are shown in Figure 42. In pH 12 polymer mass distribution is narrow. It is observed that at pH 3 the differential fraction with lower molar mass is higher and it decreases as molar mass increases. AB 005V has lower molar mass aggregates than high molar mass aggregates in pH 3. At pH 7.4, the reverse behavior is observed with a major fraction of material in higher molar mass aggregates. Differential weight fraction increases as molar mass increases in pH 7.4. Uniform distribution of molar mass is observed in the case of pH 12 as compared to the distributions of polymer in pH 7.4 and pH 3.

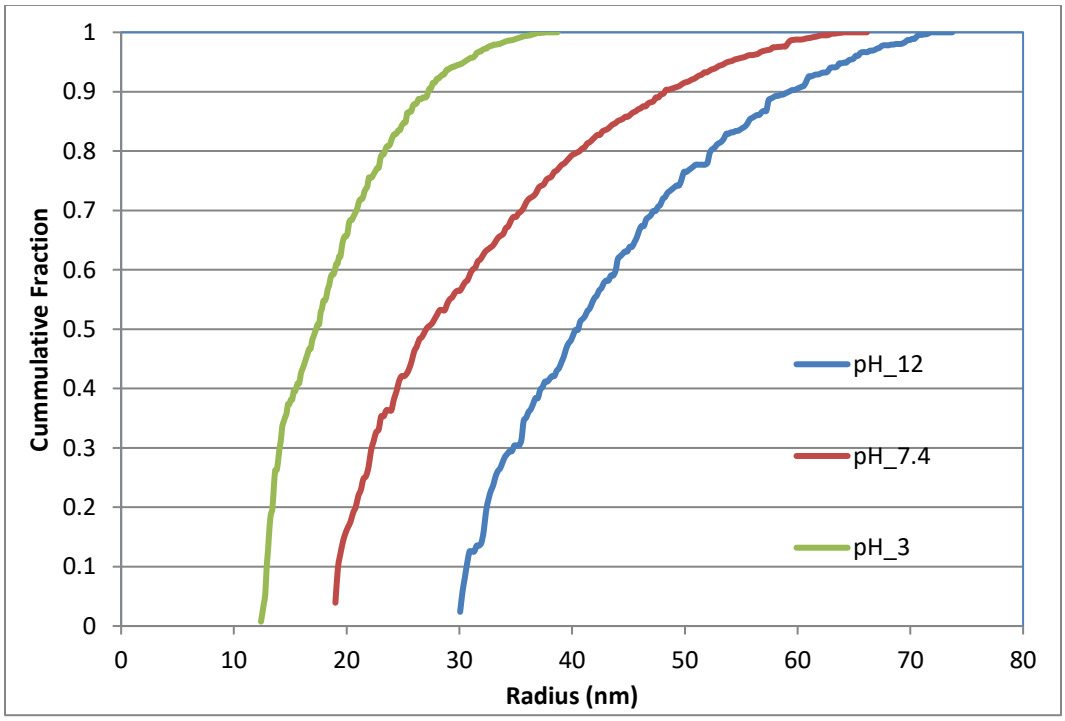

Figure 43: Cumulative Radius Fraction of AB 005V.

Shortest radius distribution is observed at pH 3. Overall, distribution curve shifting towards higher values as the solution pH increases (Figure 43). The curve for pH 3 starts near to

10 nm which increases to near 20 nm for pH 7.4 and 30 nm for pH 12. The gap between the curve for pH 12 and 7.4 decreases as cumulative fraction reaches 1 and it ends close to each other. On the contrary gap between the curves for pH 7.4 and 3 increases as fraction reaches 1. Figure 44 shows differential radius fraction for AB 005V. Overall in all the cases, the value of radius fraction decreases as radius value increases which indicate the predominant presence of low radius polymer aggregate. A visible large spike in pH 3 and relative steepness of the curve points out radius distribution is narrow with the dominant presence of 12-15 nm polymer aggregates. pH 7.4 and pH 12 shows similar curve characteristics with a small spike in the start of the curve and then a gradual decline. For pH 7.4 peak is observed near 20-22 nm and for pH 12 peak is observed around 34-36 nm. It can also be noted that curve for pH 7.4 is more smoother in decline than the pH 12. It implies that radius distribution with increasing radius value is more uniform at pH 7.4.

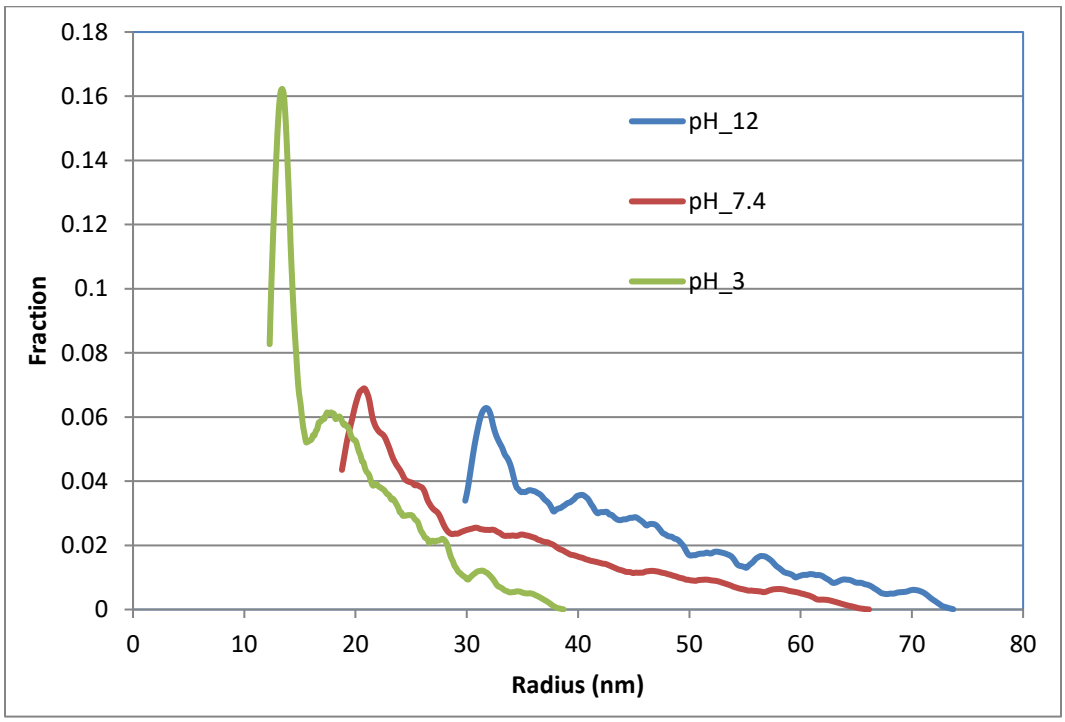

Figure 44: Differential Radius Fraction of AB 005V.

5.3.2 3130 S

The average values of radius and molar mass for 3130 S in different pH environment are presented in Table 9. 3130 S radius increases from an average value of 94 nm in pH 3 to 128.5 nm in pH 7.4 to 142.7 nm in pH 12. Rn and Rz also substantiate the trend. Rn changes from 62.5 nm to 142.1 nm and similarly Rz increases from 123.2 nm to 143.2 nm. Molar mass shows a clear trend of decrement with an increase in pH. Molar mass of 3130 S decreases from ~2.95 × 10^6 g/mol to ~2.05 × 10^6 g/mol when the solution pH changes from pH 3 to pH 7.4 and further decreases to 1.65 × 10^6 g/mol when pH increases to 12. The trend is more noticeable in Mz where it decreases from 4.5× 10^6 g/mol in pH 3 to 1.6 × 10^6 g/mol in pH 12.

Table 9: Molar Mass and Radius of 3130 S under different pH.

	Mn(g/mol)	Mw(g/mol)	Mz(g/mol)	Rn(nm)	Rw(nm)	Rz(nm)
pH 3	1.500E+06	2.956E+06	4.502E+06	62.5	94.6	123.2
pH 7.4	1.823E+06	2.053E+06	2.221E+06	121.2	128.5	133.8
pH 12	1.628E+06	1.647E+06	1.663E+06	142.1	142.7	143.2

Figure 45 shows molar mass and radius vs. retention time for 3130 S in all brines. Conformation plot of 3130 S can be in Figure 46. It is evident that slope value of the conformation plot increases as pH decreases. With the value of .3702 when pH is 12 to 0.5011 when pH is near neutral (pH 7.4) and further to 0.5661 in pH 3, decrement in slope value is significant. 3130 S is more linear in an acidic environment and polymer coils more and more as basic nature of the brine

increases. It can also be noticed that change in slope value is higher from pH 7.4 to pH 12 suggesting that conformational sensitivity is higher when brine changes from neutral to basic than the case when brine changes from neutral to acidic.

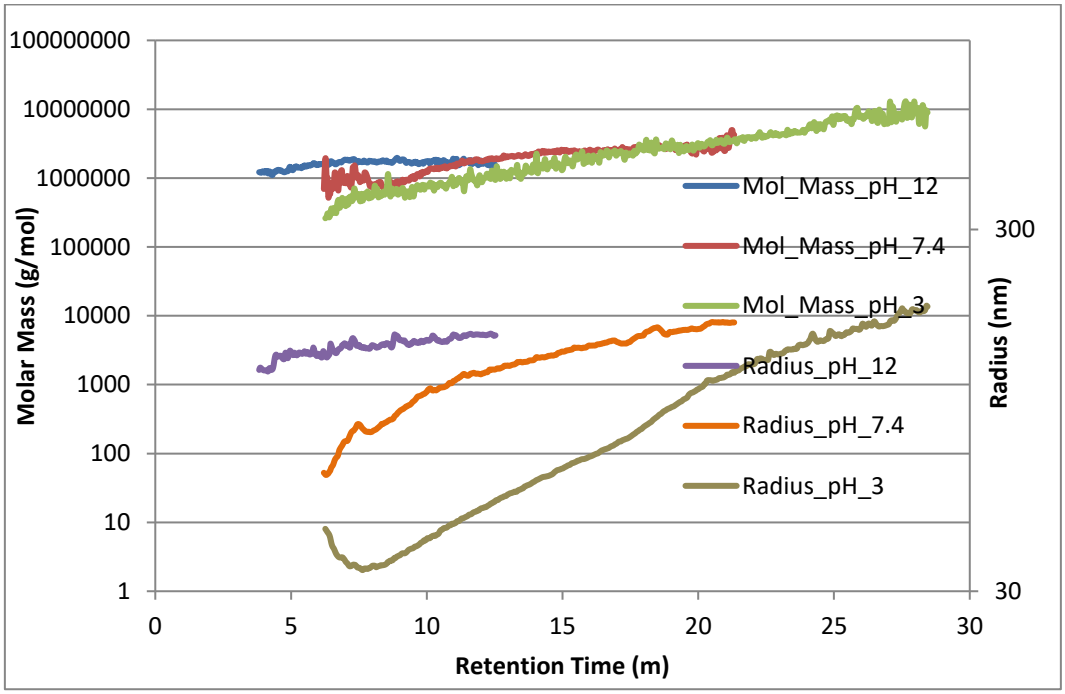

Figure 45: Molar mass and radius v/s retention time of 3130 S.

From cumulative molar mass distribution (Figure 47) it is clearly evident that the molar mass distributions of 3130 S under different pH conditions are widely different. 3130 S in pH 3 exhibits a broad distribution which extends till 1×10^7 g/mol

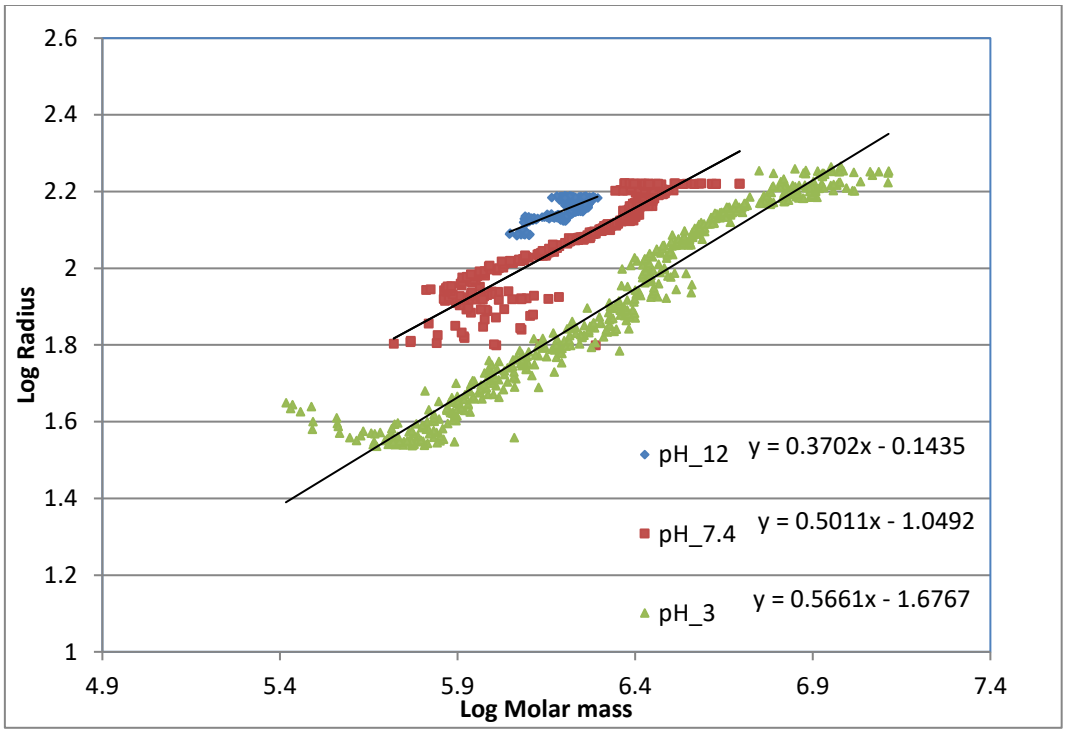

Figure 46: Conformation Plot for 3130 S.

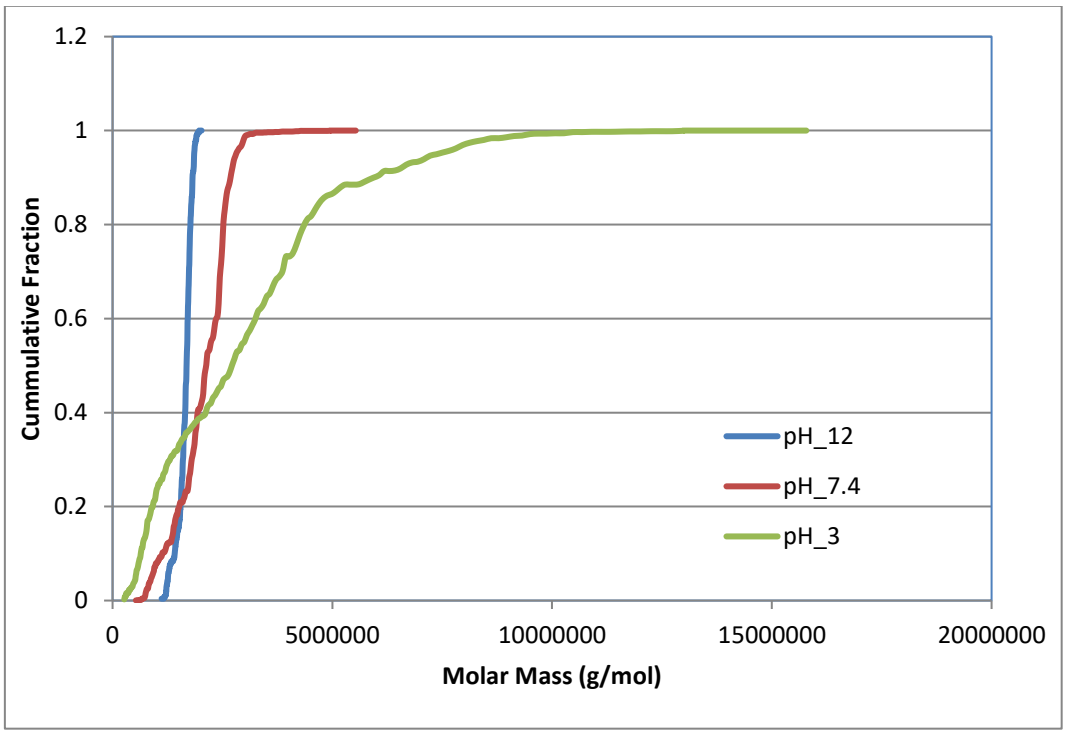

Figure 47: Cumulative Molar Mass Fraction of 3130 S.

In basic condition, mass distribution line imitates a straight line indicating a narrow mass distribution. In pH 7.4 distribution behavior is in between pH 12 and 3 and leaning more towards pH 12. Figure 48 is differential fraction plot for molar mass. As discussed earlier that 3130 S in pH 12 has a narrow distribution, it indicates the predominant presence of polymer aggregate of similar characteristics. A Large spike in pH 12 in differential fraction plot confirms the presence of polymer aggregate of molar mass 1×10^6 g/mol – 2×10^6 g/mol. It is also seen that differential fraction curve in pH 3 ends at around 1×10^7 g/mol and is also the broadest curve as inferred earlier from cumulative fraction plot. Differential mass distribution for pH 7.4 is in between pH 3 and pH 12; same was the case in cumulative fraction plot. A moderate spike can be observed in pH 7.4 curve which lays on the right of pH 12 differential fraction curve.

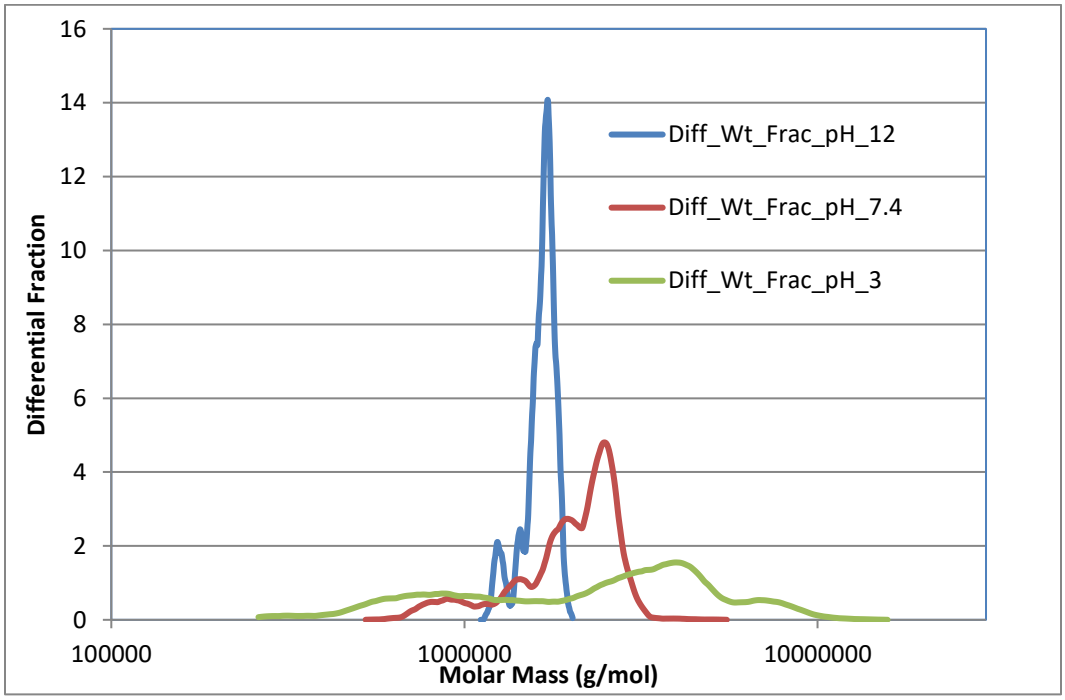

Figure 48: Differential Mass Fraction of 3130 S

Nature of radius distribution for 3130 S can be seen in Figure 49. Individual curve characteristic for cumulative fraction radius is similar to that of the cumulative fraction molar mass plot. The cumulative fraction molar mass curves starts close to each other and ends far apart. 3130 S in pH 3 has the broadest radius distribution; it starts from around 40 nm and extends up till 190 nm. Steepest curve is observed in pH 12 as per expectation. The curve for pH 7.4 starts out with lenient gradient and then progressively becomes stepper. All the curves briefly intersect at around cumulative fraction of 0.9.

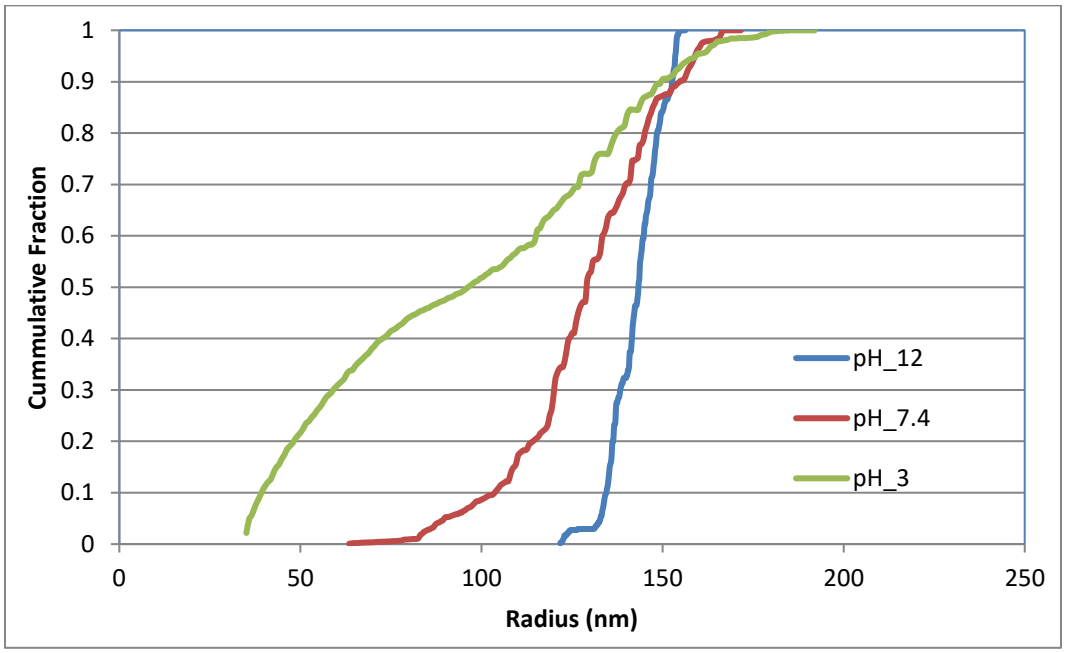

Figure 49: Cumulative Radius Fraction of 3130 S.

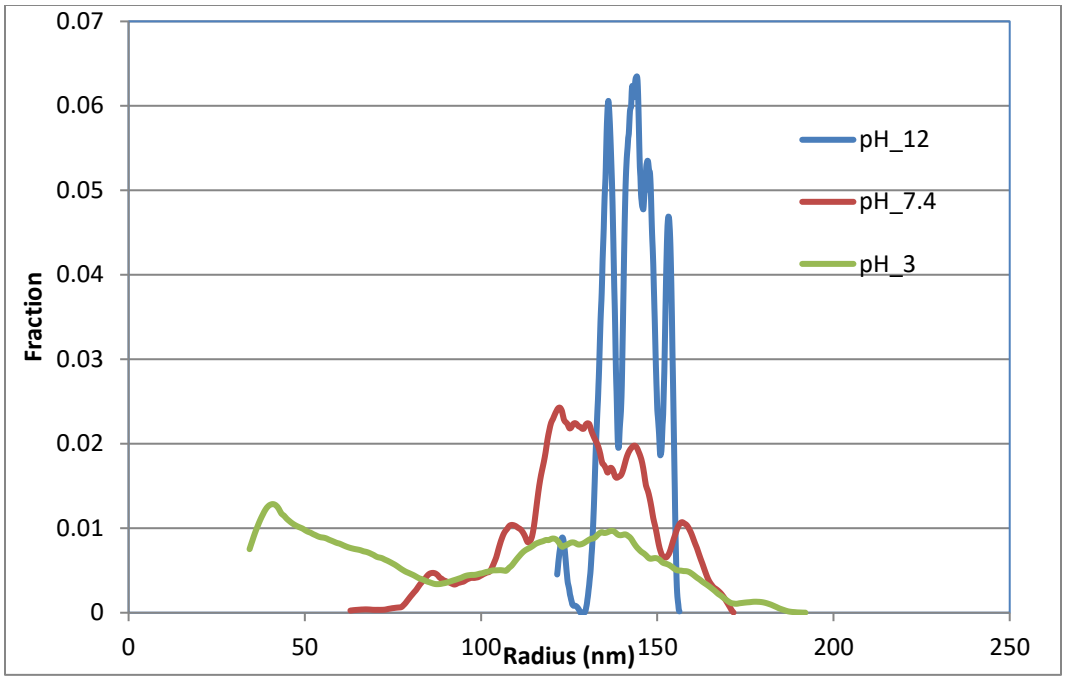

Figure 50: Differential Radius Fraction of 3130 S.

A large spike in pH 12 curve in differential radius fraction plot (Figure 50) is evident due to the steep curve in cumulative fraction plot (Figure 49). It indicates a dominating presence of polymer aggregate with radius 130 nm – 145nm. It is also to be noticed that no polymer aggregate is below 100 nm at pH 12. In pH 3, number of small radius polymer aggregates is present than aggregates above 150nm and the curve exhibits more or less uniform behavior. The curve for pH 7.4 starts around 60 nm and shows a high near 120 nm – 135 nm region.

5.3.3 3330 S

The values of radius and molar mass for 3330 S in different pH environment are presented in Table 10. A clear increment in radius values can be observed. Rw increases from 174.5 nm in pH 3 to 201.7 nm in pH 7.4 which further increases to 209 nm in pH 12. Similarly, Rn also increases from 137.8 nm in pH 3 to 175.7 nm in pH 7.4 to 200 nm in pH 12. In the case of Rz, it can be seen that it increases to 215.3 nm in pH 7.4 from 182.9 nm in pH 3 but only a negligible increment is observed when pH changes from 7.4 to 12. Molar mass value is halved from ~6.7 $\times 10^6$ g/mol to ~3.36 $\times 10^6$ g/mol when the solution pH changes from pH 3 to pH 7.4, a similar trend is also observed in the Mn and Mz. Mn decreases to 1.9 $\times 10^6$ g/mol from 4 $\times 10^6$ g/mol and Mz decreases to 3.9 $\times 10^6$ g/mol from 7.5 $\times 10^6$ g/mol. When pH changes from 7.4 to 12, Mw shows marginal change.

Table 10: Molar Mass and Radius of 3330 S under different pH.

	Mn(g/mol)	**Mw(g/mol)**	**Mz(g/mol)**	**Rn(nm)**	**Rw(nm)**	**Rz(nm)**
pH 3	4.070E+06	6.691E+06	7.522E+06	137.8	174.5	182.9
pH 7.4	1.969E+06	3.362E+06	3.981E+06	175.7	201.7	215.3
pH 12	3.209E+06	3.837E+06	4.324E+06	200.0	209.0	215.7

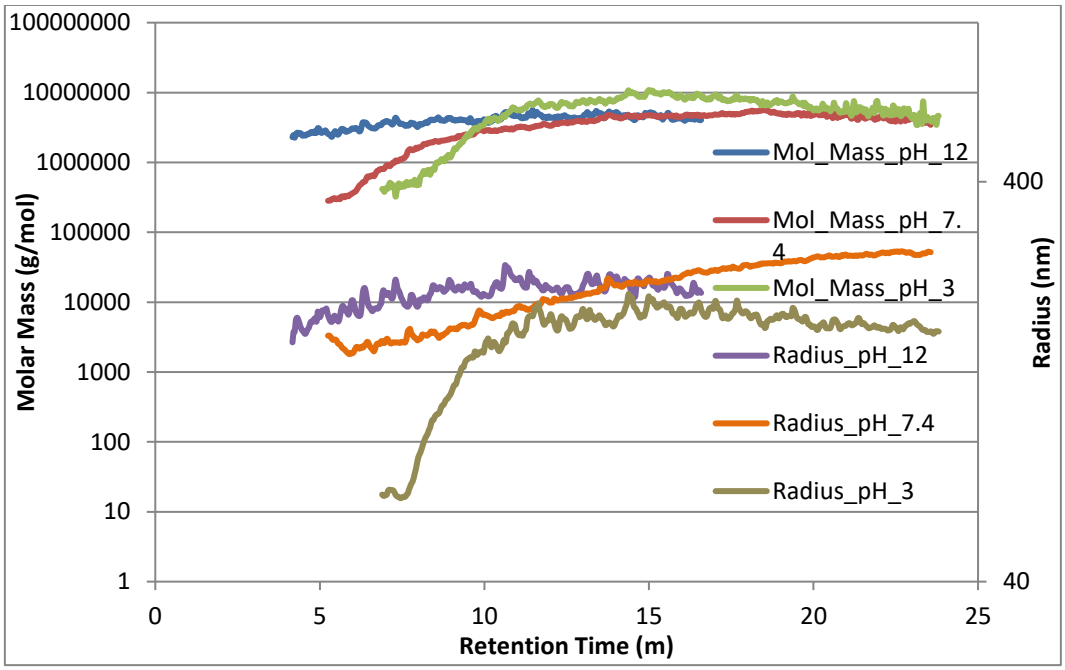

Figure 51: Molar mass and radius v/s retention time of 3330 S.

Figure 51 shows molar mass and radius vs. retention time for 3330 S in all brines. The conformation plots for 3330 S under different pH can be seen in Figure 52. Value for slope is in the range of 0.2 to 0.4 which indicates that conformational nature of 3330 S is compacted or coiled. As observed in 3130 S, the value of the slope decreases as pH changes from pH 3 to pH 7.4. It indicates that 3330 S gets more compacted and resembles coiled sphere as pH moves to 7.4. Contrary to previous observation, slope value increases to 0.36 as pH changes to 12 which suggests that 3330 S gets relatively uncoiled as it moves from pH 7.4 to pH 3. 3330 S gets more compacted in the presence of neutral environment in comparison to acidic or basic environment where it is relatively linear.

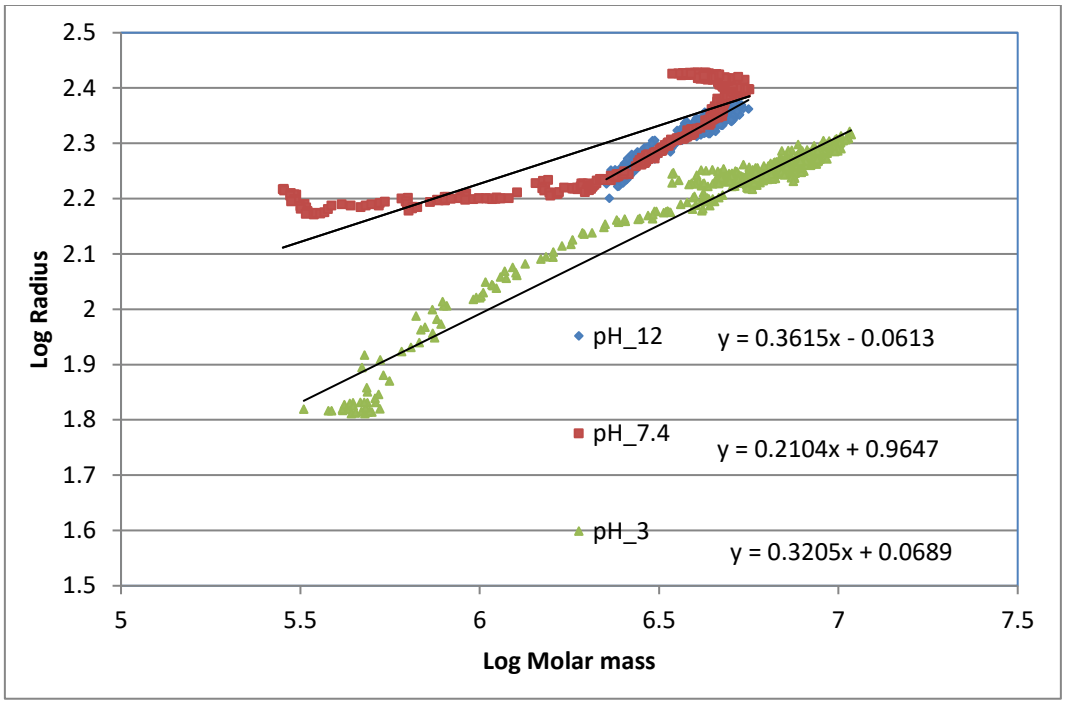

Figure 52: Conformation Plot for 3330 S.

Cumulative weight fraction for 3330 S can be seen in Figure 53. Cumulative mass distribution plot shows some similar characteristics as observed in 3130 S. Mass distribution in pH 3 extends to a fairly long range of molar mass values, and similarly mass distribution in pH 12 is relatively short, and its curve is steep. It can also be noticed that curve for pH 7.4 starts with a gradual slope and then after a cumulative fraction of 0.6 becomes steeper. Also, curve for pH 7.4 and pH 3 starts in a similar range but ends way apart, signifying changed behavior of 3330 S with a change in pH. Similarly, curve for pH 12 and pH 7.4 which starts with a reasonable gap between them, but it ends at an almost same point. Also, curve for pH 12 and pH 7.4 exhibits significant layover above cumulative weight fraction of 0.6.

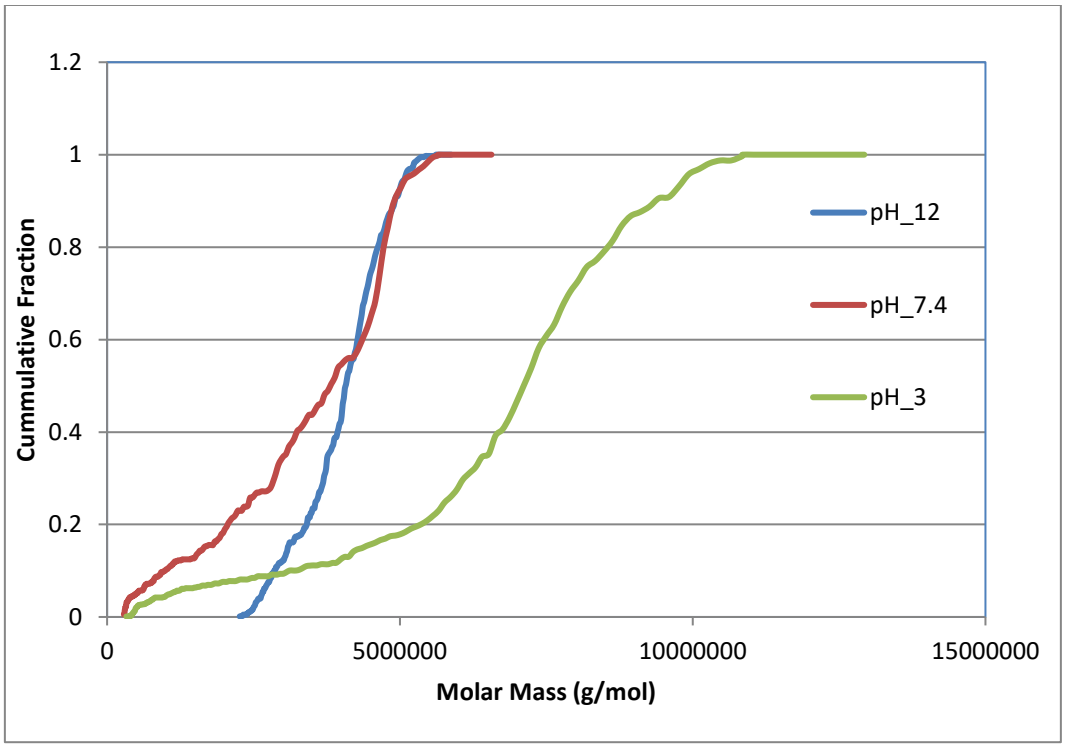

Figure 53: Cumulative Mass Fraction of 3330 S.

Differential mass fraction plot significantly aids in understanding the mass distribution of the polymer species. Figure 54 shows a differential mass fraction of 3330 S under different pH environment. A large spike in the curve of pH 12 of pH 12 is seen as expected because of the steep curve in cumulative mass fraction plot. It points towards the predominant presence of polymer aggregate weighing in the range of 3×10^6 g/mol - 5×10^6 g/mol. Differential mass fraction curve for pH 3 and pH 7.4 have similar behavior. They both show a spike towards the end of the curve and start out low and smooth. It indicates that both have a uniform presence of low molar mass aggregates. The presence of polymer aggregates increases with increasing molar mass of aggregates.

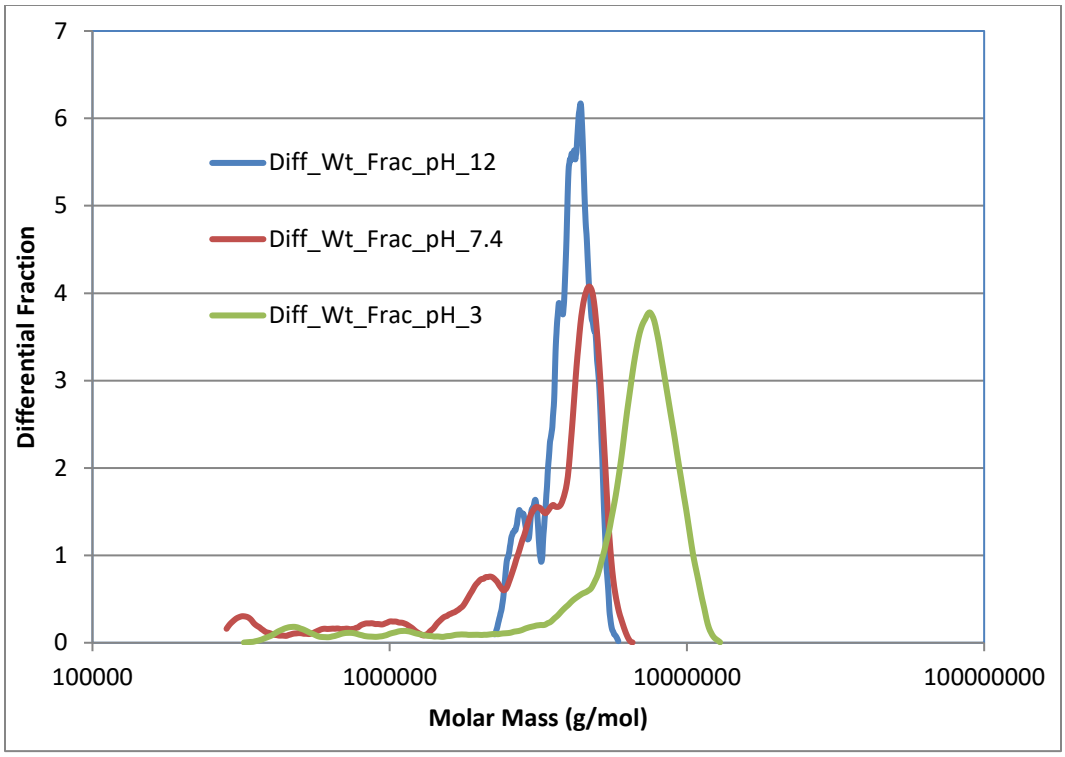

Figure 54: Differential Mass Fraction of 3330 S.

Figure 55 shows cumulative radius fraction plot of 3330 S under different pH. It can be seen that unlike cumulative molar mass plot for 3330 S, cumulative radius plot for 3330 S starts and ends in a relatively close range. It is noticeable that curve for pH 7.4 and pH 12 starts near to each other with the curve for pH 7.4 starting around 150 nm and curve for pH 12 starting around 160 nm. They also end close to each other with a crossover at a cumulative fraction of 0.5. The curve for pH 3 starts around 65 nm and slowly increases till 150 nm. From 150 nm, a sudden change in the curvature of the curve is noticed. The curve for pH 3 suddenly becomes steeper at around fraction of 0.2, it also layovers briefly on pH 7.4 curve and finally ends at around 200 nm.

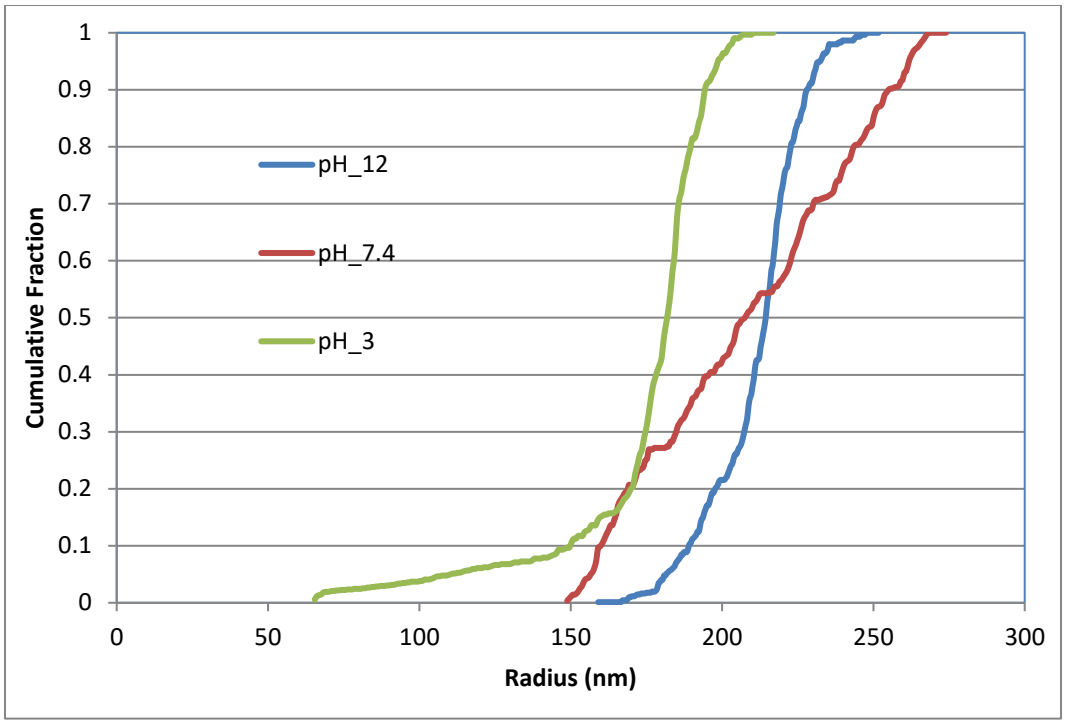

Figure 55: Cumulative Radius Fraction of 3330 S.

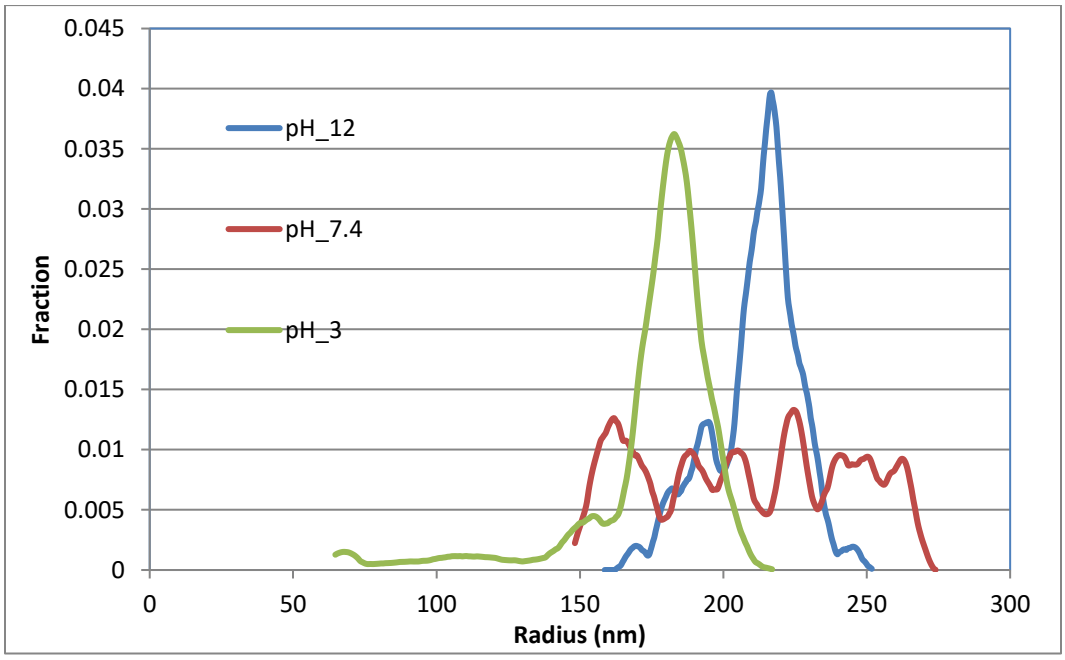

Figure 56: Differential Radius Fraction of 3330 S.

Figure 56 shows differential radius fraction plot for 3330 S in different pH. No major peak is noticeable in differential radius curve at pH 7.4. It indicates that 3330 S in the neutral environment will exhibit a relatively uniform distribution of the polymer aggregate with a radius ranging from 150 nm to 280 nm. No one species with a particular radius is dominant at pH 7.4. The differential radius curves for pH 12, and pH 3 somewhat shows similar characteristics. The curve for pH 12 shows a prominent peak around 225 nm and a smaller peak around 190 nm. It shows that under pH 12, aggregate with size around 225 nm is dominant with a presence of aggregate of size 190 nm. For pH 3, a spike is observed near 180 nm with a low steady line from 65 nm to 140 nm. It indicates that it has a low but uniform presence of low radius polymer aggregate and a prevalent presence of aggregate of 180 nm. It can be inferred that 3330 S displays a uniform distribution in neutral surrounding and it shows a peculiar distribution with the predominating presence of a specific size aggregate in acidic and basic environment.

5.3.4 3630 S

Table 11 shows values of molar mass and radius for 3630 S under pH 3 and pH 12. It is clearly observable that molar mass decreased as pH changed from 3 to 12. Mw changed from 1.1×10^7 g/mol to 5.4×10^6 g/mol. Mn also decreased from 1.0×10^7 g/mol to 5×10^6 g/mol. Finally, Mz reduced from 1.2×10^7 g/mol to 5.8×10^6 g/mol. The radius values increase with an increase in pH. Observations are as per trend is seen in previous polymers. Rw value increases from 201.7 nm in pH 3 to 242.8 nm in pH 12. Rn also increases to 239.5 nm from 196.5 nm. Rz shows the value of 245.3 nm in pH 12 and 205.1 nm at pH 3.

Table 11: Molar Mass and Radius of 3630 S under different pH.

	Mn(g/mol)	**Mw(g/mol)**	**Mz(g/mol)**	**Rn(nm)**	**Rw(nm)**	**Rz(nm)**
pH 3	1.041E+07	1.129E+07	1.187E+07	196.5	201.7	205.1
pH 12	5.037E+06	5.448E+06	5.808E+06	239.5	242.8	245.3

Figure 57 shows molar mass profile and radius profile with time for 3630 S. Conformation plot can be observed in Figure 58. It can be seen that conformance plot exhibit low value for the slope for 3630 S indicating that 3630 S has a strong tendency to behave in a highly coiled manner. The slope value of 0.2522 can be observed for 3630 S under pH 3. Conformational slope value reduces to .1013 for 3630 S in pH 12.

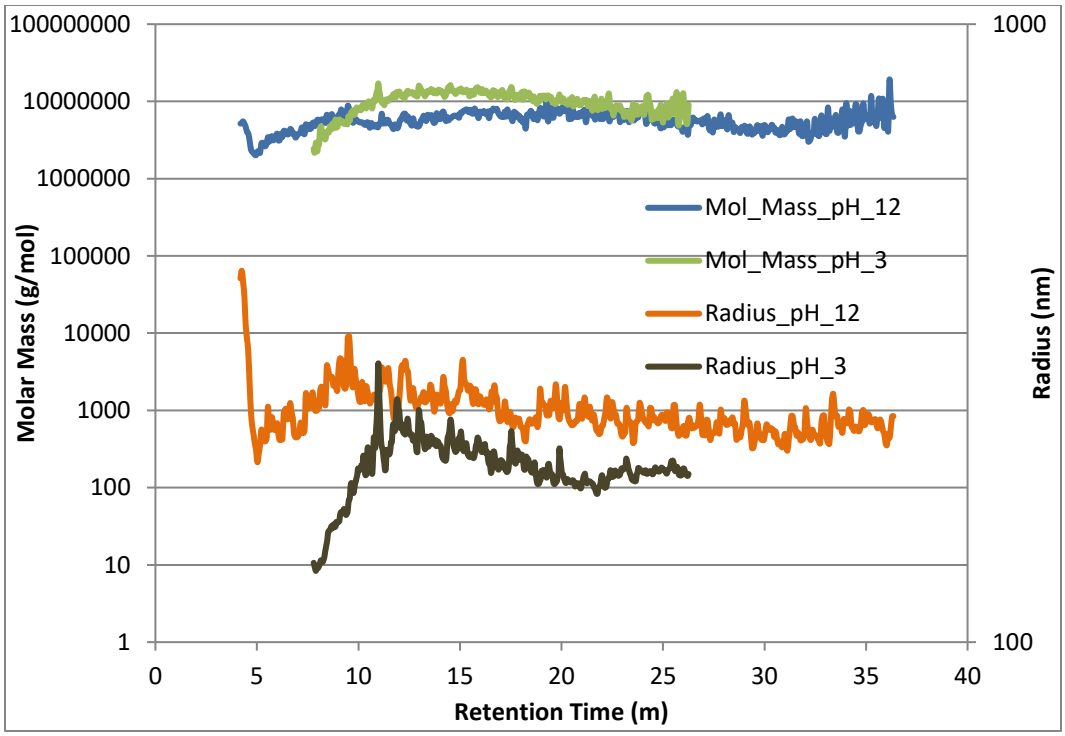

Figure 57: Molar Mass and Radius to Retention Time for 3630 S.

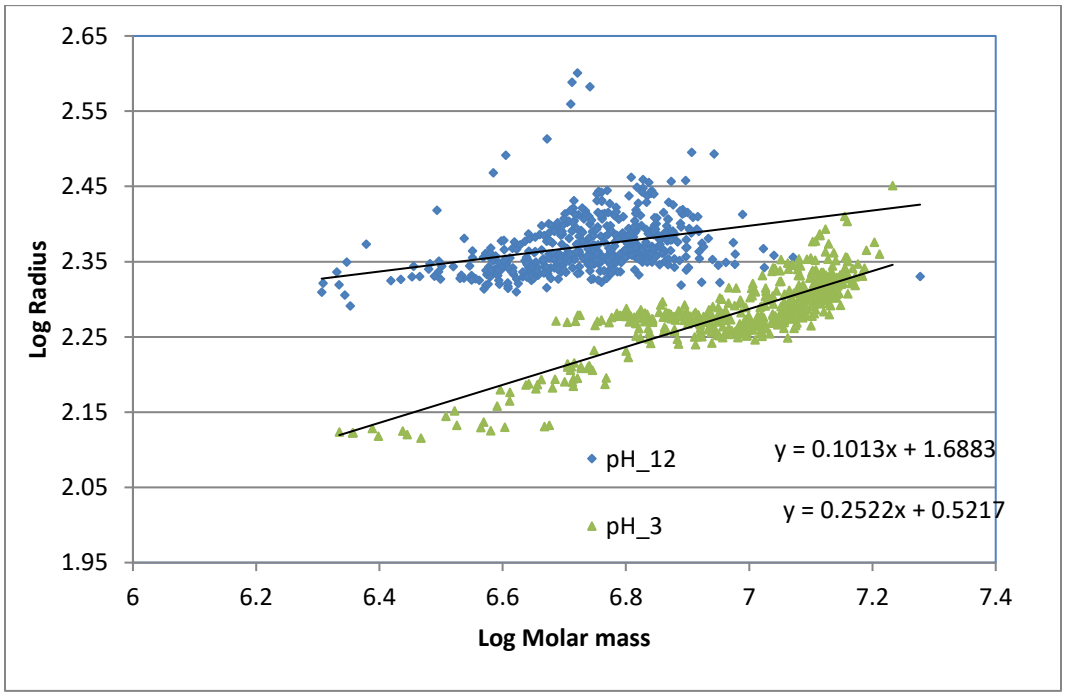

Figure 58: Conformation Plot for 3630 S.

Similar conformational behavior was also seen in 3130 S where slope value decreases with increase in pH. The value of 0.1013 strongly indicates that under basic condition, 3630 S conforms to a nearly spherical shape. The value of 0.2522 in the acidic environment also suggests that it 3630 S has highly compacted structure such as a sphere.

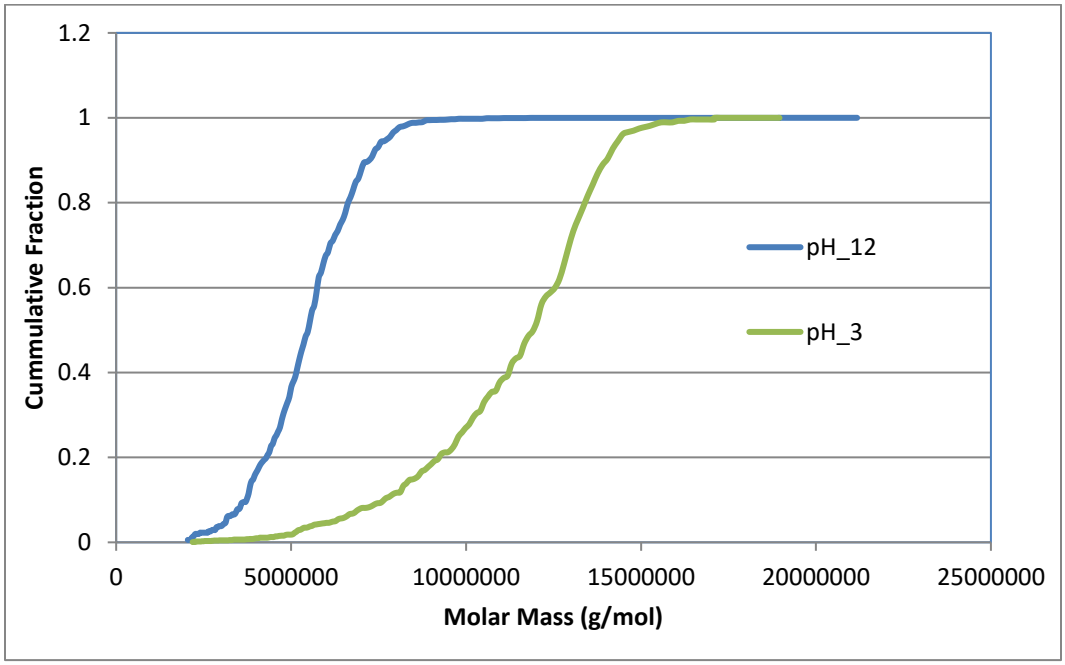

Figure 59: Cumulative Mass Fraction of 3630 S.

Figure 59 shows cumulative mass fraction plot for 3630 S under pH 3 and pH 12. It can be seen that curve for both scenarios starts nearly together. The curve for pH 12 can be seen to be steeper than pH 3 till cumulative fraction of 0.4 which indicates that pH 12 has a higher presence of aggregate with a mass around 5×10^6 g/mol. It is observed that the curve for pH 12, in the end, extends to a large molar mass with a nearly horizontal line. This indicates the small presence of high molar mass aggregate. The cumulative mass curve for pH 3 starts with a gradual slope and

continues till fraction of 0.6. After which the curve steepens up in a similar fashion to that of pH 12 curve. Both the curve ends far apart with pH 12 curve attaining cumulative fraction value of 0.8 around 7×10^6 g/mol and pH 3 reaching cumulative fraction value of 0.8 around 13×10^6 g/mol.

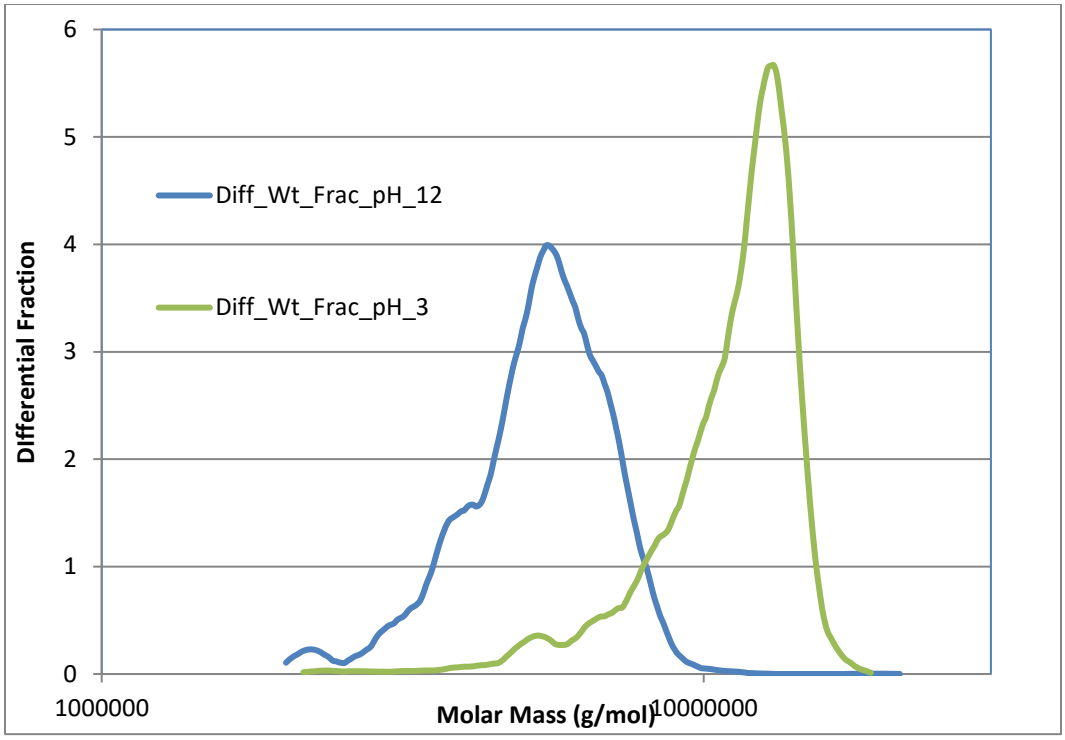

Figure 60: Differential Mass Fraction of 3630 S.

Figure 60 shows differential mass fraction plot for 3630 S. Similar to cumulative mass fraction curve, the curve for pH 12 and pH 3 also starts from a similar point in differential mass fraction curve. A clear peak is observed in the curve of pH 12; it is also to be noticed that the peak is relatively broad and it covers more range of molar mass under its peak. In the end of the curve near 1×10^7 g/mol, a nearly horizontal line can be seen near a differential mass fraction of 0 depicting a minor

presence of high molar mass aggregate which is in tandem to the observation in Figure 59. The curve for pH 3 also shows a prominent peak. The curve starts out low with a gradual increase in differential mass fraction and then showcases a peak later in the curve. This peak is larger and sharper than that of observed in pH 12.

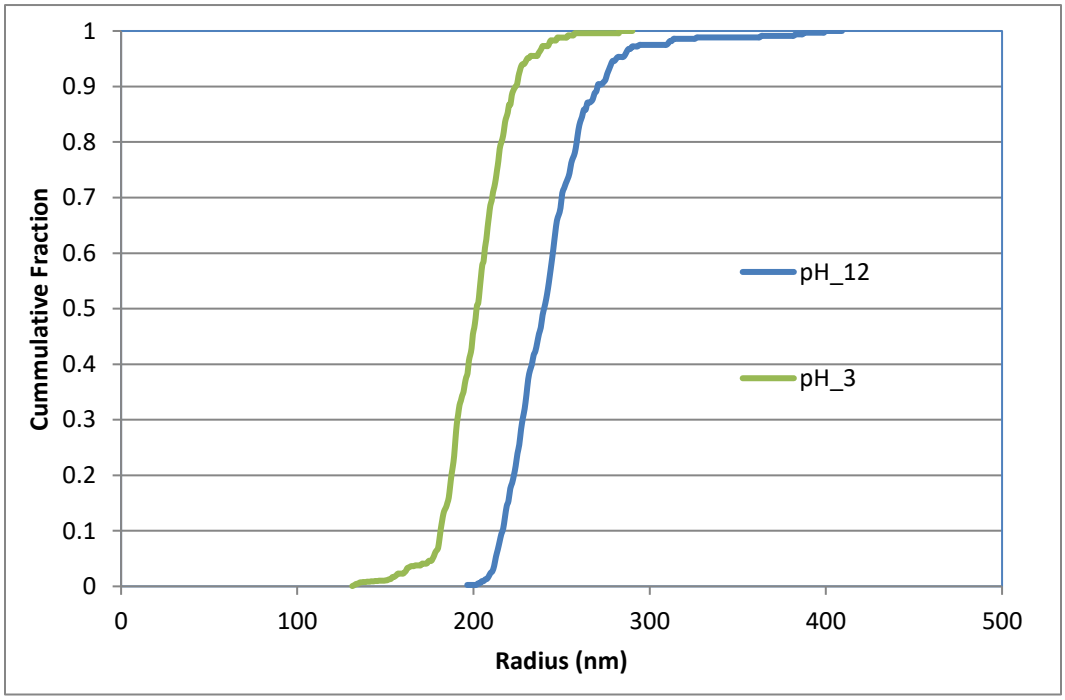

Figure 61: Cumulative Radius Fraction of 3630 S.

Cumulative radius plot for 3630 S can be seen in Figure 61. From observation, it is obvious that cumulative radius curve for pH 3 and pH 12 shows similar characteristics. Both the curve runs visibly parallel from cumulative fraction of 0.1 to fraction of 0.9. Cumulative radius curve for pH 12 starts at around 200 nm and steadily reaches a cumulative fraction of 0.9. After that, the curve extends till a little over 400 nm. The curve for pH 3 starts its steepness little late than in pH 12. After it increases till fraction of 0.9 and then eventually ends. Differential radius plot for

3630 S can be seen in Figure 62. Differential radius curve for pH 3 starts at around 130 nm then shows a little kick before the peak observed at around 200 nm. It indicates the dominant presence of aggregate measuring 200 nm.The curve ends a little short of 300 nm. It is to be observed that peak is taller and marginally narrower than the peak observed for pH 12. The curve for pH 12 starts with a peak which ends at 300 nm and then continues further. It indicates the small presence of high radius polymer aggregate with leading presence of aggregate measuring around 250 nm.

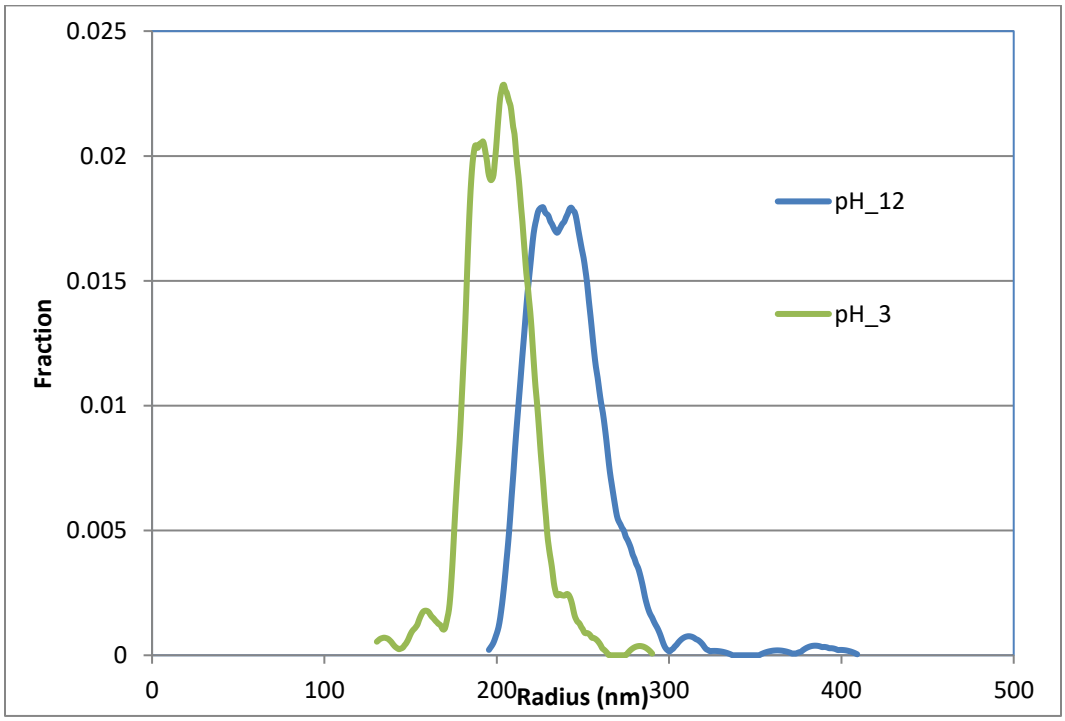

Figure 62: Differential Radius Fraction of 3630 S.

5.1 Summary

AB 005V

Molar mass value decreases as environment changes from basic to acidic. However, this effect diminishes as acidic nature increases in the environment. Radius values show a clear increment as pH changes from acidic to basic. Polymer conformation is more linear in basic medium, and it changes to more branched conformation in acidic medium. Conformational sensitivity is higher in an acidic environment. High molar mass aggregate dominates in a neutral environment. Low radius aggregate dominates in an acidic environment.

3130 S

A Clear decrease in molar mass with increasing pH is observed. Also, increase in radius with decreasing pH is clearly observed. Polymer conformation is more linear in acidic medium, and it changes to more compact conformation in a basic environment. Extremely narrow mass distribution with the dominant presence of a specific molar mass aggregate exists in basic conditions. Extremely narrow radius distribution with the dominant presence of a specific radius aggregate exists in basic conditions.

3330 S

Radius increases with increase in pH. Molar mass decreases as environment changes from acidic to neutral. Overall the polymer displays branched and compacted conformation. Narrow mass distribution with the prevalent presence

of specific molar mass aggregate exists in basic conditions. Polymer exhibits uniform distribution under a neutral condition.

3630 S

Molar mass decreases as environment changes from acidic to basic. Radius value increases as environment changes from acidic to basic. Polymer shows extremely compact conformation with near sphere like structure in acidic medium. Mass and Radius distribution show similar traits in the acidic and basic environment.

Chapter 6

Effect of Monovalent ion on HPAM

6.1 Polymer Used

Three different types of polymers namely 3630 S, Post Hydrolyzed 3630, Super Pusher C319, were used. SNF SAS supplied all the polymers in dry powder form. Super Pusher C319 is an associative polymer with both hydrophobic and hydrophilic moieties. Post Hydrolyzed 3630 differs from 3630 S by the method of manufacture. 3630 S is cohydrolyzed polymer while Post Hydrolyzed 3630 is not a cohydrolyzed polymer. In Post hydrolyzed 3630, acrylic acid is hydrolyzed after polymerization of acrylamide. These polymers are anionic and water soluble with a degree of hydrolysis of 25-30 mol %.

6.2 Solution preparation

Solutions of different salinity were made by adding specific quantity chemicals into the deionized water. NaCl was used to make a solution of different salinity. Three different solutions with different salinity were prepared, salinity was 1000 ppm, 5000 ppm, and 10000 ppm. Solutions were made by adding NaCl to deionized water; NaCl was supplied by Fisher Tropsch. Polymers were added to the solutions and were mixed with using a magnetic stirrer at 260 rpm for 24 hours. All the sample solutions were clear after three hours of mixing. In total, nine different polymer solutions were prepared (each polymer at three different salinity conditions).

6.3 Results and Observations

6.3.1 3630 S

Table 12 shows molar mass value and radius value for 3630 S for all three salinity cases i.e. 1000 ppm, 5000 ppm and 10000 ppm. It is evident from the observation that molar mass value decreases as salinity increases of the brine. Mw decreased from 18.54× 10^6 g/mol in 1000 ppm brine to 11.43 × 10^6 g/mol in 5000 brine and further decreases to 10.77 × 10^6 g/mol in 10000 ppm brine. A similar trend is also observed for Mn and Mz. Mn value decreases from 14.96 × 10^6 g/mol to 10.85 × 10^6 g/mol as salinity increases from 1000 ppm and 5000 ppm. It further decreases marginally to 10.08 × 10^6 g/mol in 10000 ppm salinity. Mz also decreases from 20.20 × 10^6 g/mol to 12.01 × 10^6 g/mol to 10.77 × 10^6 g/mol as salinity increases. It is to be noted that effect of salinity on molar mass ceases as salinity increases from 5000 ppm to 10000 ppm. It suggests that 3630 S undergoes rapid degradation in low to medium salinity environment.

Table 12: Molar Mass and Radius of 3630 S under different salinity (mono-valent ion).

	Mn (g/mol)	**Mw (g/mol)**	**Mz (g/mol)**	**Rn (nm)**	**Rw (nm)**	**Rz (nm)**
1000 ppm	14.96 E+06	18.54 E+06	20.20 E+06	322.6	361.6	395.2
5000 ppm	10.85 E+06	11.43 E+06	12.01 E+06	200.7	207.3	213.9
10000 ppm	10.08 E+06	10.77 E+06	11.28 E+06	184.1	189.8	194.2

Radius values also decrease as salinity increases. Rw decreases from 361.6 nm in 1000 ppm to 207.3 nm in 5000 ppm, and it further reduces to 189.8 nm in 10000 ppm. Radius decreases by ~150 nm as salinity changes from 1000 ppm to 5000 ppm and radius decreases by only ~20 nm when salinity changes from 5000 ppm to 10000 ppm. The salinity effect on Rw ceases as salinity increases from 5000 ppm to 10000 ppm. A similar trend was observed with molar mass as well; it indicates that 3630 S degrades rapidly in low to medium salinity environment. Rn and Rz values also decrease as salinity increases. Rn value decreases from 322.6 nm to 200.7 nm and further decreases to 184.1 nm. Similarly, Rz values decrease from 395.2 to 213.9 nm and finally to 194.2 nm. The decrease in radius is due to the charge shielding effect of cation (Na^+) of negative charge on the backbone of the HPAM aggregate. Shielding effect leads to decreases electrostatic repulsion between negative charge on the backbone and thus polymer aggregate tends to coil. Coiling of the polymer aggregate leads to decrease in radius.

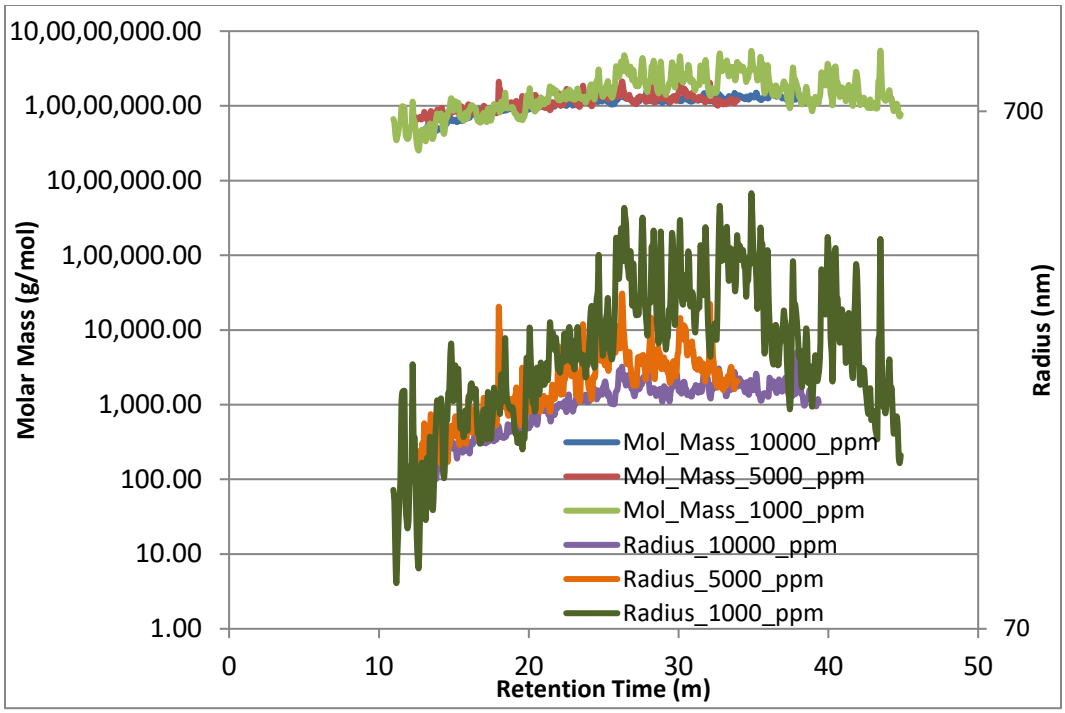

Figure 63: Molar Mass and Radius to Retention Time for 3630 S.

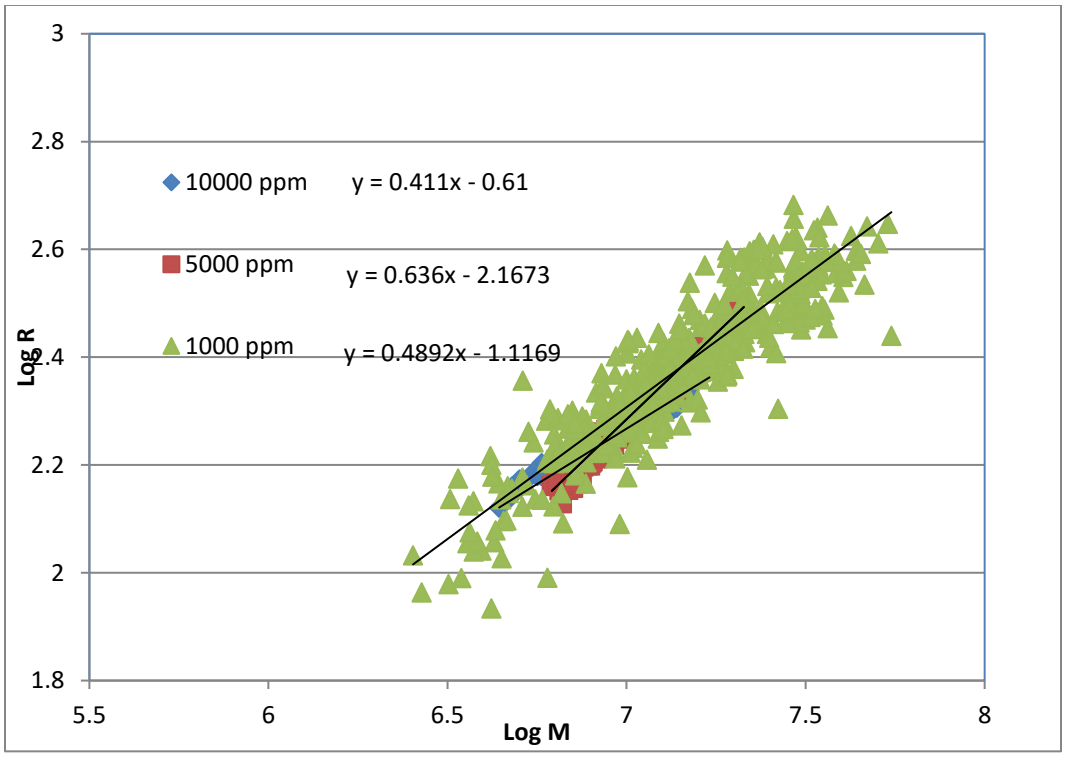

Figure 64: Conformation Plot for 3630 S.

The conformational plot for 3630 S under all salinity scenarios can be seen in Figure 64. The conformational slope values are between 0.41 and 0.64; this suggests that overall conformation for 3630 S is compact/branched to linear conformation. It can be observed that the conformation slope value is 0.636 in the case of 5000 ppm indicating random coil linear conformation. It is the highest value among other salinity which demonstrates that polymer in 5000 ppm has relatively linear most conformation. Conformation slope value of 0.41 is observed in 10000 ppm; it implies that 3630 S has most compact conformational structure about conformational structure in other salinity cases. In the case of 1000 ppm, conformational slope value is 0.49; this is in between 10000 ppm and 5000 ppm slope value.

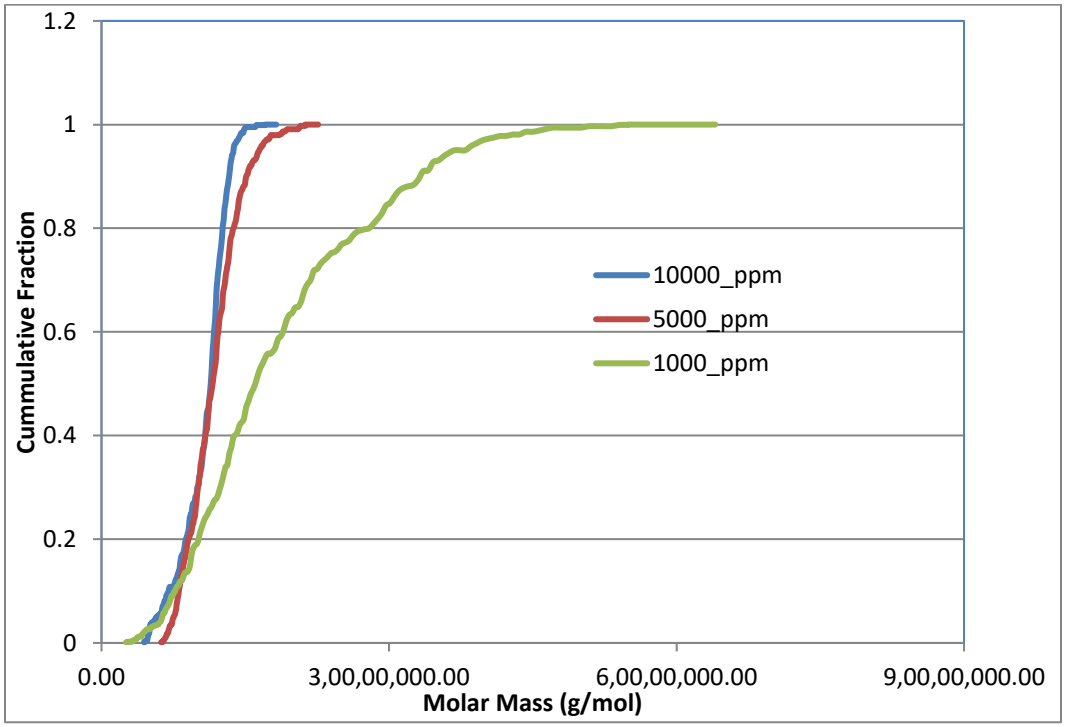

Figure 65: Cumulative Mass Fraction of 3630 S.

Cumulative mass fraction for HAPM-A for 1000 ppm, 5000 ppm, and 10000 ppm salinity is seen in Figure 65. It is evident from the graph that curve for 1000 ppm has maximum horizontal extent which means that it exhibits a broader molar mass distribution covering polymer aggregates with wide molar mass distribution. The curve for 5000 ppm and 10000 ppm displays similar characteristics. They start close to each other and briefly overlap from a cumulative fraction of 0.2 to fraction of 0.5; this suggests that molar mass distribution in the polymer species in the fraction of 0.2 to 0.5 is extremely similar.

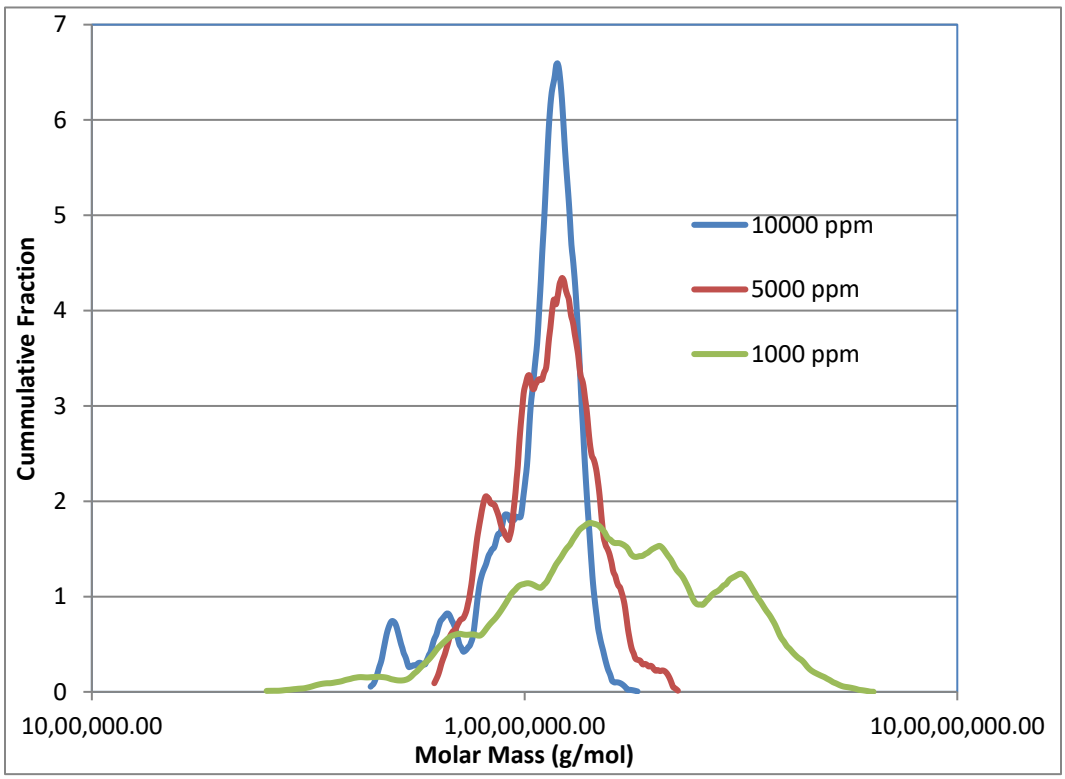

Figure 66: Differential Mass Fraction of 3630 S.

Differential mass fraction plots 3630 S under all salinity scenarios are given in Figure 66. It can be clearly observed that in the curve for 10000 ppm case, a large prominent peak is observed. It signals at the dominating presence of a specific molar mass polymer aggregate. As the peak is around 1×10^7 g/mol, polymer aggregate with a molar mass around 1×10^7 g/mol dominates when salinity is 10000 ppm. Similarly, in the curve for 5000 ppm salinity, a peak is observed at the same location as in 10000 ppm salinity. The height or extent of the peak is smaller than 10000 ppm indicating that polymer aggregate with a molar mass around 1×10^7 g/mol dominates in 5000 ppm as well, but the extent of domination is less than that of observed in 10000ppm salinity. It is also to be observed that 3630 S showcases a narrow molar mass distribution in high and medium salinity environment. In the case of 1000 ppm, a relatively uniform molar mass distribution is observed. 3630 S also exhibits widest molar mass distribution with the relative high observed near 11×10^7 g/mol - 12×10^7 g/mol.

Figure 67 shows cumulative radius fraction plot for HPAM – A. As seen in the plot, curve for 1000 ppm salinity shows maximum horizontal coverage which extends almost up to a radius of 500 nm. It indicates that 3630 S has a broad radius distribution. The curve for 5000 ppm and 10000 ppm salinity displays similar curve behavior; both are relatively steeper. The curve for 10000 ppm becomes steeper from a cumulative fraction of 0.4 while the curve for 5000 ppm develops steadily with no visible change in slope. It is also to be observed that curve ending (cumulative fraction from 0.9 to 1) is broadest/extended most as salinity decreases. In 1000 ppm case curve ending is broadest which reduces in 5000 ppm salinity and

finally in 1000 ppm salinity a narrow ending can be seen. It reflects on radius distribution of polymer aggregates in the polymer species.

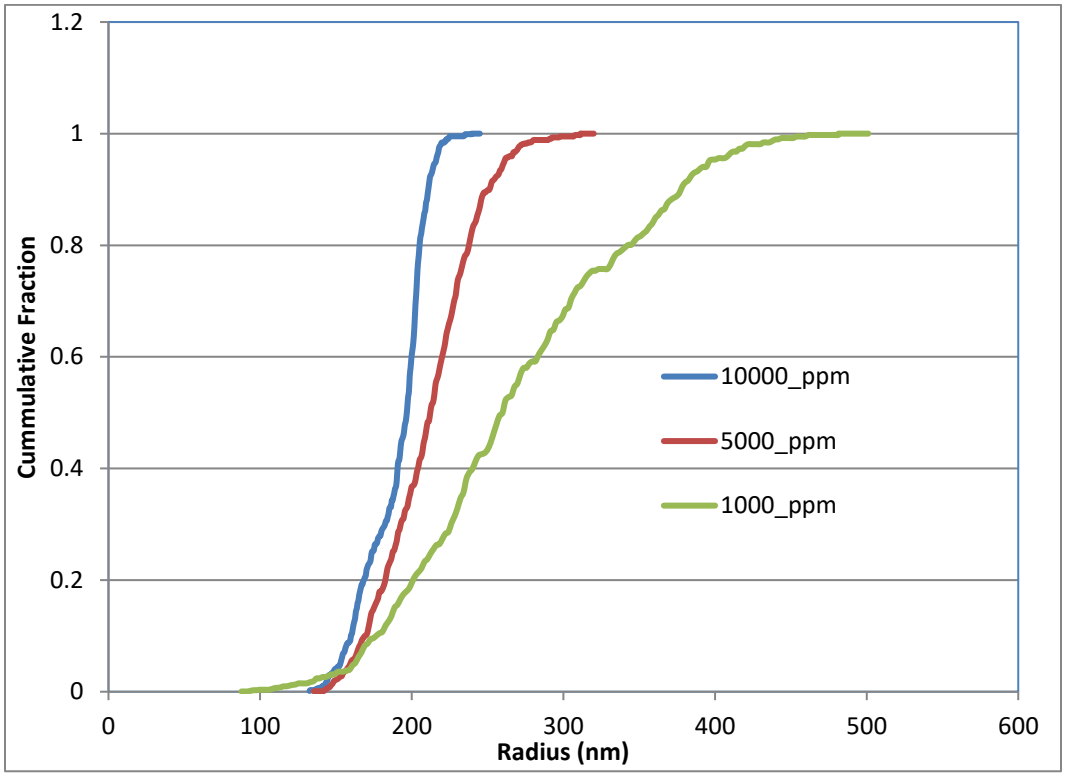

Figure 67: Cumulative Radius Fraction of 3630 S.

The differential radius plot for 3630 S under different brine is given in Figure 68. The curve for 10000 ppm displays a conspicuous large peak. The peak is at 200 nm which means that polymer aggregate with a radius of 200 nm dominates 3630 S radius distribution in high salinity. Also, a smaller peak can be seen around 170 nm in the curve of 10000 ppm, the peak of similar height is observable in the curve for 5000 ppm. The curve of 5000 ppm and 10000 ppm starts from the similar point, but the curve for 5000 ppm extend longer and end at around 310 nm.

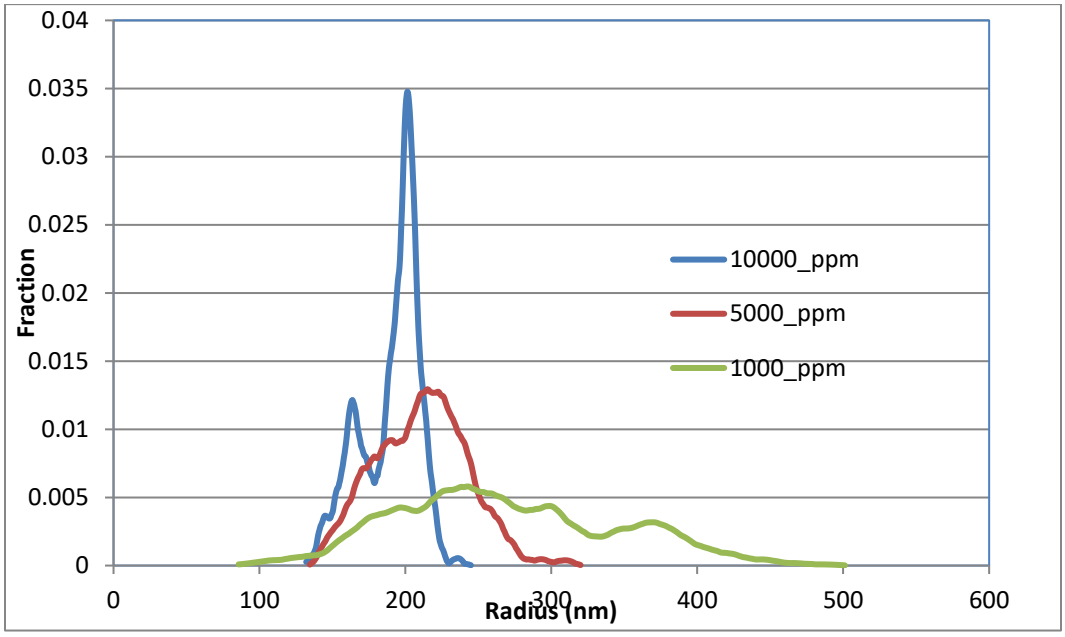

Figure 68: Differential Radius Fraction plot for 3630 S.

The peak observed around 220 nm indicates that polymer aggregate with a radius of 220 nm are present in the majority when salinity is 5000 ppm. 3630 S displays a relatively uniform radius distribution when salinity is 1000 ppm. It has the broadest distribution as inferred from the cumulative radius fraction plot. A high plateau is seen around 230 nm -250 nm. Overall, 3630 S radius distribution gets narrower as the salinity of the environment increases.

6.3.2 Post Hydrolyzed 3630

The value of molar mass and radius for Post Hydrolyzed 3630 can be seen in Table 13. It can be observed that molar mass decreases the salinity of the brine increases. The value of the Mw is 19.81 × 10^6 g/mol, and it decreases to 13.59 × 10^6 g/mol when salinity increases to 5000 ppm. Molar mass further decreases to 9.88 × 10^6 g/mol when salinity is 10000 ppm. A similar trend is also observed in Mn, Mn decreases from 15.56 × 10^6 g/mol in 1000 ppm to 9.98 × 10^6 g/mol in 5000 ppm to 8.65 × 10^6 g/mol in 10000 ppm. Also, Mz can be seen to decrease from 24.49 × 10^6 g/mol in 1000 ppm salinity brine to 17.12 × 10^6 g/mol in 5000 ppm salinity and finally to 9.88 × 10^6 g/mol in 10000 ppm.

Table 13: Molar Mass and Radius of Post Hydrolyzed 3630 under different salinity (mono-valent ion).

	Mn (g/mol)	**Mw (g/mol)**	**Mz (g/mol)**	**Rn (nm)**	**Rw (nm)**	**Rz (nm)**
1000 ppm	15.56 E+06	19.81 E+06	24.49 E+06	326.4	368.7	407.3
5000 ppm	9.98 E+06	13.59 E+06	17.12 E+06	267.8	317.2	359.4
10000 ppm	8.65 E+06	9.88 E+06	10.81 E+06	205.5	218.2	227.3

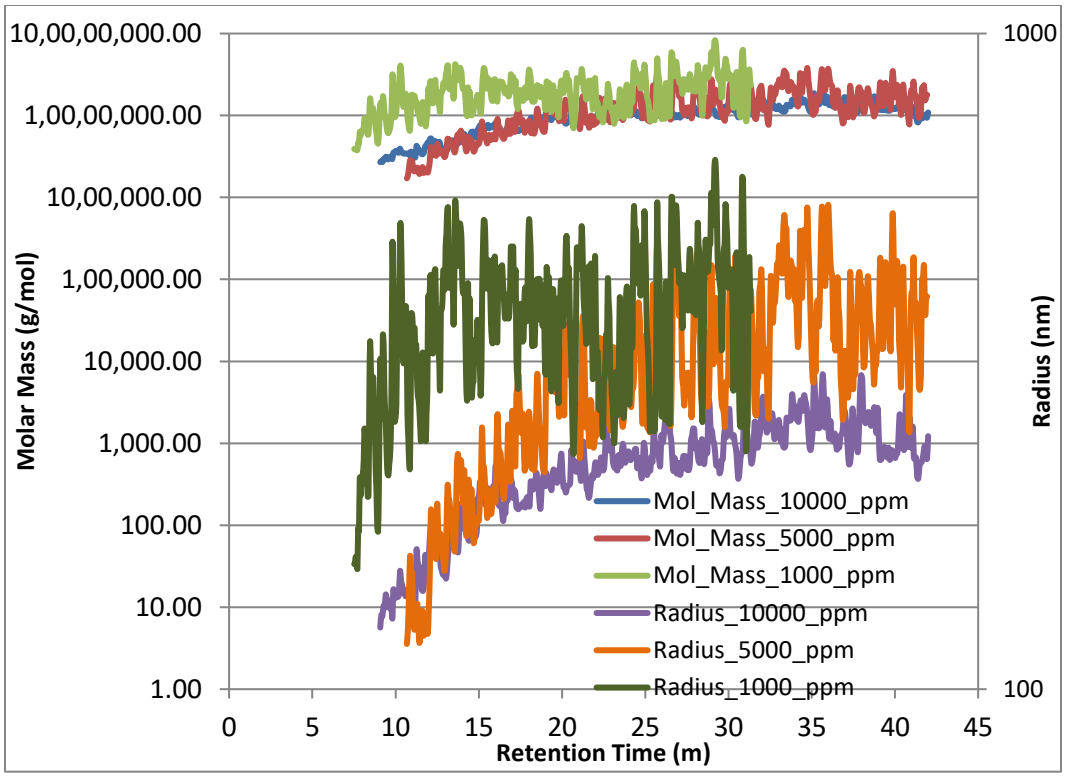

Figure 69: Molar Mass and Radius to Retention Time for Post Hydrolyzed 3630.

Radius values also decrease systematically as salinity increases. The Rw value in 1000 ppm salinity brine is 368.7 nm which reduces to 317.2 nm when salinity increases to 5000 ppm and further decreases to 218.2 nm when 10000 ppm salinity. Rn and Rw also show similar trend. The decrease in radius is due to charge shielding effect of added cation from the negative charge on the backbone of HPAM aggregate. Molar mass values and radius values on retention time for Post Hydrolyzed 3630 can be seen in Figure 69. Responses of Post Hydrolyzed 3630 under all salinity conditions can be seen in the same figure. Figure 70 shows conformational plot for Post Hydrolyzed 3630 under all three salinity conditions. It is observed that all the conformational slope values are between 0.4 to 0.511, it can be said that overall polymer conformation in the presence of salinity is branched

structure. It is obvious from observation that conformational value in 5000 ppm and 1000 ppm scenario is same. It means that the polymer exhibits same conformational behavior under 1000 ppm and 5000 ppm salinity scenario. It implies that salinity effect on Post Hydrolyzed 3630 is uniform i.e. it affects the polymer molecules in the similar fashion and only magnitude changes as salinity changes (as molar mass and radius value changes). As salinity further increases to 10000 ppm, slope value decreases to 0.4 which means that polymers become more branched/compacted as salinity increases from 5000 ppm to 10000 ppm.

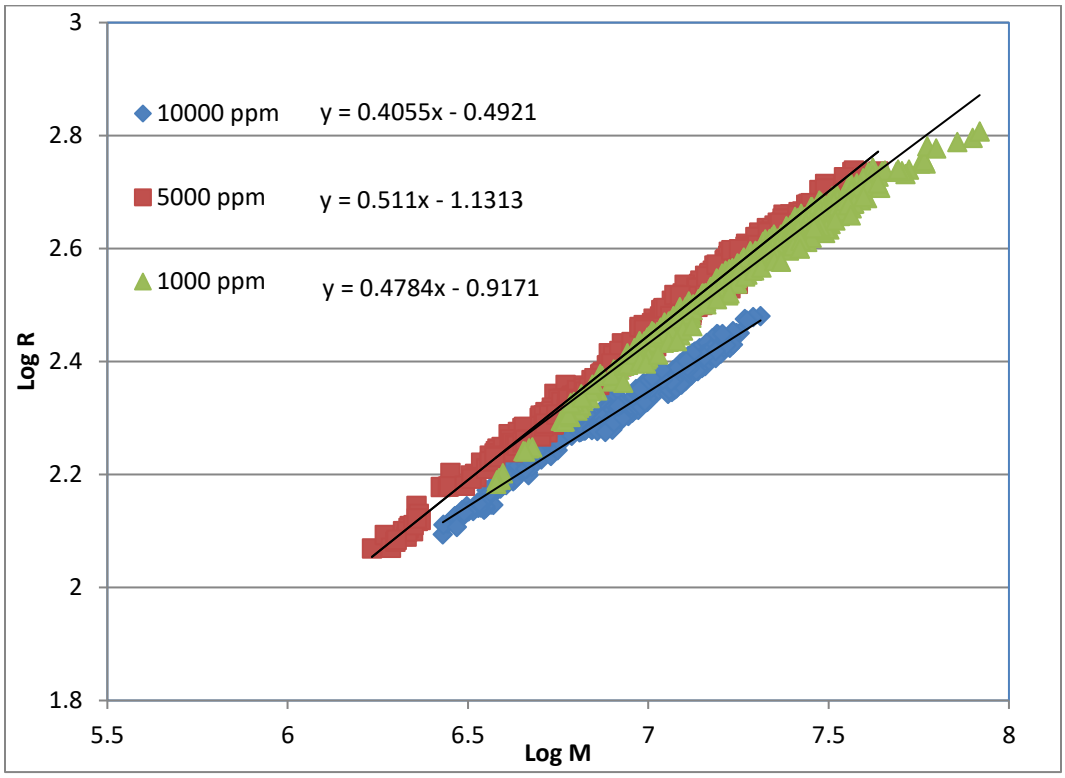

Figure 70: Conformation Plot for Post Hydrolyzed 3630.

Figure 71 shows cumulative mass fraction plot for Post Hydrolyzed 3630 under 1000 ppm, 5000 ppm, and 10000ppm salinity. It can be observed that cumulative

mass curve for all the salinity scenarios starts near to each other, but the curves end far from each other. The curve for 5000 ppm and 1000 ppm salinity displays similar characteristics. The cumulative mass curve for 10000 ppm displays smaller horizontal extent. The curve for 1000 ppm has the largest horizontal extend indicating broader molar mass distribution.

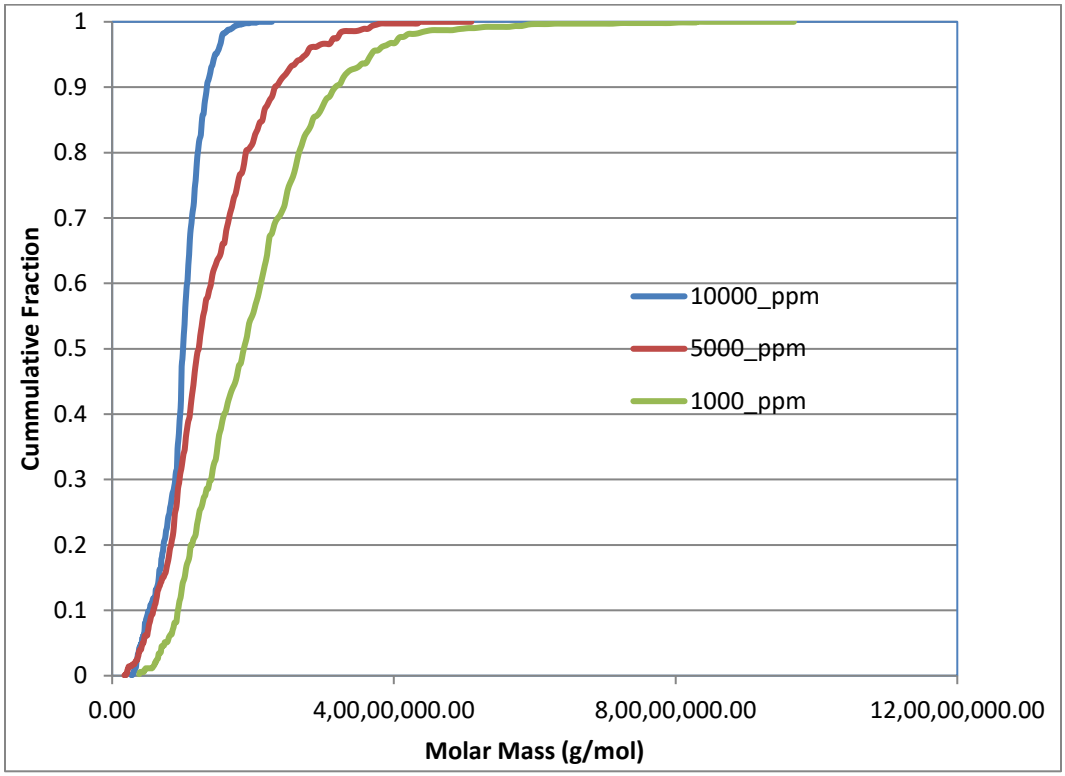

Figure 71: Cumulative Mass Fraction of Post Hydrolyzed 3630.

Differential mass fraction for Post Hydrolyzed 3630 under different salinity conditions is seen in Figure 72. One clear observation is a presence of a high peak in the curve of 10000 ppm case. It indicates a predominant presence of polymer aggregate with a mass around 1×10^7 g/mol. It showcases a narrow molar mass distribution for Post Hydrolyzed 3630 when the salinity is 10000 ppm. The curve

for 10000 ppm starts in-between 5000 ppm and 1000 ppm curve, but it ends before 5000 ppm and 1000 ppm curve. It is also seen that differential curve for 1000 ppm and 5000 ppm shows some similar characteristics. The curve for 5000 ppm and 1000 ppm differential curve shows same peak height, it signifies that extent of the presence of a single dominating polymer aggregate is same in both cases. Peak in 5000 ppm curve shows the dominant presence of polymer aggregate with molar mass 1×10^7 g/mol. Similar peak in 1000 ppm curve can be seen on the right of the peak in the curve of 5000 ppm.

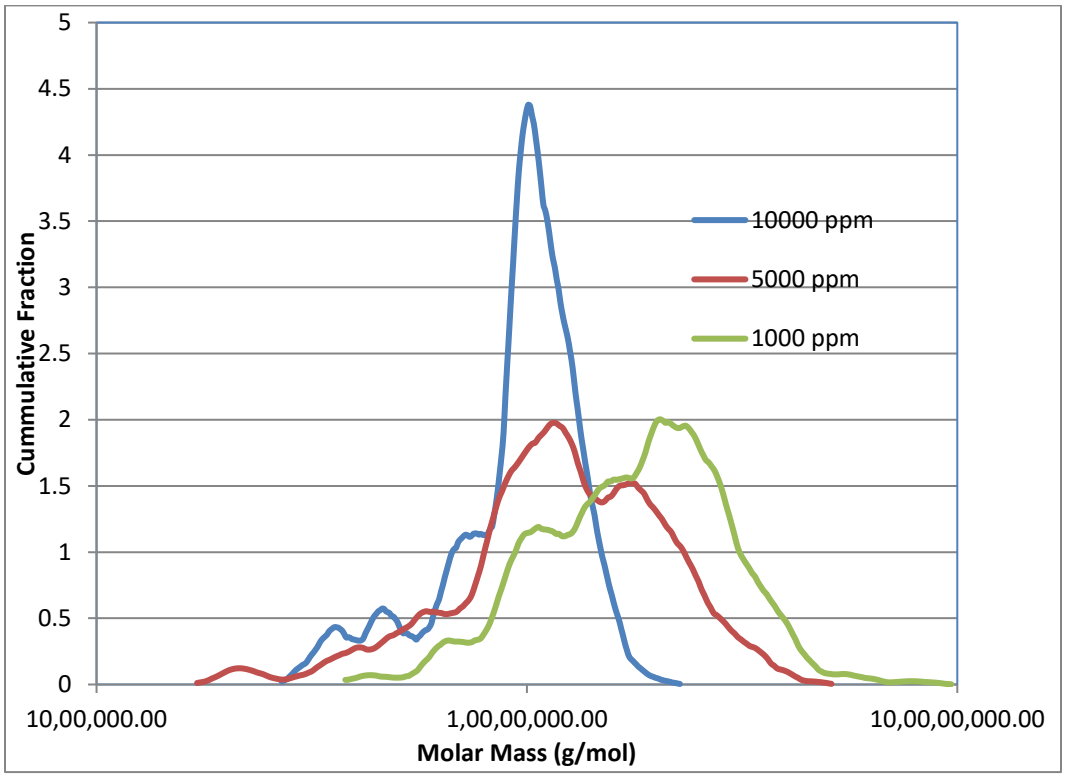

Figure 72: Differential Mass Fraction of Post Hydrolyzed 3630.

Cumulative radius fraction plot for Post Hydrolyzed 3630 under 1000 ppm, 5000 ppm, and 10000 ppm salinity can be seen in Figure 73. As seen in the figure, the

cumulative curve for 5000 ppm and 1000 ppm shows similar characteristics. The curve for 10000 ppm extends less horizontally; it indicates that Post Hydrolyzed 3630 has a shorter radius distribution. Similar to the cumulative mass fraction plot, in cumulative radius plot also curves for all salinity starts near to each other and then ends relatively far.

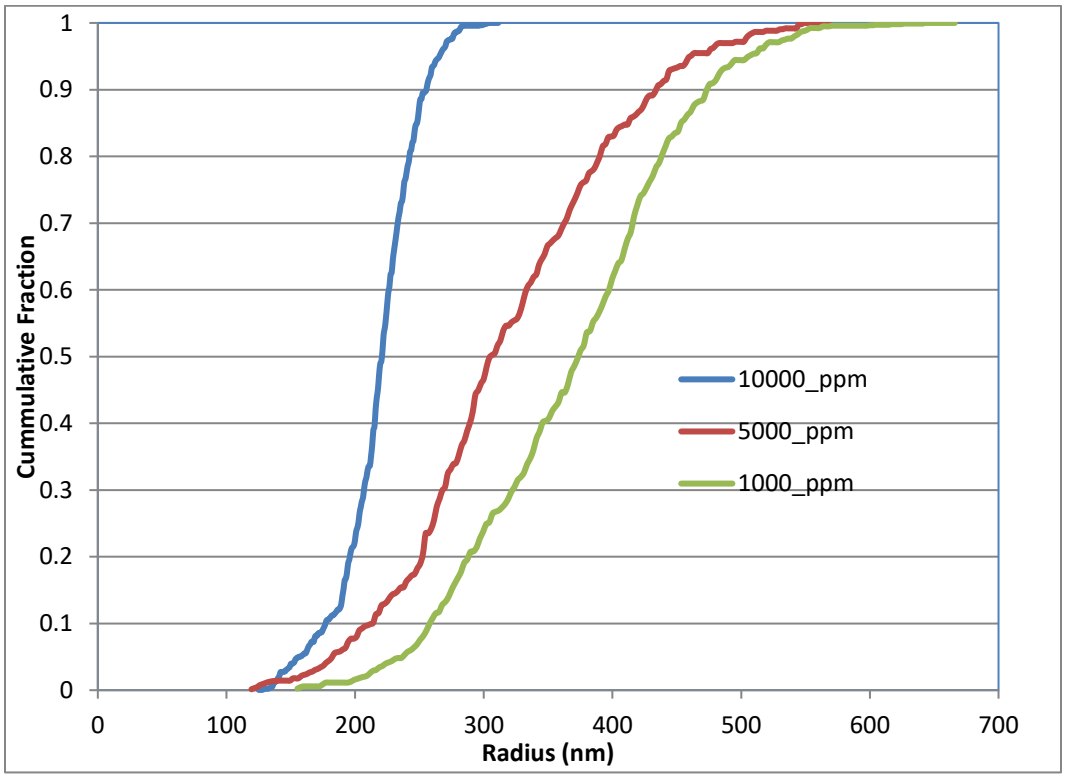

Figure 73: Cumulative Radius Fraction of Post Hydrolyzed 3630.

Figure 74 shows differential radius plot for Post Hydrolyzed 3630 in different salinity scenarios. One striking observation is the similarity between differential radius plot and differential mass plot for Post Hydrolyzed 3630. This similarity noticed reflects on the fact that polymer conformational behavior is similar; this is

validated from the conformational plot (Figure 70) where it is observed that slopes are between 0.4 and .51 with same slope value for 1000 ppm and 5000 ppm. In differential radius plot, the curve for 10000 ppm displays a large peak. It indicates the predominant presence of polymer aggregate with a radius around 220 nm -230 nm. The curve starts around 120 nm ends at around 300 nm. The curve for 5000 ppm and 1000 ppm shows more uniform distribution than 10000 ppm. A high is observed in 5000 ppm case around 280 nm -290 nm and in 1000 ppm a high is observed around 380 nm - 400 nm.

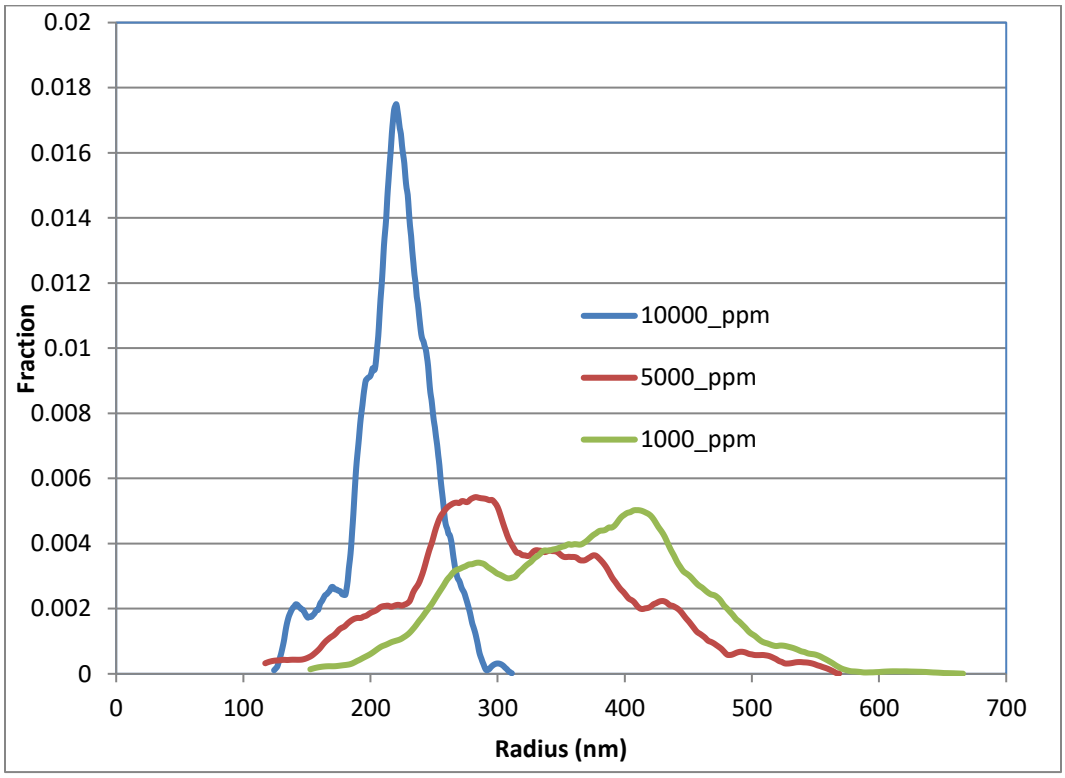

Figure 74: Differential Radius Fraction plot for Post Hydrolyzed 3630.

6.3.3 C 319

Molar mass and radius of C 319 under different salinity scenarios i.e. 1000 ppm, 5000 ppm and 10000 ppm can be seen in Table 14. It is clearly observed that molar mass of the C 319 clearly decreases as the salinity of the brine increases. Mw for the C 319 decreases from 72.2 × 10^6 g/mol in 1000 ppm brine to 54 × 10^6 g/mol in 5000 ppm. It further decreases from 54 × 10^6 g/mol to 24.67 × 10^6 g/mol in 10000 ppm. Mz also decreases from 89.4 × 10^6 g/mol to 60 × 10^6 g/mol when salinity increases from 1000 ppm to 5000 ppm; it further decreases to 29.46 × 10^6 g/mol in 10000 ppm brine. Mn in seen to increases marginally as salinity increases from 1000 ppm to 5000 ppm, it might be because of the nature of distribution of the molar mass.

Table 14: Molar Mass and Radius of C 319 under different salinity (mono-valent ion).

	Mn (g/mol)	**Mw (g/mol)**	**Mz (g/mol)**	**Rn (nm)**	**Rw (nm)**	**Rz (nm)**
1000 ppm	45.64 E+06	72.21 E+06	89.42 E+06	415.2	509.3	556.4
5000 ppm	47.45 E+06	54.08 E+06	60.12 E+06	333.2	350.1	364.9
10000 ppm	19.90 E+06	24.67 E+06	29.46 E+06	272.0	298.7	323.7

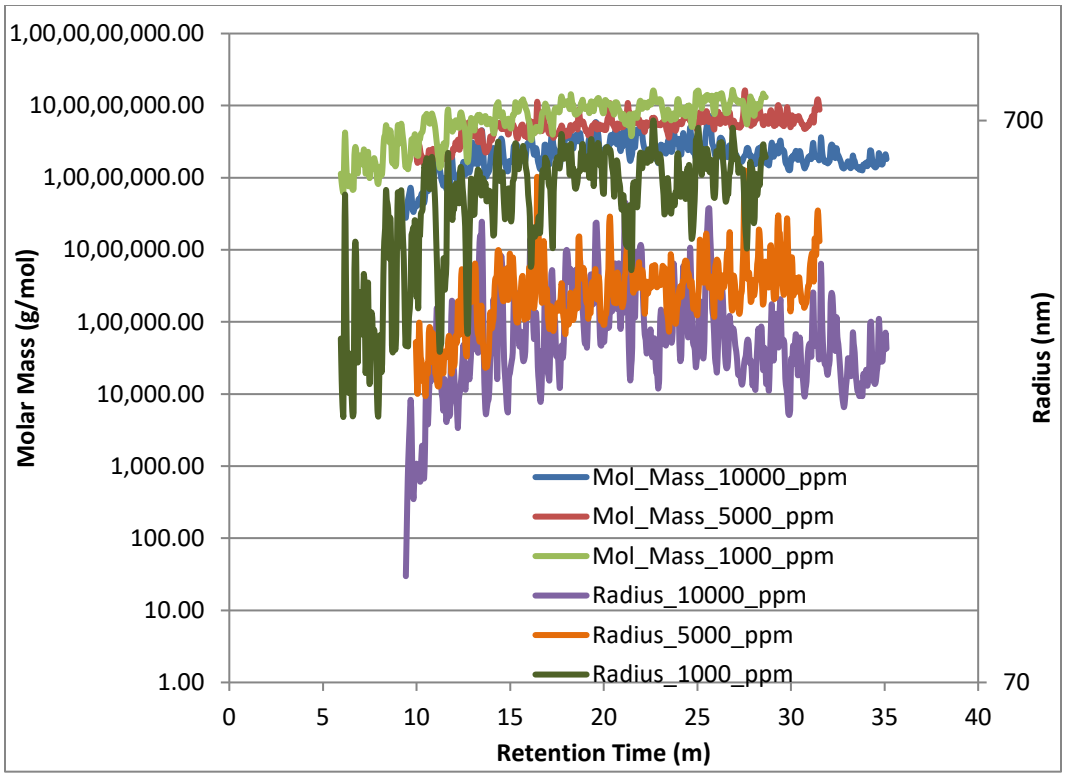

Figure 75: Molar Mass and Radius to Retention Time for C 319.

Radius also decreases as the salinity of the brine increases. Rw decreases from 509.3 nm in 1000 ppm to 350.1 nm in 5000 ppm and further decreases to 298.7 nm in 10000 ppm. Rz and Rn also decreases as salinity increases. Rz decreases from 556.4 nm to 364.9 nm and then to 323.7 as salinity increases. The shielding effect due to Na+ ion leads the polymer aggregate to coil more which results in decreases value of radius with increase in salinity. Figure 75 shows molar mass and radius to retention time for C 319 for all the salinity case. Conformational plot for C 319 for all salinity is observed in Figure 76. It can be observed that slope values for all three cases are in between 0.33 and .39. It is a very narrow range which strongly suggests that C 319 conforms in a similar way all the salinity cases. Also, the overall

conformation for C 319 in all the salinity cases is highly compacted and near sphere-like conformation. Increasing concentration of the monovalent ion does not seem to be a major factor on the effect of polymer conformation. However, salinity significantly coils the polymer which results in low values for conformation slope. C 319 shows the value of 0.33 in 1000 ppm, .34 in the case of 5000 ppm salinity and finally 0.39 when the salinity increase to 10000 ppm.

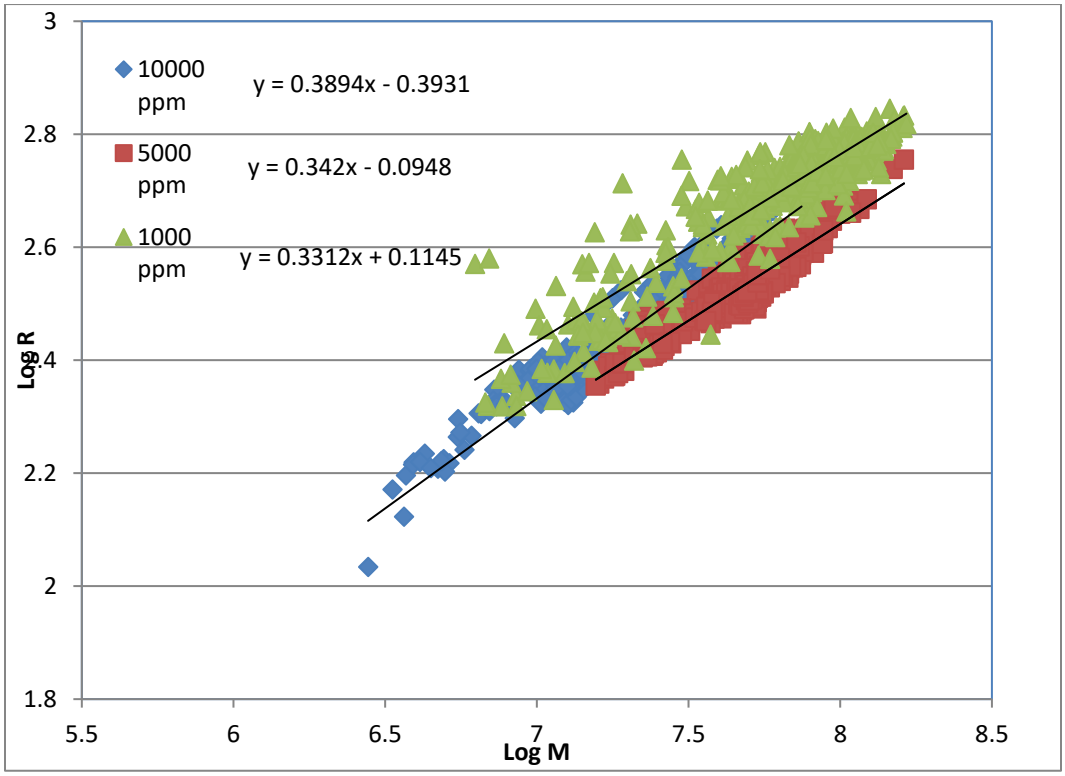

Figure 76: Conformation Plot for C 319.

Figure 77 shows cumulative mass fraction plots for C 319 in different salinity case. As seen in the figure cumulative molar mass curve for 1000 ppm salinity has the maximum horizontal extent. A similar trend was also observed in 3630 S and Post

Hydrolyzed 3630 where cumulative molar mass curve exhibits longest horizontal extend in 1000 ppm.

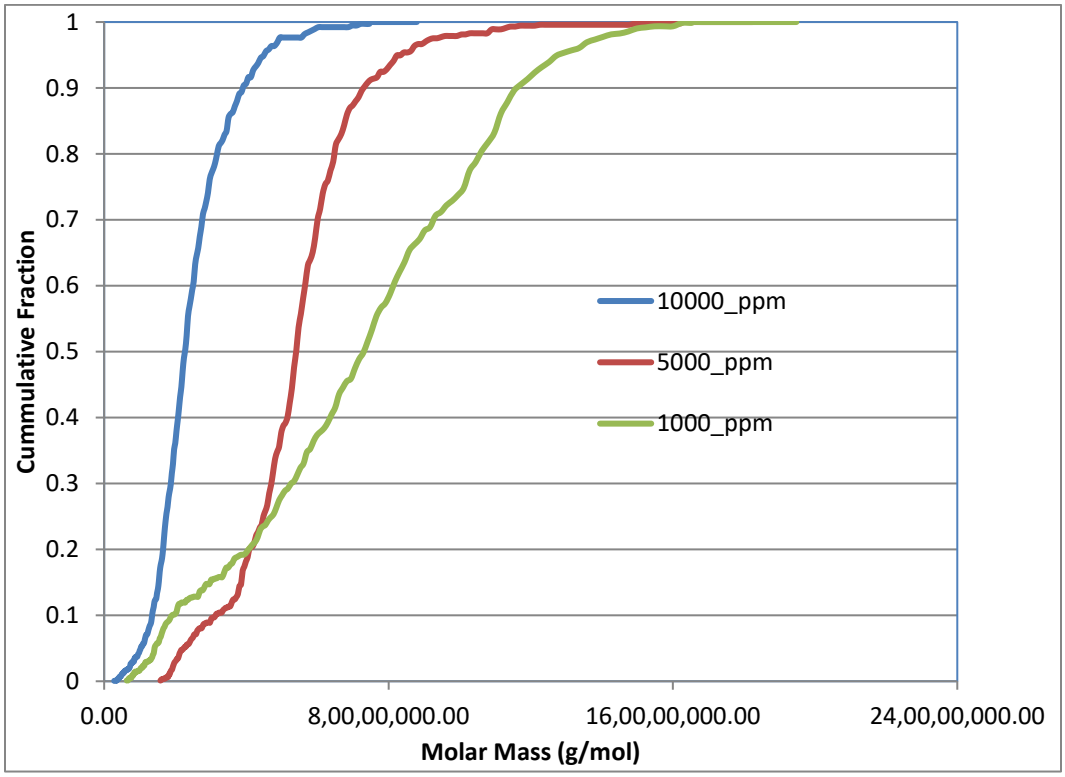

Figure 77: Cumulative Mass Fraction of C 319.

Differential mass fraction curve for different salinity for C 319 can be seen in Figure 78. It can be seen that the curve for 5000 ppm has the narrowest molar mass distribution. A large spike is clearly observable in the curve for 5000 ppm; it signifies that a particular polymer aggregates dominants in the mass distribution. The curve for 10000 ppm also shows a peak which is on the left of the peak observed in 5000 ppm. The curve for 10000 ppm ends near 1×10^8 g/mol. Finally, the curve for 1000 ppm is observed to have a peak on the right of the peak observed in 5000 ppm. It is to be observed that the peak shifts towards the right as the salinity

of the brine increases. It means that as the salinity increases, the polymer aggregate with lower molar mass dominants the molar mass distribution.

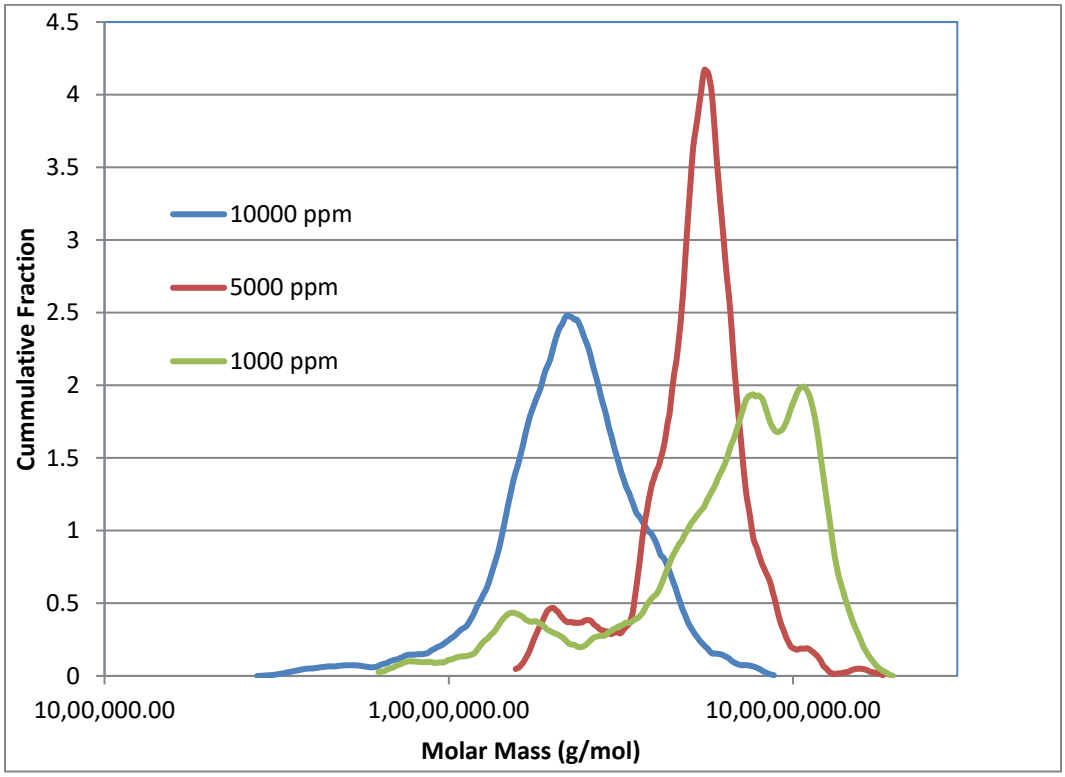

Figure 78: Differential Mass Fraction of C 319.

Figure 79 shows cumulative radius fraction for C 319 for 1000 ppm, 5000 ppm, and 10000 ppm. From the graph, it is observable that cumulative radius curve for 1000 ppm has the largest horizontal extent. Similar observation was noticed in a cumulative molar mass curve as well. It signifies that C 319 has the widest radius distribution. The curve for 10000 ppm and 5000 ppm shows similar curve characteristics.

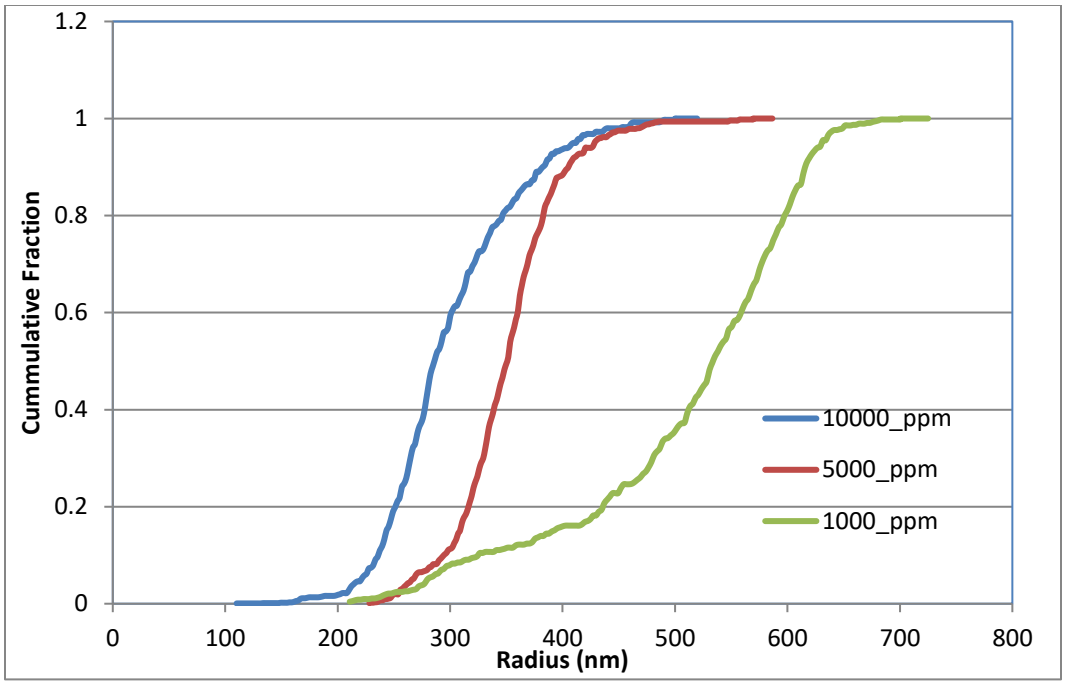

Figure 79: Cumulative Radius Fraction of C 319.

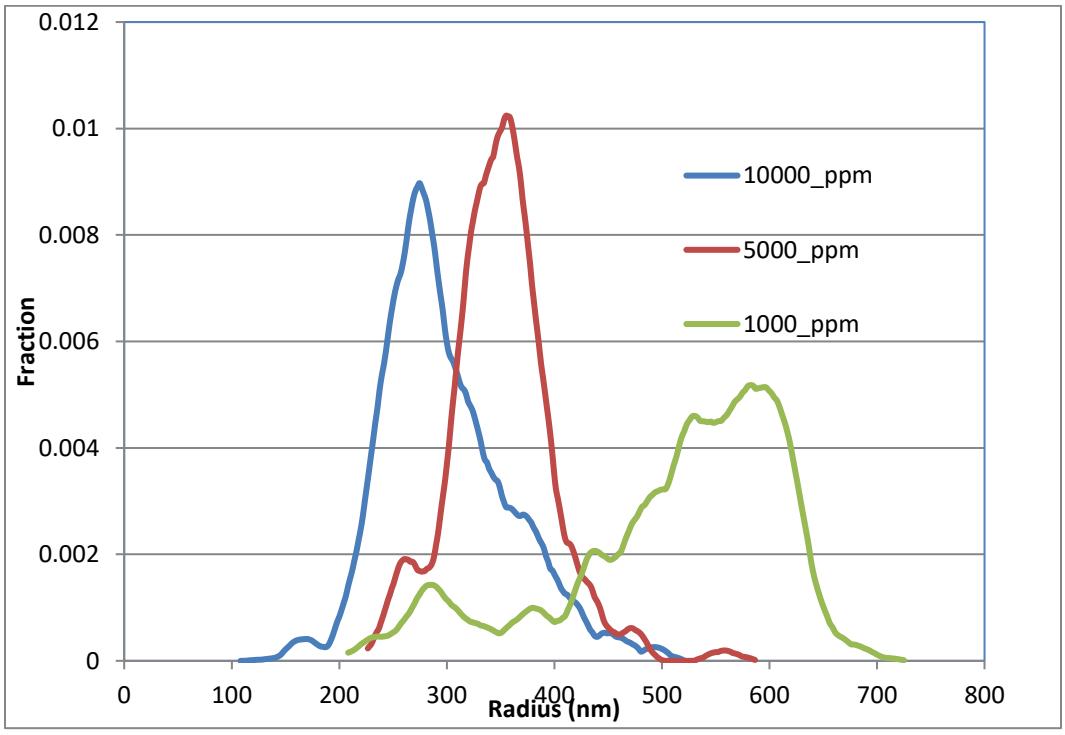

Figure 80: Differential Radius Fraction plot for C 319.

Differential radius fraction for C 319 in different salinity can be seen in Figure 80. As seen in the figure, differential radius curve for 10000 ppm and 5000 ppm shows peaks of similar magnitude. The curve for 5000 ppm shows the tallest peak which is observed near 370 nm – 380 nm. It shows that polymer aggregate with 370 nm – 380 nm radiuses dominant in the polymer species in 5000 ppm salinity. It also shows the narrowest distribution of radius; it was also seen in the differential mass fraction plot in which narrowest distribution was seen in 5000 ppm salinity. In the curve of 10000 ppm, a peak is observed near 270 nm – 280 nm. Also, it is to be noticed that peak in 10000 ppm is a little bit broader than the peak observed in 5000 ppm. In 1000 ppm the differential radius curve starts from 200 nm and ends around 710 nm making it the broadest radius distribution. A high can be seen around 550 nm – 600 nm, which means that polymer aggregate with higher radius dominant in low salinity.

6.1 Summary

3630 S

Molar mass decreases as the salinity of the environment increases. The radius of polymer aggregate decreases as the salinity of the environment increases. Effect of salinity on molar mass and radius is preeminent in low to medium salinity environment, and salinity effect tends to cease in high salinity. Polymer shows linear most conformation in 5000 ppm salinity. Polymer exhibits relatively broad and linear molar mass and radius distribution in low salinity brine. Molar mass distribution tends to get peakier as salinity increases. Radius distribution tends to get narrower and peakier as salinity increases.

Post Hydrolyzed 3630

Molar mass value changes with a change in environment salinity. Molar mass values show clear decrement with increasing salinity. Radius value changes with a change in salinity in the environment. Radius values decrease as salinity increases. The way in which Na+ ion effect polymer is similar for 5000 ppm and 1000 ppm with magnitude increasing with salinity. The polymer is more compacted in high salinity environment. In low salinity environment, polymer aggregate with high molar mass and high radius are in the majority.

C 319

Molar mass decreases as the salinity of the brine increases. Radius value changes with the salinity of the brine. Radius values decrease as salinity increases. This effect maximizes as salinity increases. Polymer conformation does not change with a change in salinity. Polymer conforms in highly branched/ near spherical conformation in all salinity. Molar mass and radius value for the dominant polymer aggregate increases as salinity decreases.

Chapter 7

Effect of Divalent ion on HPAM

7.1 Polymer Used

Two different types of polymers namely 3630 S and Post Hydrolyzed 3630. SNF SAS supplied all the polymers in dry powder form. These polymers are anionic and water soluble with a degree of hydrolysis of 25-30 mol %.

7.2 Solution preparation

Solutions of different salinity were made by adding specific quantity chemicals into the deionized water. Sodium chloride(NaCl) and Calcium chloride(CaCl2) were used to make a solution of different salinity. Four different solutions with different ion compositions were prepared. Two solutions were prepared with 1000 ppm salinity with different ion composition. In one brine, 1000 ppm salinity was made by CaCl2 alone and in other brine 500 ppm of NaCl and 500 ppm of CaCl2. Other two solutions were made of 5000 ppm salinity. Out of which, one brine was made with CaCl2 and in other NaCl and CaCl2 was used. NaCl was supplied by Fisher Tropsch. Deionized water was used to make a brine by adding the appropriate amount of salt. Salinity and ion composition is given in Table 15. Polymers were added to the solutions and were mixed with using a magnetic stirrer at 260 rpm for

24 hours. The polymer concentration of 2000ppm (2 g/liter) was used. All the sample solutions were clear after three hours of mixing.

Table 15: Different Brine Composition.

Brine Number	Total Salinity (ppm)	Sodium Chloride (ppm)	Calcium Chloride (ppm)
1	1000	0	1000
2	1000	500	500
3	5000	0	5000
4	5000	2500	2500

7.3 Results and Observations

7.3.1 3630 S

The molar mass value and radius value for 3630 S under different salinity scenarios can be seen in Table 16. In the table results for 1000 ppm NaCl and 5000 ppm NaCl are also shown, these results are taken from the previous section.

Table 16: Molar Mass and Radius of 3630 S under different salinity (mono-di valent ion)

	Mn (g/mol)	Mw (g/mol)	Mz (g/mol)	Rn (nm)	Rw (nm)	Rz (nm)
1000 ppm NaCl	14.96 E+06	18.54 E+06	20.20 E+06	322.6	361.6	395.2

500 ppm NaCl + 500 ppm CaCl2	14.32 E+06	18.82 E+06	23.90 E+06	248.1	286.1	324.3
1000 ppm CaCl2	15.28 E+06	18.42 E+06	21.49 E+06	223.5	248.2	270
5000 ppm NaCl	10.85 E+06	11.43 E+06	12.01 E+06	200.7	207.3	213.9
2500 ppm NaCl + 2500 ppm CaCl2	10.47 E+06	10.75 E+07	10.97 E+06	175.4	178.4	180.3

It is observed from the table that molar mass for 1000 ppm salinity under different scenarios remains constant, it implies that presence of mono valent (NaCl) or di-valent (CaCl2) doesn't affect the molar mass of the HPAM I when the salinity is constant. Mw is observed to be 18.54×10^6 g/mol in 1000 ppm NaCl brine which is close to 18.82×10^6 g/mol, which is observed in "500 ppm NaCl+500 ppm CaCl2" brine. In 1000 ppm CaCl2 case Mw of 18.42×10^6 g/mol is observed. Mn in 1000 ppm NaCl is 14.96×10^6 g/mol, 14.32×10^6 g/mol in 500 ppm NaCl 500 ppm CaCl2, 15.28×10^6 g/mol in 1000 ppm CaCl2. Contrary to trend observed in molar mass, radius values decrease as CaCl2 content increases in the brine. In 1000 ppm NaCl, the value of Rw is 361.6 nm. Rw value then decreases to 286.1 nm in "500 ppm NaCl+500 ppm CaCl2" brine and then further reduces to 248.2 nm in 1000 ppm CaCl2 case. The value of Rz also decreases from 395.2 nm in 1000 ppm NaCl to 324.3 nm in "500 ppm NaCl+500 ppm CaCl2" brine to 270 nm in 1000 ppm CaCl2 brine. Na+ and Ca2+ both will have shielding effect on negative charge of polyacrylamide backbone which will result in polymer coiling. However, Ca2+

has potential to bind to negative sites on the polymer chain (Thomas, 2012) (Axelos, 1994), this binding can be between negative group (carboxyl) on the same molecule or between negative group of different adjust polymer chain. Intramolecular binding will lead to rapid decrease in hydrodynamic volume of the polymer aggregate. Flory et al (Flory, 1954) demonstrated that Ca2+ caused a stronger polymer coiled conformation than the corresponding concentration of Na+ beyond the expected coiling due to shielding effect. Results in Table 16 is in accordance to the observation made by Flory, at same salinity, radius is significantly smaller in Ca2+ than Na+. Significant decrease in radius indicates intramolecular binding of negative sites on polymer backbone with Ca2+ ion.

The value of Mw in 5000 ppm NaCl is 11.43×10^6 g/mol which reduces marginally to 10.75×10^6 g/mol in 2500 ppm NaCl 2500 ppm CaCl2 brine. It can again be seen that presence of di-valent ion does not have a significant effect on the molar mass of 3630 S. However, radius value decreases as CaCl2 content increases. Rw reduces from 207.3 nm in 5000 ppm NaCl to 178.4 nm in 2500 ppm NaCl 2500 CaCl2. A similar trend is also observed in Rn and Rz as well. Rn reduces from 200.7 nm to 175.4 nm, and Rz reduces from 213.9 nm to 180.3 nm.

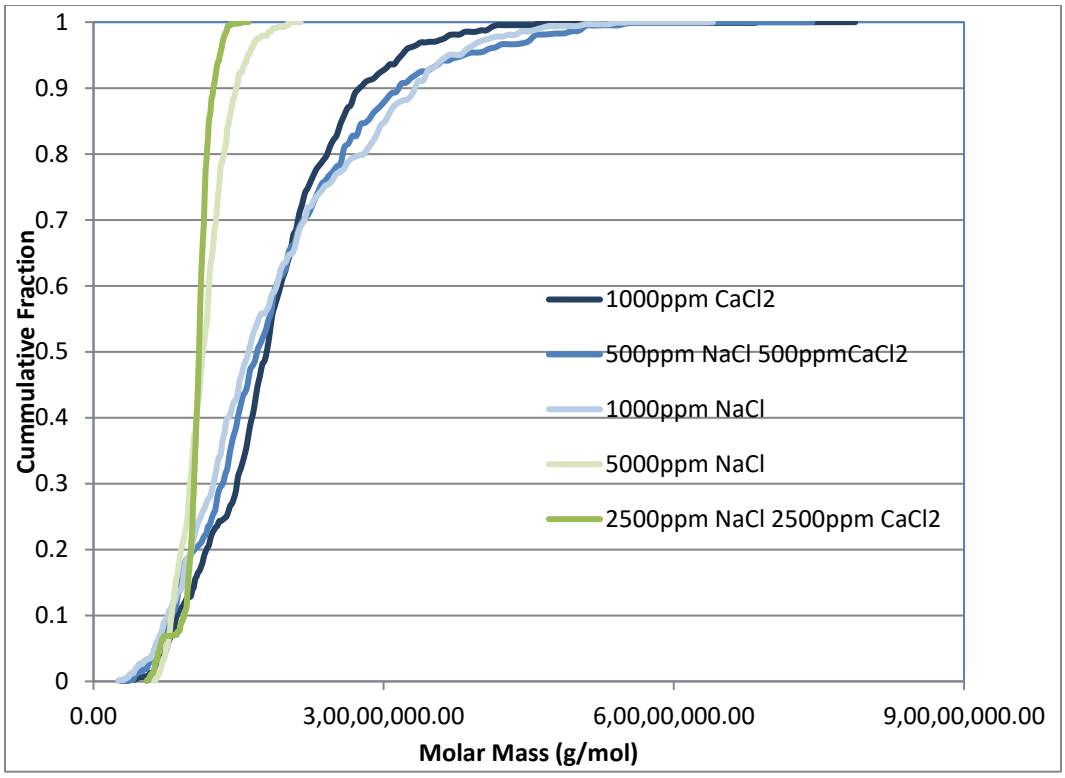

Figure 81: Cumulative Mass Fraction of 3630 S under different salinity.

Figure 81 shows cumulative mass fraction curves for 3630 S under different salinity scenarios. As seen in the plot, cumulative curves for 1000 ppm NaCl, "500 ppm NaCl+500 pp m CaCl2", 1000 ppm CaCl2 are close to each other, curves start from similar molar mass values and ends near to each other. All the curve overlay each other briefly from around cumulative mass fraction of 0.6 to 0.7. The curves for 5000 ppm NaCl and "2500 ppm NaCl+2500 ppm CaCl2" are close to each other. The curves overlap each other from a cumulative fraction of 0.3 to 0.5. Curves are significantly steeper than the curves of 1000 ppm salinity. It is also to be noticed that all the curves are jumbled together in a narrow range of molar mass till cumulative mass fraction of 0.2.

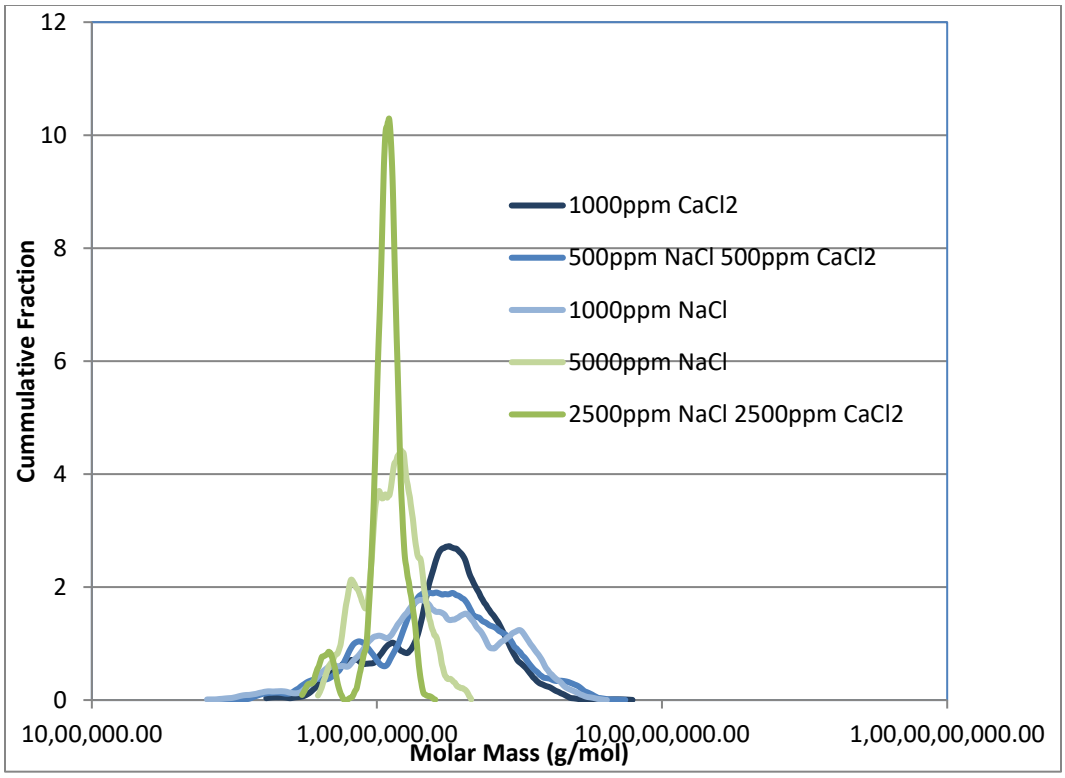

Figure 82: Differential Mass Fraction of 3630 S under different salinity.

The differential mass fraction curves for 3630 S under different salinity conditions can be seen in Figure 82. Curve with blue shade represents 1000 ppm salinity scenarios. It can be seen that all three curves in 1000 ppm salinity case exhibit similar molar mass distribution range. The curve for 1000 ppm CaCl2 shows a peak which is stronger than "500 ppm NaCl+500 CaCl2" and 1000 ppm NaCl. The curve for 500 ppm NaCl 500 ppm CaCl2 shows a little high in comparison to 1000 ppm NaCl brine. The peak for the 1000 ppm salinity scenarios is observed at the similar molar mass range. In all three 1000 ppm salinity i.e. 1000 ppm NaCl, "500 ppm NaCl+500 ppm CaCl2" and 1000 ppm CaCl2 brine, the dominant polymer aggregate has similar molar mass.

In the case of 5000 ppm NaCl and “2500 ppm NaCl+2500 CaCl2”, extend of molar mass distribution is similar to each other. A sharp and strong peak are observed in “2500 ppm NaCl+2500 ppm CaCl2” indicating that dominant polymer aggregate has a molar mass around 1×10^7 g/mol. A peak is also observed near 1×10^7 g/mol in the curve of 5000 ppm NaCl brine. The vertical extent of the peak for “2500 ppm NaCl+2500 ppm CaCl2” is more than two times than that of 5000 ppm NaCl, this signifies the extent of the dominance of a specific polymer aggregate in the distribution.

Figure 83 shows cumulative radius fraction plot for 3630 S for different 1000 ppm salinity scenarios and different 5000 ppm salinity scenarios. It can be observed that unlike in cumulative mass fraction plot, cumulative radius curves for 1000 ppm salinity scenarios are not very close to each other. The curves for 1000 ppm NaCl, “500 ppm NaCl+500 ppm CaCl2” and 1000 ppm CaCl2 starts near to each other. As the curves evolve, the gap between 1000 ppm CaCl2 curve and “500 ppm NaCl+ 500 ppm CaCl2” curve keeps on increasing and both the curve finally ends far from each other. The curve for 1000 ppm NaCl is in between the curve of 1000 ppm CaCl2 curve and 500 ppm NaCl 500 ppm CaCl2 curve. The curve of 1000 ppm NaCl overlaps the curve of 1000 ppm CaCl2 from a cumulative fraction of 0.15 to 0.4.

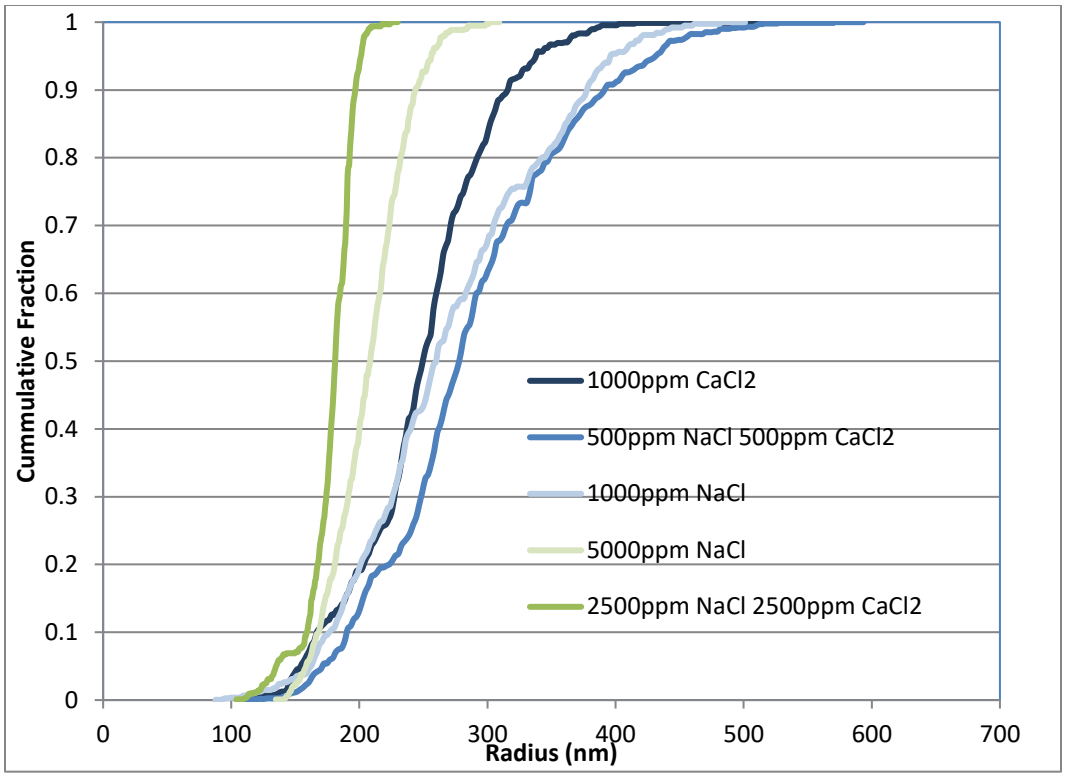

Figure 83: Cumulative Radius Fraction of 3630 S under different salinity.

As it can be observed from the plot that curves of 5000 ppm salinity are steeper than the curves of the 1000 ppm salinity scenarios. It indicates that polymer exhibits a shorter radius distribution in 5000 ppm salinity environment. It can be observed that curve for "2500 ppm NaCl+2500 ppm CaCl2" is steeper than the curve of 5000 ppm NaCl. Both the curve starts near to each other, as the curves evolve distance between the two curves keep on increasing and finally ends relatively far from each other.

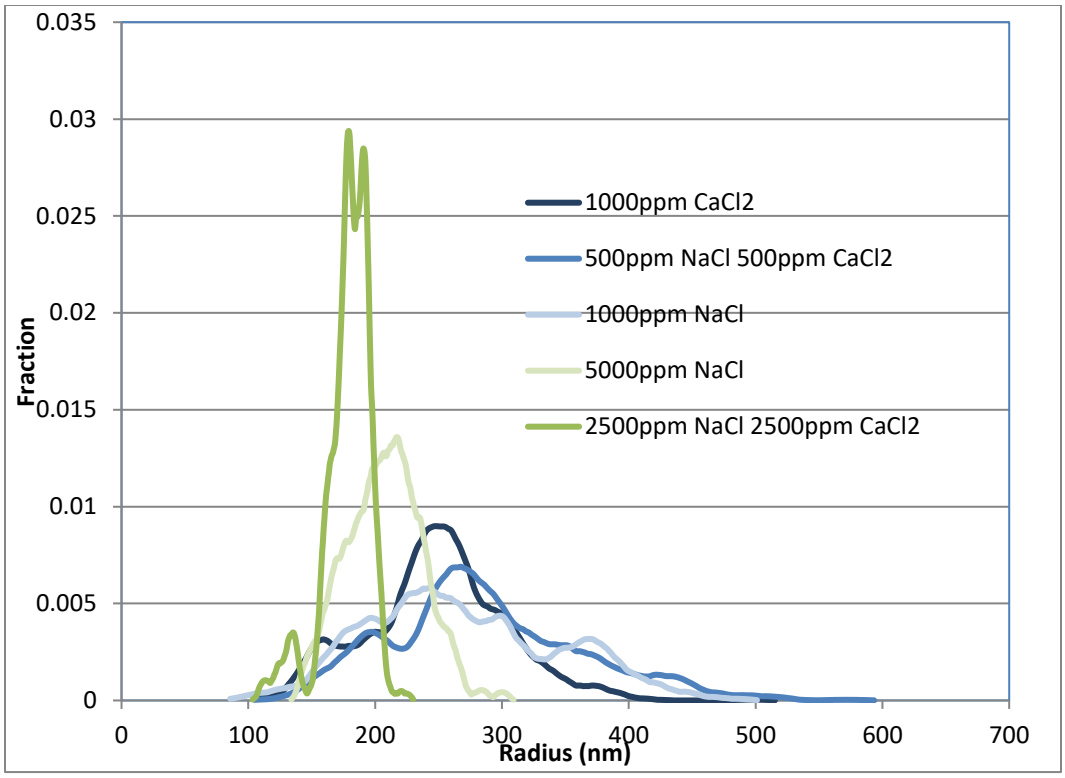

Figure 84: Differential Radius Fraction of 3630 S under different salinity.

Figure 84 shows differential radius fraction curve for 3630 S under different salinity scenarios i.e. 1000 ppm and 5000 ppm. The differential radius curve in blue shade represents 1000 ppm salinity scenarios. It can be seen that curve of 1000 ppm NaCl exhibits more uniform distribution than other 1000 ppm salinity cases. The curve of 1000 ppm CaCl2 shows a peak around 250 nm indicating the radius for the dominant polymer aggregate. It also has the narrowest distribution in 1000 ppm salinity cases. It can be observed that the high observed in "500 ppm NaCl+500 ppm CaCl2" is also around 260 nm which is very near to that of 1000 ppm CaCl2 case. It means that dominant polymer aggregates in both the cases have radius value close to each other.

A sharp and clear peak is observed in “2500 ppm NaCl+2500 ppm CaCl2” curve. This peak is observed around 180 nm – 190 nm which means that the polymer aggregate which dominates in the “2500 ppm NaCl+2500 ppm CaCl2” brine is around 140 nm- 150 nm. It is to be noted that the vertical extent observed in the peak is double to that of vertical extent observed in the peak of 5000 ppm NaCl case. The peak observed in 5000 ppm NaCl case is around 210 nm. Also, its peak has a broader base than the peak seen in “2500 ppm NaCl+2500 ppm CaCl2”. The radius distribution is broader in 5000 ppm NaCl then the “2500 ppm NaCl+2500 ppm CaCl2”.

7.3.2 Post Hydrolyzed 3630

The molar mass and radius values for Post Hydrolyzed 3630 in the presence of mono-valent and di-valent ion in different concentration can be seen in Table 17. The data for the salinity of 1000 ppm of NaCl and 5000 ppm of NaCl is same as in the previous section.

Table 17: Molar Mass and Radius of Post Hydrolyzed 3630 under different salinity (mono-di valent ion)

	Mn (g/mol)	**Mw (g/mol)**	**Mz (g/mol)**	**Rn (nm)**	**Rw (nm)**	**Rz (nm)**
1000 ppm NaCl	15.56 E+06	19.81 E+06	24.49 E+06	326.4	368.7	407.3
500 ppm NaCl + 500 ppm CaCl2	13.58 E+06	14.74 E+06	11.10 E+06	259.8	272.3	285.1
1000 ppm CaCl2	11.10 E+06	11.99 E+06	13.04 E+06	212.9	222.4	233.1
5000 ppm NaCl	9.978 E+06	13.58 E+06	17.12 E+06	267.8	317.2	359.4
2500 ppm NaCl + 2500 ppm CaCl2	9.339 E+06	9.583 E+06	9.780 E+06	160.1	162.4	164.1
5000 ppm CaCl2	8.545 E+06	8.707 E+06	8.874 E+06	140.9	142.1	143.3

It can be seen in 1000 ppm salinity molar mass (Mw) varies between 19.81×10^6 g/mol and 12×10^6 g/mol. The value of Mw is 19.81×10^6 g/mol in 1000 ppm of

NaCl, and it decreases to 14.74 × 10^6 g/mol when CaCl2 is added in equal proportion to NaCl. It further decreases to 11.99 × 10^6 g/mol when CaCl2 achieved the salinity of 1000 ppm. It is evident from the observation that effect of divalent ion is significant of the molar mass of Post Hydrolyzed 3630. A similar trend is observed in radius values as well. It decreases from 368.7 nm in 1000 ppm NaCl to 272.3 nm in "500 ppm NaCl+500 ppm CaCl2". The decrement in radius is significant in the presence of divalent calcium ions. It further reduces to 222.4 nm in the 1000 ppm CaCl2. A similar trend is also observed in Rn and Rz.

Similarly, in the case of 5000 ppm salinity, the effect of divalent ion is clearly seen. When the salinity is 5000 ppm NaCl, molar mass is 13.58 × 10^6 g/mol which decreases to 8.7 × 10^6 g/mol when the salinity is 5000 ppm of CaCl2. The molar mass in between is 9.58 × 10^6 g/mol which is observed when 5000 ppm salinity is achieved by 2500 ppm NaCl and 2500 CaCl2. Even at higher salinity effect of divalent ion is more than prominent then mono valent ion. No significant decrease in molar mass is observed when salinity changes from 5000 ppm NaCl to "2500 NaCl+2500 CaCl2", however, radius values decreases for the same change in brine. The radius decreases from 317 nm to 162.4 nm. A similar trend is also observed in Rn and Rz. Radius further decreases to 142.1 nm in 5000 ppm CaCl2. Molar mass also reduces to 8.7 × 10^6 g/mol in 5000 ppm CaCl2 case.

It is also to be noted that molar mass and radius decreases as CaCl2 content increases in the brine. At 500 ppm CaCl2, molar mass is 14.74× 10^6 g/mol with a radius of 272.3 nm, it further decreases to 11.99× 10^6 g/mol and 222.4 nm when salinity is 1000 ppm CaCl2. At 2500 ppm of CaCl2 molar mass is 9.58× 10^6 g/mol

with a radius of 162.4 nm and it decreases to the molar mass of 8.7× 10^6 g/mol and radius of 142.1 nm when CaCl2 increases to 5000 ppm. It can be observed that effect of incremental CaCl2 is demised out.

Shielding effect between negative charge on polymer aggregate and cation (Na+ and Ca2+) leads to decrease in radius values. Divalent ion such as Ca2+ can also result in intramolecular binding which leads to increased polymer coiling. The difference between radius values at 1000 ppm salinity for Na+ and Ca2+ can be explained by intramolecular binding by Ca2+.

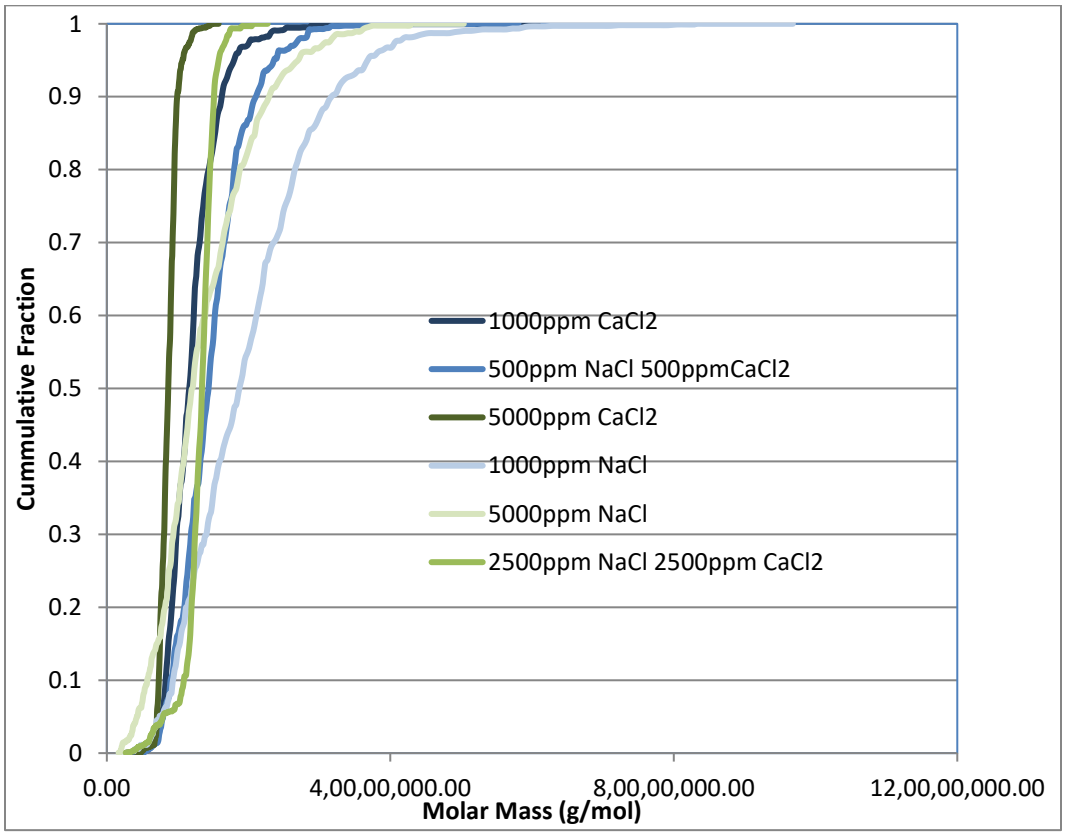

Figure 85: Cumulative Mass Fraction of Post Hydrolyzed 3630 under different salinity.

Figure 85 shows cumulative molar mass fraction for Post Hydrolyzed 3630 under different salinity scenarios. The cumulative curves in blue shades represent 1000 ppm salinity. As seen in 1000 ppm NaCl case, the cumulative curve has the broadest horizontal extent. The curve for 1000 ppm salinity with 500 ppm NaCl and 500 ppm CaCl2 is steeper than 1000 ppm NaCl curve indicating that presence of CaCl2 significantly changes cumulative curve for molar mass. It can be seen that both the curve overlaps till fraction of 0.2. The cumulative fraction curve for 1000 ppm CaCl2 is also steeper than the curve for 1000 ppm NaCl. The curve for 1000 ppm CaCl2 and "500 ppm NaCl+500 ppm CaCl2" have similar curve characterizes, and both the curve ends close to each other.

The curve for the salinity of 5000 ppm NaCl extends longest horizontally among different scenarios of 5000 ppm salinity. It can be seen that the curve for 5000 ppm CaCl2 is steeper than 5000 ppm NaCl curve. It is also a bit steeper than 1000 ppm CaCl2 curve. Also, the curve for "2500 ppm NaCl+2500 CaCl2" is steeper than 5000 ppm NaCl and is similar to 5000 ppm CaCl2. The curve for 5000 ppm CaCl2 and "2500 ppm NaCl+2500 ppm CaCl2" almost run parallel to each other and are very close to each other suggesting that the incremental effect of CaCl2 with increasing CaCl2 concentration decreases. This conclusion is also sustained by noticing that gap between the curve decreases i.e. the gap between 1000 ppm CaCl2 and "500 ppm NaCl+500 ppm CaCl2" curve and the gap between 5000 ppm CaCl2 and "2500 ppm NaCl+2500 CaCl2".

It can be observed that cumulative mass curve got steeper in the presence of CaCl2. It can be observed that cumulative mass curve was broad in 1000 ppm NaCl and 5000 ppm NaCl salinities. The curve gets steeper as CaCl2 content increases in the brine. Also, it is to be noticed that curve shifts towards positive y-axis as salinity increases, indicating that molar mass value decreases as CaCl2 content increases.

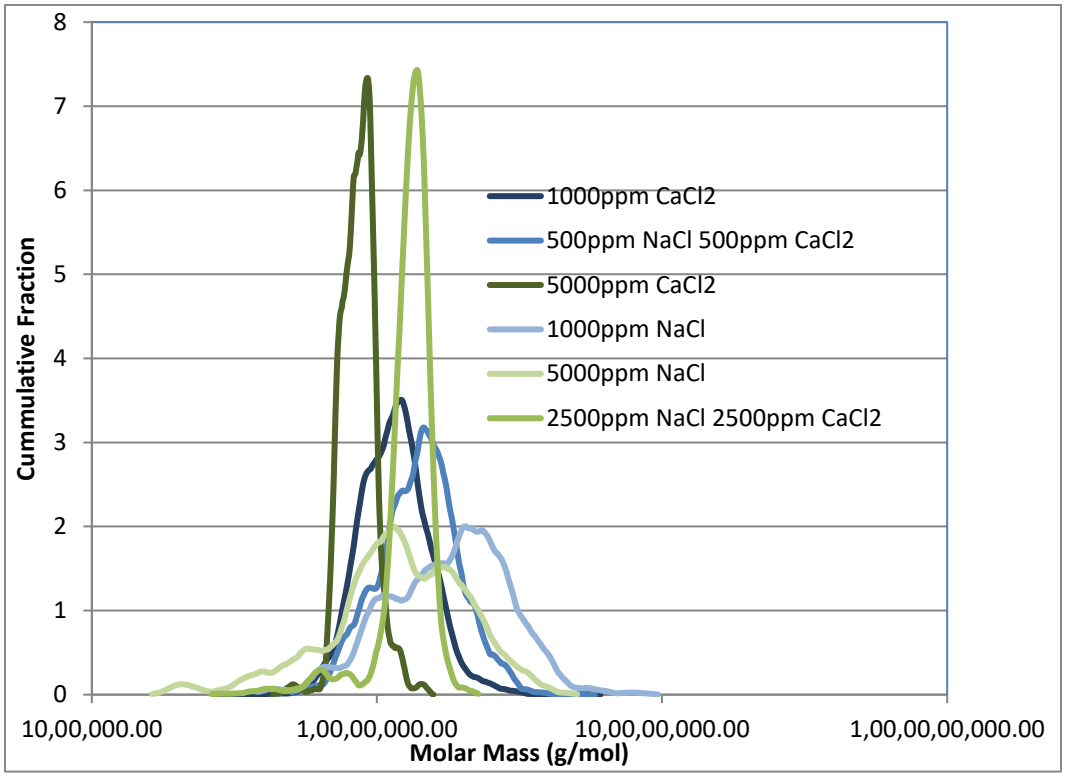

Figure 86: Differential Mass Fraction of Post Hydrolyzed 3630 under different salinity.

Figure 86 shows a differential mass fraction of Post Hydrolyzed 3630 under different salinity scenarios. Differential mass fraction reflects more information on the molar mass distribution of the polymer in the brine. As seen in the graph, curves in blue shades represent curves with 1000 ppm salinity. The curve for 1000 ppm

CaCl2 and “500 ppm NaCl+500 ppm CaCl2” exhibits similar peak with a slightly larger peak for 1000 ppm CaCl2. Both the peak also ends close to each other. The peak is observed for 1000 ppm CaCl2 curve near 1×10^7 g/mol. The similar peak is observed in “500 ppm NaCl+500 ppm CaCl2” curve on right of the peak observed in 1000 ppm CaCl2. The curve for 1000 ppm NaCl shows a relatively broad distribution with a high on the right of the peak observed in “500 ppm NaCl+500 ppm CaCl2” curve.

It is evident that curve for 5000 ppm NaCl shows the broadest molar mass distribution in 5000 ppm salinity cases. The curve also shows a relative high around 1×10^7 g/mol. The high is comparable to the high observed in 1000 ppm NaCl. A large and dominant peak is observed in the curve for 5000 ppm CaCl2 curve and “2500 ppm NaCl+2500 ppm CaCl2” peak indicating the presence of a specific polymer aggregates which dominates the molar mass distribution. The curve for “2500 ppm NaCl+2500 ppm CaCl2” curve shows the highest peak with a shorter base. In the curve for 5000 ppm CaCl2, a peak is observed which has a relatively broader base. Both the curves intersect and overlap each other in the peak envelope which indicates that predominant polymer aggregates in both the salinity cases have a molar mass close to each other.

It can also be examined that with the addition of CaCl2, the differential curve for molar mass exhibits peakier characteristics. The extent of peak increases as CaCl2 content increases indicating that with an increase in CaCl2, the dominance of a specific polymer aggregates increases. It is also to be observed that peak observed shifts towards positive y-axis as CaCl2 contain increases in the brine.

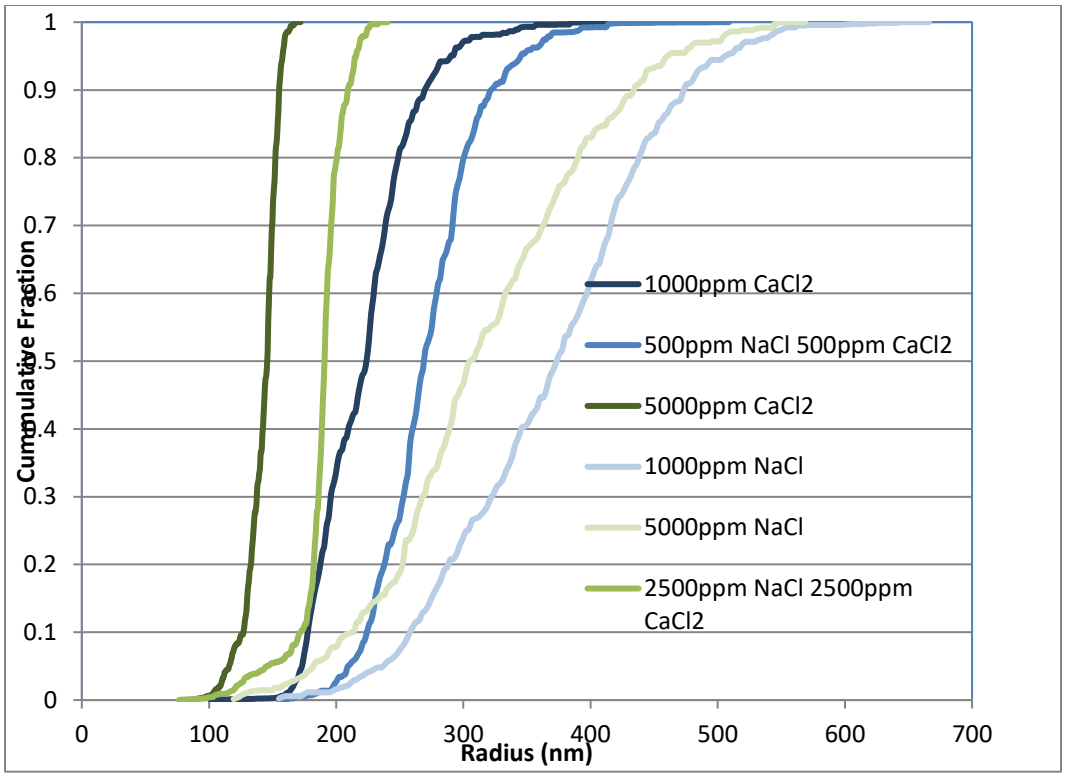

Figure 87: Cumulative Radius Fraction of Post Hydrolyzed 3630 under different salinity.

Cumulative radius fraction of Post Hydrolyzed 3630 in different salinity environment can be seen in Figure 87. The cumulative radius curve for 1000 ppm NaCl shows a greater horizontal extent which indicates that it has a broader radius distribution. The curve for "500 ppm NaCl+500 ppm CaCl2" is steeper than the curve for 1000 ppm CaCl2. Both the curves start close to each other and end far from each other. Effect of CaCl2 is evident as the slope of the cumulative radius curve clearly, changes from smoother to a steeper curve. Further, the curve of 1000 ppm CaCl2 exhibits similar curve characteristics as seen in "500 ppm

NaCl+500 ppm CaCl2" salinity curve suggesting that in the presence of both NaCl and CaCl2, Post Hydrolyzed 3630 tends to be more affected by CaCl2 than NaCl.

The radius distribution curve for 5000 ppm NaCl have largest horizontal extend in 5000 ppm salinity scenarios, which means that it is widest radius distribution which extends almost from 100 nm to 500 nm. The radius distribution for "2500 ppm NaCl+2500 CaCl2" is steeper than 5000 NaCl curve. The curve for 5000 ppm CaCl2 shows similar behavior as "2500 ppm NaCl+2500 ppm CaCl2" radius distribution, also both the curves are extremely steep indicating a dominant presence of a specific polymer species. Both the curves are close to each other, which signify that effect of CaCl2 is not linear with increase in its concentration. The effect of CaCl2 subdues as CaCl2 concentration increases. This conclusion is also evident from the gap between the curves; the gap in between 500 ppm NaCl 500 ppm CaCl2 and 1000 ppm CaCl2 is bigger than the gap between 2500 ppm NaCl 2500 ppm CaCl2 curve and 5000 ppm CaCl2 curve.

It is noticed that cumulative radius curve tends to be steeper in the presence of CaCl2. It means that a particular polymer species with a radius value prevails in the radius distribution of the polymer. Also with the increase in CaCl2 content the cumulative radius curve shifts closer to the positive y-axis, which means that radius value for the distribution curve decreases of Post Hydrolyzed 3630 as CaCl2 increases.

The differential radius curves for Post Hydrolyzed 3630 under different salinity conditions can be seen in Figure 88. As seen in the graph, the curve for 1000 ppm NaCl is the broadest curve which extends till 600 nm. The curve also has a high around 400 nm indicating the radius of the dominant polymer aggregate. With the addition of CaCl2, the curve for "500 ppm NaCl+500 ppm CaCl2" is clearly peakier than 1000 ppm NaCl. Its peak is seen around 280 nm. The vertical extent of the peak is almost double than that of 1000 ppm NaCl which shows that even small quantity of CaCl2 has a significant impact on radius distribution of Post Hydrolyzed 3630. The radius distribution for 1000 ppm CaCl2 shows a similar curve with a peak at around 230 nm. It also shows a second smaller peak around 180 nm.

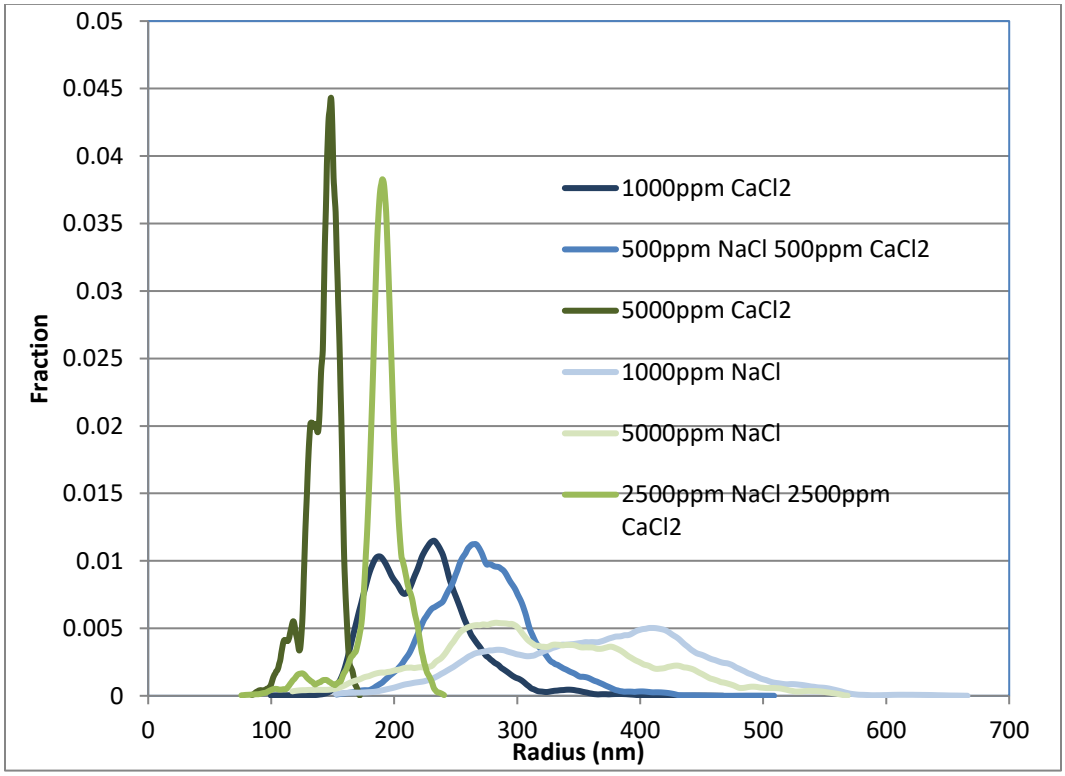

Figure 88: Differential Radius Fraction of Post Hydrolyzed 3630 under different salinity.

The differential radius curve for 5000 ppm NaCl is similar to 1000 ppm NaCl curve. The curve extends till 550 nm and shows a peak around 280 nm. The curve for 5000 ppm CaCl2 and “2500 ppm NaCl+2500 CaCl2” shows a sharp and dominant peak. Also, both the curves show similar characteristics. The curve for “2500 ppm NaCl+ 2500 CaCl2” starts at 100 nm and ends around 195 nm. It shows the peak around 170 nm indicating the polymer aggregate radius which dominates the distribution in the given environment. Similarly, the curve for 5000 ppm CaCl2 starts at 90 nm and ends at around 180 nm. The peak observed is around 140 nm.

It is to be noticed that with the addition of CaCl2 in even small amount changes the differential radius distribution. The curve tends to be peakier with the addition of CaCl2. Also, radius distribution tends to be narrower as CaCl2 content increases. It implies that presence of CaCl2 is significant to the macromolecular structure. Also polymer aggregate with smaller radius dominants the radius distribution as CaCl2 concentration increases in the environment.

7.4 Summary

3630 S

The presence of CaCl2 has no significant impact on the molar mass of the polymer at same low to medium salinity. The presence of CaCl2 has a significant impact on the radius of the polymer. The increase in CaCl2 decreases the radius of the polymer at same salinity. Effect of CaCl2 on the distribution of molar mass is limited at same salinity. Polymer aggregate with lower molar mass dominates with increasing salinity. Effect of CaCl2 on the distribution of radius is limited at same salinity. Polymer aggregate with lower radius dominates with increasing salinity.

Post Hydrolyzed 3630

The presence of CaCl2 has a significant impact on the molar mass of the polymer. The increase in CaCl2 decreases the molar mass of the polymer at same salinity. The presence of CaCl2 has a significant impact on the radius of the polymer. The increase in CaCl2 decreases the radius of the polymer at same salinity. The effect of CaCl2 is more prominent in lower salinity, and its incremental effect decreases as salinity increases. The increase in CaCl2 in absolute term and at same salinity makes a molar mass distribution to exhibit dominance of a specific polymer aggregate with a lower molar mass with increasing CaCl2. The increase in CaCl2 in absolute term and at same salinity makes radius distribution peakier with increasing dominance of low radius polymer aggregate with increasing CaCl2.

Chapter 8

Conclusion

Asymmetrical Flow fluid flow fractionation method coupled with MALS and RI detector was successfully used to characterize oil field application polymer used in enhanced oil recovery application. The elution of high molar mass polymer aggregate and high radius polymer aggregate as seen in the later part of the graph shows that large polymer aggregates can be detected in AF4-MALS-RI. The absence of shear degradation, as well as the fact that no filtration is required of polymer solution before sample injection strongly indicates that results obtained, are a true representation of the polymer solution. A positive correlation exists between molar mass and radius for the polymers studied. Polymer concentration has no serious effect on molar mass and radius values. The signal strength for MALS-RI response increases as polymer concentration increases.

Different polymer behaves differently under changing pH conditions. Overall the polymers show a decrease in molar mass and increase in radius as pH changes from basic to acidic. A broader molar mass and radius distribution are observed in acidic surrounding and as surrounding changes to basic, molar mass distribution and radius distribution becomes narrower. Conformation changes as salinity change from high salinity environment to low salinity environment. Polymer exhibits more coiled and compacted structure in the presence of high salinity. AB 005V shows linear most polymer conformation in an acidic environment in comparison of 3130 S, 3330 S, and 3630 S. 3630 S polymer macromolecules are near sphere like and exhibits most compacted polymer structure compared to 3130 S, 3330 S and AB 005V in the presence of acidic environment. AB 005V is most sensitive to change in radius values with varying pH in compared to other polymers. It shows 40 % drop in radius when the environment changes from basic to neutral and

further 40 % drop when the environment changes from neutral to acidic. 3330 S is most resistance to radius change with varying pH. It shows just 3.5 % drop in radius when surrounding changes from basic to neutral. Similarly, it is most resistance when pH changes from neutral to acidic with 13.5 % radius change. In absolute terms 3630 S has higher radius and molar mass than other polymers under acidic and neutral surrounding. Similarly, AB 005V has smallest radius and molar mass than other polymers. 3130 S has the most uniform molar mass and radius distribution in an acidic environment when compared to AB 005V, 3330 S and 3630 S. 3330 S has uniform radius distribution in the neutral surrounding in compared to other polymers.

Different polymer behaves differently in the presence of mono valent ions. In general, molar mass and radius of the polymers reduce as the mono-valent ion increases in the brine. Molar mass distribution and radius distribution of the polymers tends to be narrower and peakier as the mono-valent ion increases in the environment. The molar mass and radiydfus value decreases of the dominant polymer aggregate increase as mono valent ion increases. 3630 S is more salinity resistance in radius value and molar mass value than Post Hydrolyzed 3630 and C 319 in 5000 ppm – 10000 ppm salinity range. It shows radius decrement of 9 % only and molar mass decrement of 5.8 % when salinity increases from 5000 ppm to 10000 ppm. C 319 is more stable in 1000 ppm -5000 ppm range regarding molar mass values than other polymers studied. It shows decrement of 25%, which is lowest when compared to other polymers. Post Hydrolyzed 3630 is more stable radius value in the range of 1000 ppm – 5000 ppm. 14 % radius decrement is observed in Post hydrolyzed 3630. In absolute terms, C 319 retains highest molar mass values and radius values when compared to 3630 S and Post hydrolyzed 3630 under all salinity conditions. 3630 S displays most uniform molar mass and radius distribution in 1000 ppm salinity in compared to post hydrolyzed 3630 and C 319.

The presence of divalent ion has a significant impact on the radius of the polymer. The increase in di-valent ion at same salinity significantly decreases the radius of the polymer. The presence of divalent ion can have a different effect on molar mass depending on the polymer. HPAM 3630 exhibits no significant effect of a divalent ion at same salinity on its molar mass. However, Post Hydrolyzed 3630 shows a prominent effect on its molar mass as divalent ion increases at same salinity. HPAM 3630 shows the limited effect of the divalent ion on its molar mass distribution and radius distribution. In Post Hydrolyzed 3630, increase in divalent ion in absolute term and at same salinity makes molar mass distribution and radius distribution to exhibit dominance of a specific polymer aggregate, whose molar mass and radius decreases as divalent ion increases. 3630 S is more resistance than post hydrolyzed 3630 to the presence of di valent ion at same salinity. Its molar mass remains similar as ions changes from Na^+ to Ca^{2+} at same salinity and radius shows a decrease of 31 % as ions changes at same salinity.

Future Work

- With the knowledge of the exact composition of the reservoir brine, this method can be used to investigate the behavior of polymer in the reservoir. It can provide valuable information on molar mass distribution, radius distribution and conformational tendency of the polymer.
- With correct instrumentation coupled with the AF4 system it is possible to represent reservoir temperature and pressure, thus providing more accurate polymer behavior at reservoir conditions.
- It is a tremendous tool for characterization of novel polymers developed for the specific purpose. It can be used to investigate the behavior of the novel polymer under various external conditions.
- A matching study between the pore throat diameter distribution of the reservoir and the polymer radius distribution in the reservoir brine can be investigated.
- Investigation and prediction of injectivity based on reservoir characterization based on porosity and permeability along with polymer characterization regarding radius distribution.

References

Abdel-Alim, A. H. (December, 1973). Shear degradation of water soluble polymers. *Journal of Applied Polymer Science, 17*(12), 3769-3778.

Agarwal, S. P. (1980). Shear degradation of poly(vinyl acetate) in toluene solutions by high speed stirring. *Journal Of Applied Polymer Science, 25*(2), 173-185.

Akstinat, M. (28-30 May, 1980). Polymers for enhanced oil recovery in reservoirs of extremely high salinities and high temperature. SPE 8979-MS. *SPE Fifth International Symposium on Oilfield and Geothermal Chemistry.* Stanford, CA.

Al-Sabagha, A. K.-G.-D.-S. (2013). Synthesis and characterization of high molecular weight hydrophobically modified polyacrylamide nanolatexes using novel nonionic polymerizable surfactants. *Egyptian Journal of Petroleum, 22*(4), 531-538.

Alvarado, V. E. (2010). *Enhanced Oil Recovery: An Update Review. Energies*, 3(9): p. 1529-1575.

Andersson, M. W. (2001). Ultra high molar mass component detected in ethylhdroxyethyl cellulose by AF4 couples with MALS. *Analytical Chemistry, 73*(20), 4852-4861.

Andersson, M. W. (2003). Accuracy in Multi Scatternig Measurements for Molar mAss and Radius Estimations. Model Calculations and Experiments. . *Anal. Chem., 75*(16), 4279-7291.

Armstrong, T. (1967). Polymer Floods Attacking Recovery Gap. *Oil and Gas Journal, 65(1)*, 46-48.

Aronofsky, J. R. (1956). Mobility Ratio - Its Influence on Injection o Production Histories in Five Spot Water Flood. *Journal of Petroleum Technology. SPE-641-G, 8*(9).

Aust, N. (2003). Application of size-exclusion chromatography to polymers of ultra-high molar mass. *Journal of Biochemical and Biophysical Methods, 56*(1-3), 323-334.

Axelos, M. M. (1994). Phase Diagrams of Aqueous Solutions of Polycarboxylates in the Presence of DIvalent Cations. . *Macromolecules, 27*, 6594-66.

Barth, H. C. (1984). A review of Polymer Shear Degradation in Size Exclusion chromatography. *Journal Of Liquid Chromatography, 7*(9), 1717-1738.

Basedow, A. E. (1979). Effects of mechanical stree on the reactivity of polymers:Shear degradation of polyacrylamide and dextran. *Macromolecualer Chemistry and Physics, 180*(2), 411-427.

Baviere, M. (1991). Critical Reports on Applied Chemistry Volume 33. Basic concepts in Enhanced Oil Recovery Processes. . London and New York: Elsevier Applied Science.

Botana, A. R. (September 7, 1995). Field programmed flow field flow fractionation. *J. Microcolumn*, 395-402.

Bragg, J. M. (October, 1983). Control of xanthan-degradation organisms in the Loudon Pilot:approach, methodology, results. SPE 11989-MS. *SPE 58th Annual Fall Conference.* San Francisco, CA.

Brandrup, J. I. (1999). *Polymer Handbook.* New York: Wiley.

Buchholz, B. B. (2001). The use of light scattering for precise charaterization of polymers for DNA sequencing by capillary electrophoresis. *Electrophoresis, 22*, 4118-4128.

Buckley, S. L. (1942). Mechanism of FLuid Displacment in Sands. *Soceity of Petroleum Engineers. SPE-942107-G, 146*(01).

Castor, T. S. (1981). Recovery mechanisms of alkaline flooding. *Surface Phenomena in Enhanced Oil Recovery. Plenum Press, New York City*, 249-291.

Cave, R. S. (2009). Characterization of Starch by Size-Exclusion Chromatography: The Limitations Imposed by Shear Scission. *Biomacromolecules, 10*(8), 2245-2253.

Chang, L. Z. (2006). Advances in Polymer Flooding an Alkaline/Surfactant/Polymer Process as Developed and Applied in the People's Republic of China. *JPT, 58*(2), 84-89.

Chauveteau, G. a. (1991). Critical Reports on Applied Chemistry Volume 33.Basic Concepts in Enhanced Oil Recovery Process. Published by Elsevier Applied Science. . 43-47.

Chemical Flooding Polymer. (2001). Retrieved from http://www.chemicalflooding.com/

Chen, Z. D. (2016). Study of Factors Influencing Polymer Hydrodynamic Retention in Porous Media. SPE -179607-MS. *SPE Improved Oil Recovery Conference. .* Tulsa, Oklahoma, USA.

Christopher, C. C. (1988). Performance and Operation of a Successul Polymer Flood in the Sleep Hollow Reagan Unit. *SPE Enhanced Oil Recovery Symposium. SPE-17395-MS.* Tulsa, Oklahoma.

Clampitt, R. R. (September 28 - October 1, 1975). An economic polymerflood in the North Burbank Unit Osage County . *SPE 5552 presented at 50th Annual Fall Meeting of SPE of AIME held in Dallas, TX,USA.*

Dake, L. (1978). *Fundamentals of Reservoir Engineering.* New York City: Elsevier.

Davinson, P. M. (June 1982). Polymer flooding in North Sea reservoir. SPE 9300 PA. *Soc. Pet. Eng. J., 22*(03), 353-362.

Dominguez, J. W. (April, 1977). Retention and flow charateristics of polymer solutions in porous media. SPE 5835 PA. *Society of Petroleum Engineers Journal*, 111-121.

Dupas, A. H. (2012). Mechanical degradation onset of polyethylene oxide used as a hydrosoluble model polymer for enhanced oil recovery. *Oil & Gas Science and Technology, 67*(6), 931-940.

Farouq Ali, S. S. (1970). Increased oil recovery by improved waterflooding. *Earth and Mineral Science , 39*(4), January, pp. 25-28.

Flory, P. O. (1954). Intrinsic Viscosities of polyelectrolytes. Poly- (arcylic acid). *J. Phys. Chem., 58*, 653-661.

Fraunhofer, W. W. (2004). The use of asymmertrical flow field flow fractionation in pharmaceutics and biopharmaceutics. *European Journal of Pharmaceutics and Biopharmaceutics, 58*(2), 369-383.

Fraunhofer, W. W. (2004). The use of asymmetrical flow field flow fractionation in pharmaceutics and biopharmaceuics. *European Journal of Pharmaceutics and Biopharmaceutics, 58*(2), 369-383.

Giddings, J. C. (1979). Flow programmed flow fluid flow fractionation. *Analytical chemistry, 51*(1), 30-33.

Gumpenberger, T. D. (November, 2012). Experiments and simulation of the near wellbore dynamics and displacement efficiences of polymer injection, Matzen Field. SPE- 161029-MS. *Abu Dhabi International Petroleum Exhibition & Conference. .* Abu Dhabi, UAE.

Hill, H. B. (1974). The behaviour of polymers inporous media. SPE 4748MS . *SPE Improved Oil Recovery Symposium .* Tulsa, OK.

Huh, C. C. (1990). Polymer Retention in Porous Media. SPE 20235-MS. *SPE Enhanced Oil Recovery Symposium.* Tulsa, Oklahoma.

(2013). *IEA World Energy Outlook.*

Jung, J. K. (2013). Rheology and polymer flooding charateristics of partially hydrolyzed polyacrylamide for enhanced heavy oil recovery. *Journal of Applied Polymer Science , 127*(6), 4833-4839.

Jungmann, N. S. (2001). Charaterization of polyorganosiloxane nanoparticles in aqueous dispersion by AF4. *Macromolecules, 34*(23), 8347-8353.

Kasaai, M. (2005). Intrinsic Viscosity- Molecular Weight Relationship and Hydrodynamic Volume for Pullulan. *Journal of Applied Polymer Science, 100*(6), 4325-4332.

Kirkland, J. (1976). Porous silica microspheres for high-performance size exclusion chromatography. *Journal of Chromatography A, 125*(1), 231-250.

Lee, H. W. (2001). Analysis of self-assembled cationic lipid-DNA gene carrier complexes using flow field-flow fractionation and light scattering. *Anal Chem, 73*(4), 837-843.

Lee, L. R. (December, 1991). Adsorption of polyacrylamide on the different faces of kaolinites. *Journal of Colloid and Interface Science, 147*(2), 351-357.

Leenders, L. (2014). *Miniaturization in asymmetrical flow field flow fractionation.* Amsterdam .

Leourtier, L. L. (1990). Adsorption of Polyacrylamides on Siliceous Minerals. *Colloids and Surfaces, 40*, 219-231.

Liberatore, M. B. (2004). Turbulent drag reduction of polyacrylamide solutions: effect of degradation on molecular weight distribution. *Journal of Non-Newtonian Fluid Mechanics, 123*(2-3), 175-183.

Limited, S. A. (2013). *An Introduction to Enhanced Oil Recovery Techniques.*

Ling., Y. H. (1982). A Study Of Mechanical Degradation of polymer in high performance GPC. *Journal of Liquid Chromatography, 5*(7), 1259-1267.

Liu, R. (2014). Research on chemical degradation of PAM in oil recovery application. *Advanced Material Research, 936*, 1556-1559.

Manichand, R. S. (2014). Field vs Laboratory Polymer Retention Values for a Polymer Flood in Tambaredjo Field. *SPE Improved Oil Recovery Symposium.* Tulsa, Oklahoma, USA.

Menard, H. (1981, January). Toward a Rational Strategy for Oil Exploration. *Scientific American* , 244(1): 47-57.

Moffitt, P. Z. (May 1993). Application of Freshwater and brine Polymer Flooding in the North Burbank Unit, Osage County, Oklahoma. *8*(3), SPE-20466-PA.

Moradi -Araghi, A. D. (May, 1987). Hydrolysis and precipitation of polyacryamide in hard brines at elevated temperatures. SPE 13033- PA. *SPE Reservoir Engineering, 2*(02), 189-198.

Needham, R. D. (1987). Polymer Flooding Review. SPE -17140- PA. *Journal of Petroleum Technology, 39*(12).

Noik., C. D. (February, 1995). Physico-chemical charaterics of polyacrylamide solutions after mechanical degradation through a porous medium. *Proceedings of SPE International Symposium on Oilfield Chemistry.* Texas, USA.

(2013). *OPEC World Outlook.*

Ouyanga, L. W. (2011). Synthesis and nucleation mechanism of inverse emulsion polymerization of acrylamide by RAFT polymerization: A comparative study. *Polymer, 52*(1), 63-67.

Pourjavadi, A. F. (2013). Novel cationic-modified salep as an efficient flocculating agent for settling of cement slurries. *Carbohydrates Polymers, 93*(2), 506-511.

Putz, A. B. (1994). Commercial Polymer Injection in the Courtenay Field, 1994 Update. *SPE Annual Technical Conference and Exhibition. SPE 28601-MS.* New Orleans, Louisina.

Pye, D. (1964). Improved Secondary Recovery by Control of Water mobility. *J.Pet.Tech., 16(8)*, 911-916.

Ram, A. K. (1970). Shear degradation of polymer solutions. *Journal Of Applied Polymer Science, 14*(8), 2145-2156.

Rayleigh, L. (1910). The Incidence of Light upon a Transparent Sphere of Dimenions Comparable with the Wave Length. *Proc. R. Soc., 84*, 25-46.

Richardson. (1965). Miscible Processes. *Reprint Series,SPE*, p. 205.

Roger, P. B. (2001). Charaterization of starch polysaccharides by flow field flow fractionation multi angle laser light scattering differential refractometer index. . *Journal of Chromatography, 917*(1-2), 179-185.

Ryles, R. (1983). Elevated Temperature testing for mobility control reagent. SPE 12008-MS. *SPE Annual Technical Conference and Exhibition.* San Francisco, California.

Ryles, R. C. (April, 1986). New Polymers for EOR Application. SPE 14947-MS. *SPE Enhanced Oil Recovery Symposium.* Tulsa, Oklahoma .

Seright, R. C. (June 2010). Stability of Partially Hydrolyzed Polyacrylamides at Elevated Temperatures in the Absence of Divalent Cations. *Society of Petroleum Engineers, 15*(02), 341-348.

Seright, R. S. (October 2009). Injectivity Charateristics of EOR Polymers. SPE 115142. *SPE Reservoir Evalutions and Engineering Journal, 12*(05), 783-792.

Singhal, A. (2011). *Preliminary Review of IETP Projects Using Polymers.* Calgary: Premier Reservoir Engineering Services LTD.

Slagowski, E. F. (1974). Upper Molecular Weight Limit for the Characterization of Polystyrene in Gel Permeation Chromatography. *Macromolecules, 7*(3), 394-396.

Smith, F. (Feb, 1970). The Behavior of Partially Hydrolyzed Polyacrylamide solutions in porous media. SPE 2422-PA. *Journal of Petroleum Technology, 22*(02), 148-156.

Sorbie, K. (1991). *Polymer - Improved Oil Recovery.* Boca Raton, Florida: CRC Press Inc. .

Sorbie, K. (1991). *Polymer - Improved oil recovery. Blackie USA and Canada.* CRC Press.

Southan, M. M. (1999). Molecular weight distriibution of wheat protien . *Cereal Chem, 76*, 827-836.

Su, X. Z. (2008). Stereocontrol during photo-initiated controlled/living radical polymerization of acrylamide in the presence of Lewis acids. *European Polymer Journal, 44*(6), 1849-1856.

Sydansk, R. a. (Spetember 27-30, 1998). More than 12 years of experiance with a successful conformance control polymer gel technology. *SPE 49315 presented at SPE-ATC held in New Orleans, LA, USA*.

Szabo, M. (August, 1975). Some aspects of polymer retention in porous media using a c14 tagged hydrolyzed polyacrylamide. *Society Of Petroleum Engineers Journal , 15*(4), 323-337.

Tay, A. O. (2015). Adsorption Inhibitors:A new route to mitigate adsorption in chemical enhanced oil recovery. SPE-174603-MS. *Society of Petroleum Engineers.* Kuala Lumpur, Malaysia.

Tekin, N. D. (2005). Adsorption of cationic polyacrylamide onto kaolinite. *Microporous and Mesoporous Material , 85*(3), 340-350.

Thomas, A. G. (2012). Some Key Features to Consider When Studying Acrylamide- Based Polymers for CHemical Enhanced Oil Recovery. *Oil Gas Sci. Technol., 67*(6), 887-902.

Thompson, G. M. (1969). Thermal field flow fractionation of polystyrene samples. *Anal. Chem., 41*(10), 1219-1222.

Vela, S. P. (April, 1976). Evaluation of Polymer Flooding in a Layered Reservoir With Crossflow, Retention and Degradation. *Society of Petroleum Engineers, 16*(2), 82-96.

Vela, S. P. (April, 1976). Evaluation of Polymer flooding in the Layered reservoir with cross flow, retention and degradation. *Society of Petroleum Engineers Journal, 16*(02), 82-96.

Wan, H. S. (2016). Is Polymer Retention Different Under Anerobic vs Aerobic Conditions . SPE- 179538-MS. *SPE Improved Oil Recovery Conference.* Tulsa, Oklahoma, USA.

Warner, H. J. (1976). Analysis Of Mechnical Degradation Data On Partially Hydrolyzed Polyacrylamide Solutions. SPE 6502-MS. *Society of Petroleum Engineers .*

Wever, D. P. (2013). Branched polyacrylamides: Synthesis and effect of molecular architecture on solution rheology. *European Polymer Journal, 49*(10), 3289-3301.

White, R. (1997). FFF MALS A New Tool for the charaterization of polymers and particles. *Polymer international, 43*(4), 373-379.

Willhite, G. (1986). *Waterflooding.* Texas: Textbook Series, SPE.

Wittgren, B. B. (1998). Conformational change and aggregation of kappa carregeenan studied by flow field flow fractionation and multipleangle light scattering. *Biopolymers, 45*(1), 85-96.

(2006). *World Energy Outlook.* International Energy Agency.

Xin, X. X. (15 September, 2007). The effect of CaCl2 on the interaction between hydrolyzed polyacrylamide and sodium sterate: Rheological property study. *Colloids and Surfaces, 305*(1-3), 138-144.

Young, R. L. (1991). *Introduction to Polymers, 2nd Edition. .* New York: Chapman & Hall.

Zaitoun, A. K. (1988). Teo Phase Flow Through Porous Media:Effect of an Adsorbed Polymer Layer. SPE 18085-MS. *SPE Annual Technical Conference and Exhibition.* Houston, USA.

Zaitoun, A. P.-M.-H.-G. (2012). Shear Stability of EOR Polymers. SPE - 141113-PA. *Society of Petroleum Engineers, 17*(02).

Zhang, G. S. (13-15 April, 2015). Hydrodynamic retention and rheology of EOR polmers in porous media. SPE 173728-MS. *SPE International Symposium on Oilfield Chemistry.* Woodlands, Texas, USA.

Zhang, G. S. (2014). Effect of Concentration on HPAM Retention in Porous Media. SPE 166265-PA. *Society of Petroleum Engineers, 19*(3), 373-380.

Zhu, D. Z. (2013). Laboratory Study on the Potential EOR use of HPAM/VES hybrid in High Temperature and High Salinty Oil Reservoir. *Journal of Chemistry*, Article ID 927519.

Žigon, M. T. (1997). Degradation of High Molecular Weight Polystyrenes During the SEC Separation Process, as Demonstrated by SEC Coupled with Lalls and by Static Light Scattering. *Journal of Liquid Chromatography & Related Technologies, 20*(14), 2155-2167.

Appendix

Replicate Analysis

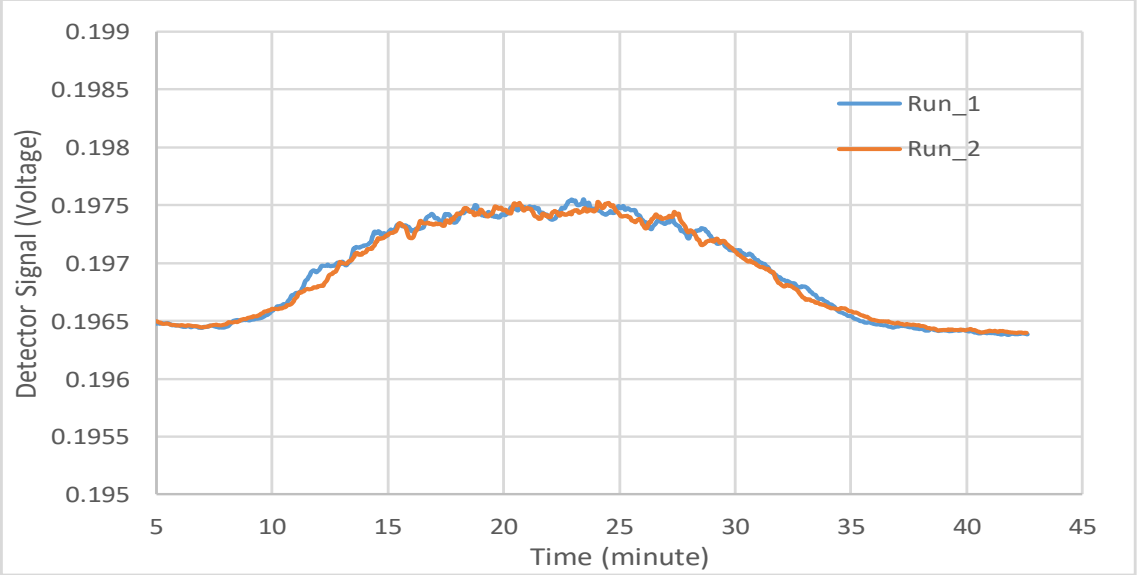

Figure A 1: Replicate runs for HPAM 3630 at 1500 ppm in 5000 ppm NaCl.

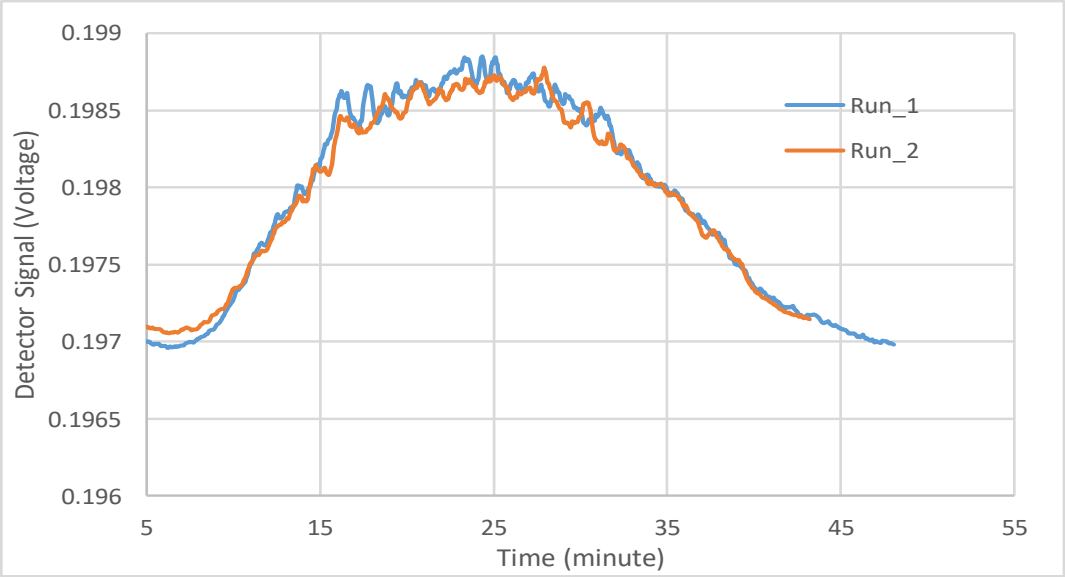

Figure A 2: Replicate runs for HPAM 3630 at 2000 ppm in 10000 ppm NaCl.

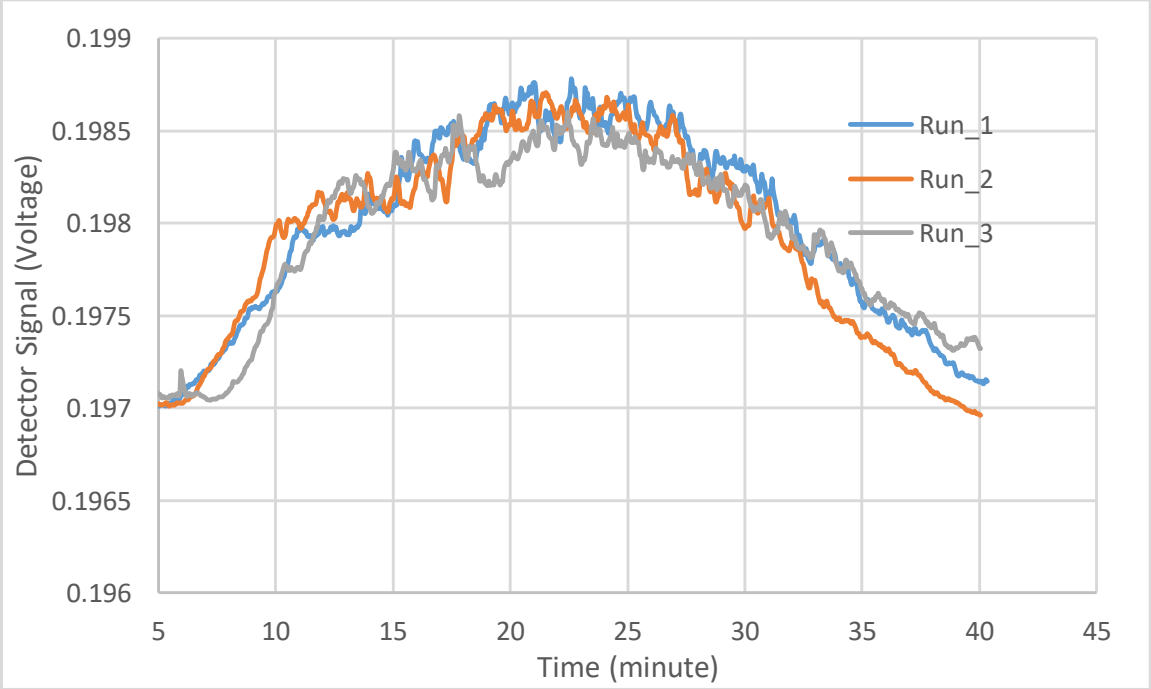

Figure A 3: Replicate runs for C319 at 2000 ppm in 5000 ppm NaCl.

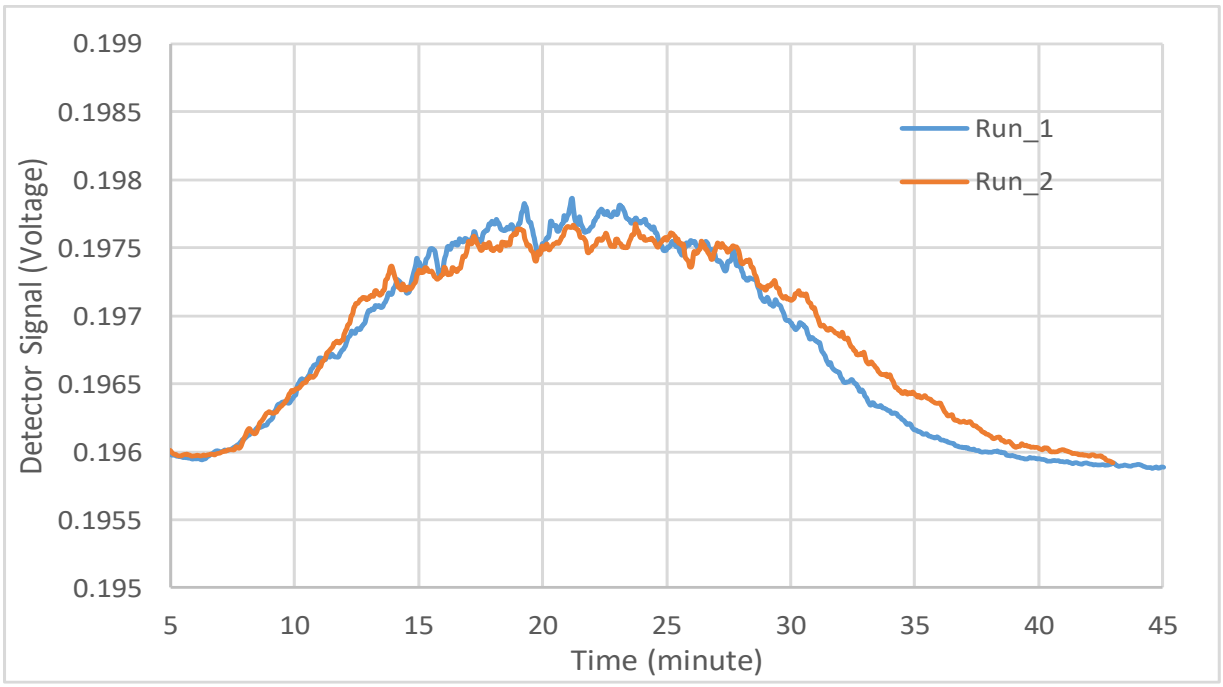

Figure A 4: Replicate runs for C319 at 2000 ppm in 10000 ppm NaCl.

Concentration Runs

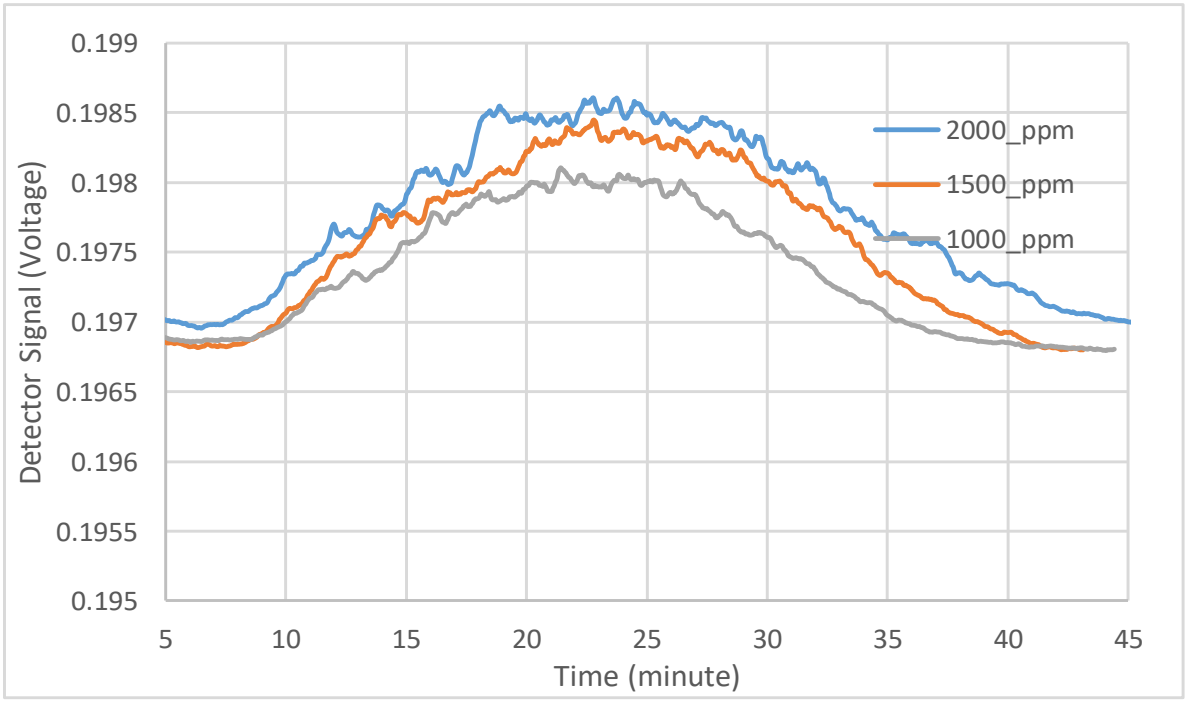

Figure A 5: Different Polymer concentration run for Post-Hydrolyzed polymer in 10000 ppm NaCl.

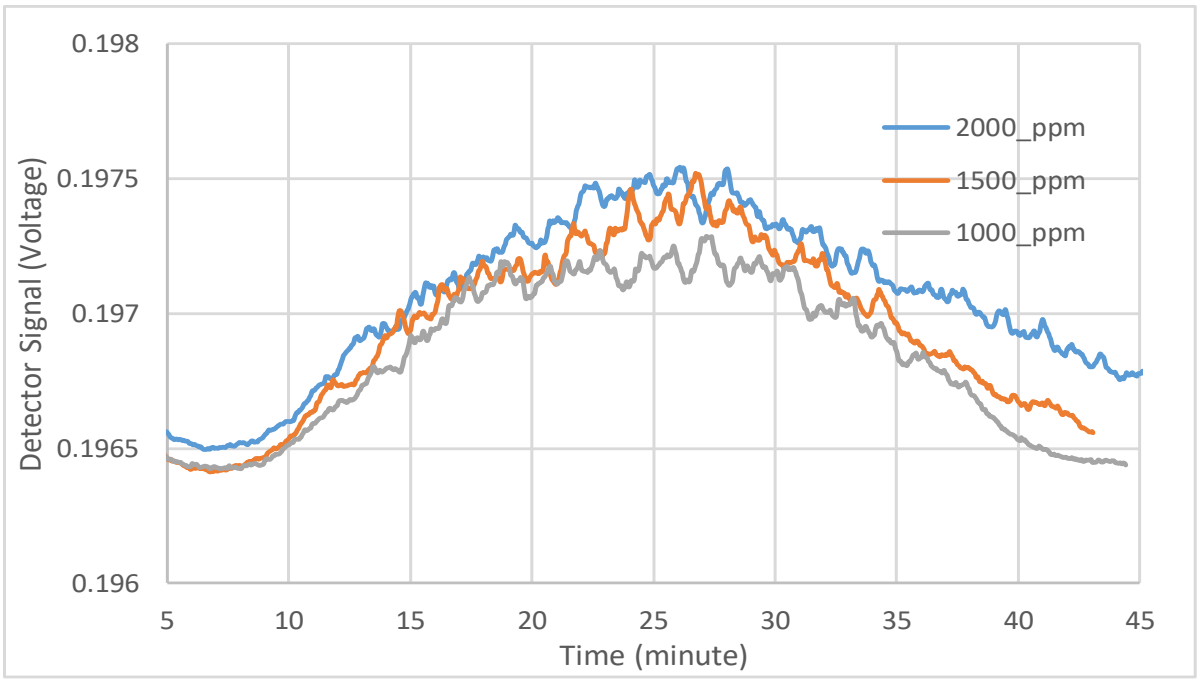

Figure A 6: Different Polymer concentration run for Post-Hydrolyzed polymer in 5000 ppm NaCl.

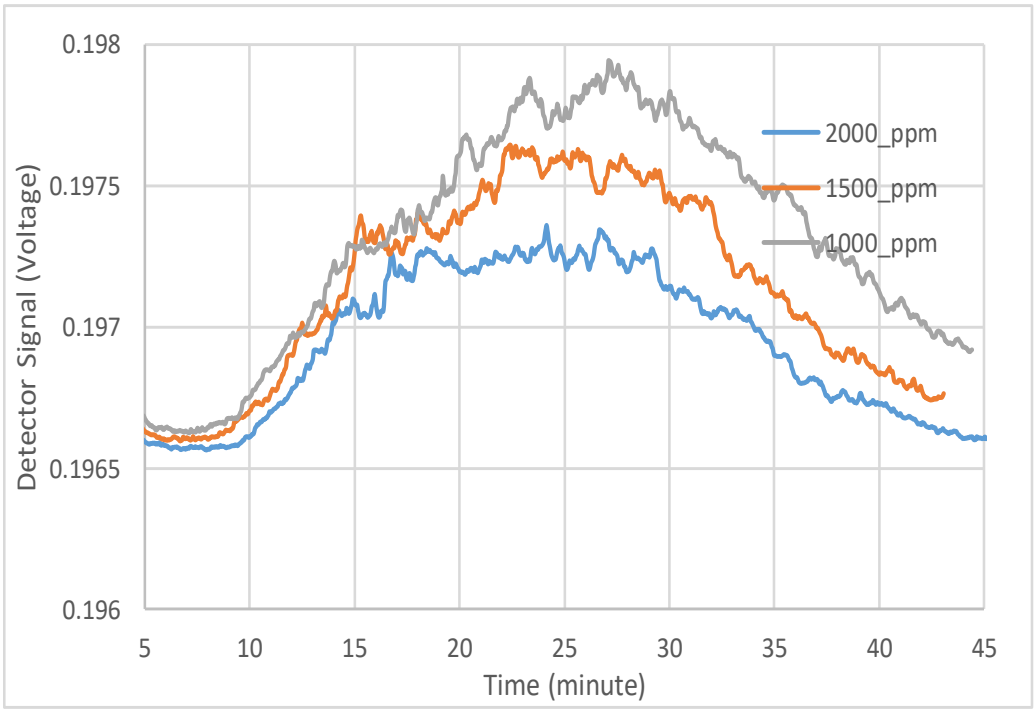

Figure A 7: Different Polymer concentration run for Post-Hydrolyzed polymer in 500 ppm NaCl.

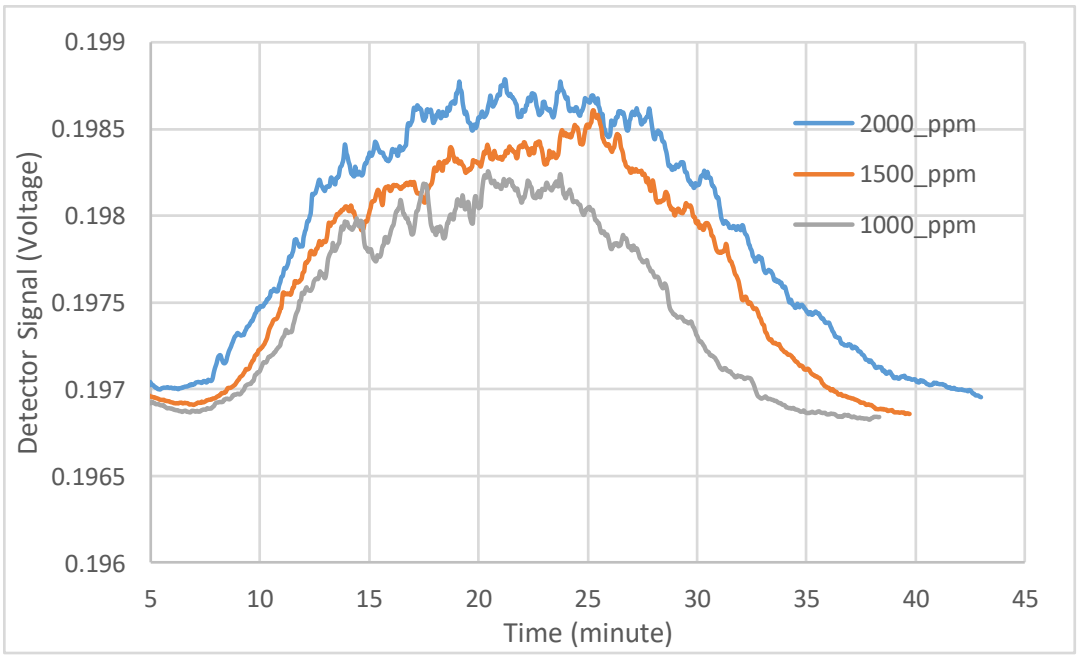

Figure A 8: Different Polymer concentration run for C319 in 10000 ppm NaCl.

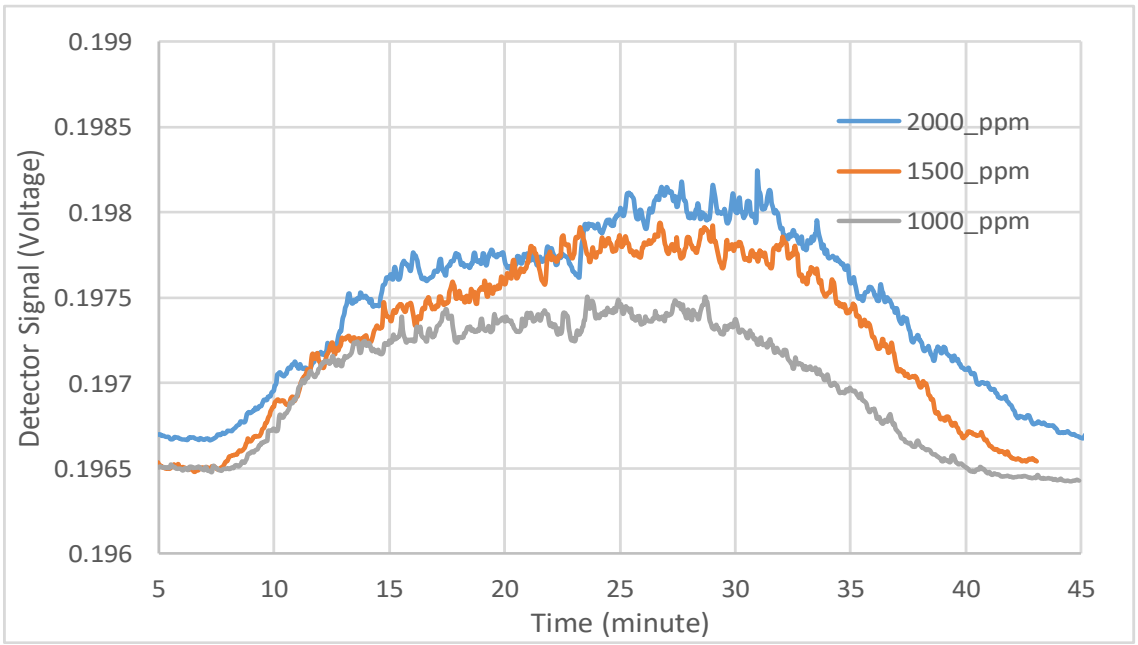

Figure A 9: Different Polymer concentration run for C319 in 5000 ppm NaCl.

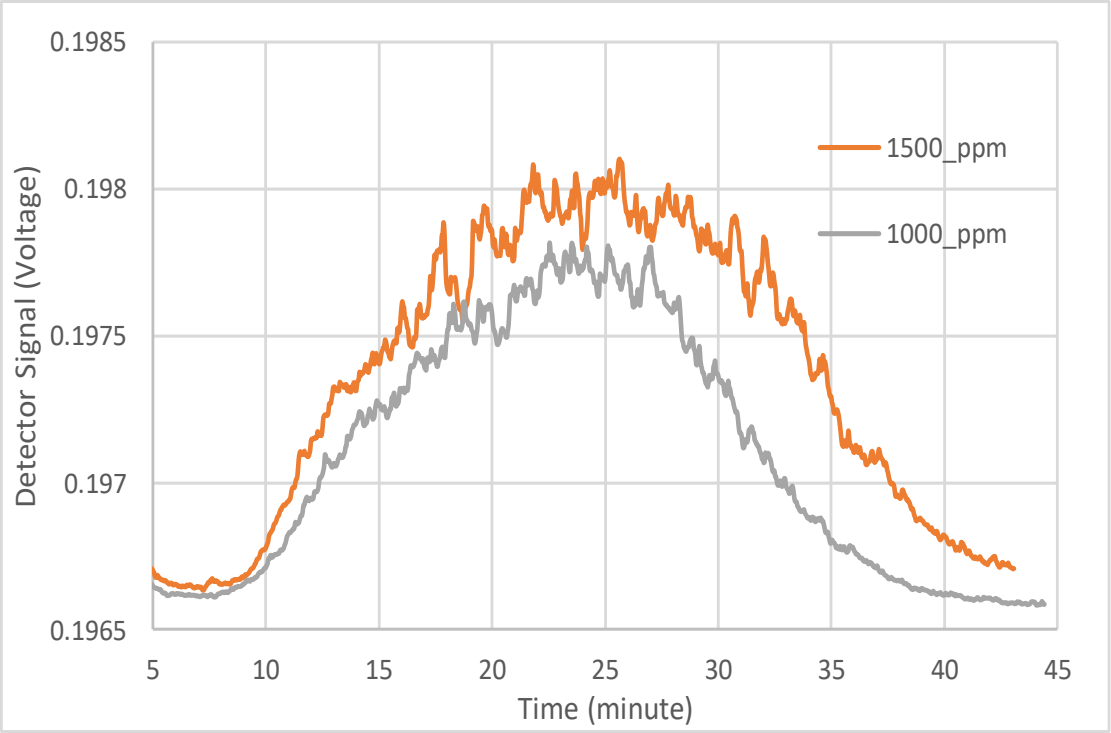

Figure A 10: Different Polymer concentration run for C319 in 500 ppm NaCl.

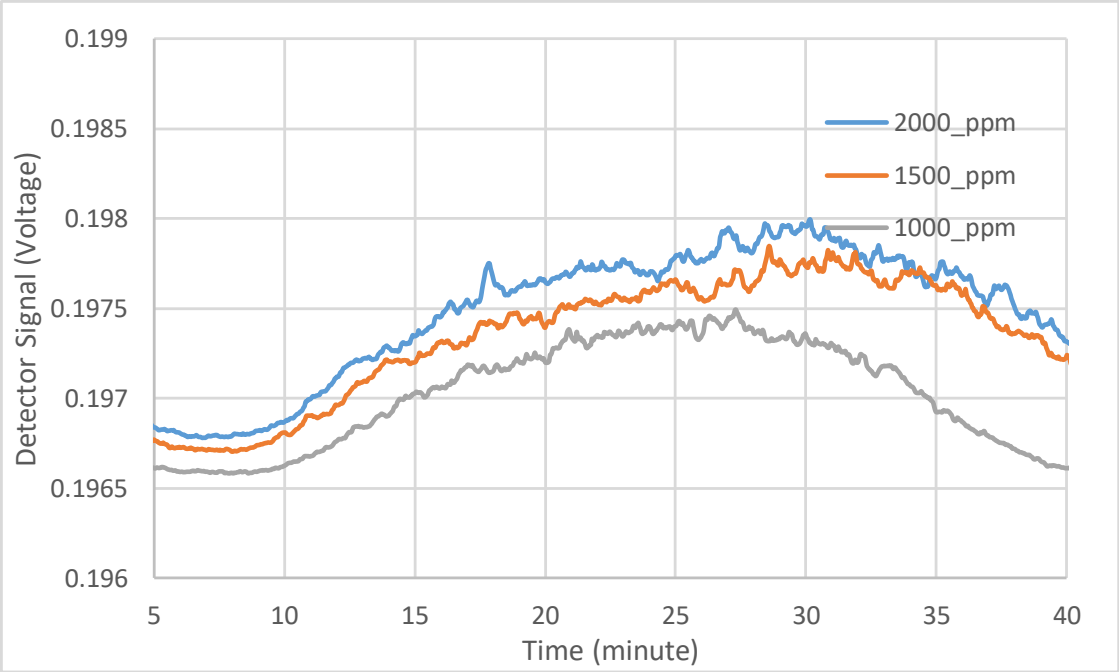

Figure A 11: Different Polymer concentration run for HPAM 3630 in 500 ppm NaCl.